A cognitive robotics approach to the human reaching process

Simulating goal-directed reaching and choice-reaching tasks with a closed-loop model

Soeren Strauss

A thesis submitted to the
University of Birmingham
for the degree of
Doctor of Philosophy

School of Psychology
College of Life and Environmental Sciences
University of Birmingham
September 2013

Abstract

In this thesis a robotics-based model for simulating reaching experiments is presented. First, I will focus on simulating visual attention in choice-reaching tasks. In such experiments participants are asked to make rapid reach movements towards a target that is presented with distractors. Interestingly, these studies found that in a high number of trials movements were initially directed towards a distractor and only later were adjusted towards the target (e.g. Song & Nakayama, 2008b). In order to understand the complex behaviour in such tasks I will follow a robotics based approach and simulate numerous choice-reaching tasks.
The second part of this thesis will deal with phenomena of goal-directed reaching such as the speed-accuracy trade-off of Fitts' law (Fitts, 1954) which states that the movement time of reaching movements increases with the distance and decreases with the size of the target object. In the simulations I will demonstrate the human-like goal-directed reaching behaviour of my model. Moreover, due to its feedback-based architecture my model offers an alternative explanation to the popular two-component models of the goal-directed reaching process (e.g. Meyer, Smith, Kornblum, Abrams, & Wright, 1990).
My model utilises a real-world LEGO robot and required the implementation of multiple underlying processes and the handling of different sources of noise. To link the model with the control of the robot I applied the neurological plausible framework of the dynamic field theory of Erlhagen and Schoener (2002). The successful simulations demonstrated that my model can give further insight in the nature of goal-directed reaching and the choice-reaching tasks.

Acknowledgements

First I would like to thank my supervisor Dr Dietmar Heinke for having given me the opportunity to do a PhD here at the University of Birmingham and for the successful work together in the last years.
Furthermore, I want to thank my colleagues of my office and my department. Whether we did projects together or had conversations about more or less work-related topics often new ideas arose from this exchange of information.
Finally I thank my friends and my family for their patience and helpful support.
My PhD also was supported by the Engineering and Physical Sciences Research Council (EPSRC, UK).

Contents

List of Figures

List of Tables

1. Introduction

1.1. Motivation

Humans possess a highly efficient vision-action system which enables them to interact with their environment. One important example for such an interaction is reaching. I will focus on the underlying processes that are involved to successfully plan and execute reaching movements and on how these processes are encoded in the human brain.

Even for a seemingly simple task such as reaching for a target on a table with objects several steps have to be completed to eventually land with the hand on the target. First, the target needs to be attended and identified whereas nearby distractor objects have to be ignored. Next, the movement has to be planned by specifying a trajectory and selecting an appropriate movement speed in order to interact with the selected object. Finally, potentially occurring changes in the environment like moving objects have to be detected and after the movement initiation the movement itself has to be supervised in order to react towards unexpected perturbations and the noise in the human motor system.

In this PhD a cognitive robotics approach will be taken to understand the mechanisms behind these processes. Hereby the aim is two fold: First, I develop a model utilising a robotic arm that mimics human reaching behaviour in choice-reaching tasks. Recent experimental evidence in cognitive psychology suggests that such tasks can shed new

light on cognitive processes, such as visual attention, memory, or language processing (see Song & Nakayama, 2009; for a review). In these experiments participants are asked to make rapid visually-guided reaching movements towards a target. The trajectories of these movements often reflect important characteristics of the underlying cognitive processes that are involved in order to determine the target and to coordinate the reaching process. For instance Song and Nakayama (2008b) found evidence for the fact that the target selection process operates in parallel with the movement planning process and can affect an already initiated movement. Experiments applying the choice-reaching task paradigm can unveil the complex interactions of those cognitive processes better than traditional reaction time experiments. Examples for such tasks that I will focus on are the odd-colour task on visual attention of Song and Nakayama (2008b), tasks regarding the spatial averaging effect by Chapman et al. (2010a) and the Simon effect (e.g. Scherbaum, Dshemuchadse, Fischer, & Goschke, 2010). The model that I will develop accounts for their empirical findings focusing on evidence for visual attention from reach movements in visual search tasks and the influence of visual attention on the movement execution. Moreover, I aim to simulate these experiments with human-like behaviour, i.e., with a straight, jerk-free trajectory and a bell-shaped velocity profile as it typically is observed in human reaches (e.g. Jeannerod, 1984).

In the second part of this thesis I focus on the question how the brain plans and executes goal-directed movements. Until recently, there has been consensus that reaching is controlled by two phases like it is suggested by the two-component model. The origins of this model go back to Woodworth (1899) (see Elliott, Helsen, & Chua, 2001; for a review). It suggests that the first part of a reaching movement is a ballistic pre-planned impulse where no feedback is used. In contrast, the second component consists of an online controlled reaching movement that guides the hand to the target. However, recently it has become increasingly clear that even the early

phase is influenced by visual information (see Elliott et al., 2010; for a recent review). Moreover, it is possible to go so far to say that reaching is under continuous control of visual information as proposed by the model of Hoff and Arbib (1993) (or see Saunders & Knill, 2005; for a recent instalment). Crucial for their model is the assumption of an internal model based on the control theory which generates movements by minimising the jerk of the trajectory. The application of internal models in the reaching process that are able to deal with the visual processing delay later was established by Miall and Wolpert (1996). In fact, my model of the choice-reaching tasks implements online control in a neurologically plausible manner. Crucially, my model assumes that such an internal model exists and enables a fairly good online control. Hence, the choice-reaching model seems to be a good base for simulating goal-directed reaching experiments. However, besides visual feedback (which my model uses) humans have access to a broader range of sensory feedback (e.g. proprioceptive feedback) and can even estimate the hand position with forward models. Hence, my model should be considered as a simplified internal model in order to study the consequences of target properties and perturbation effects on various measures. The simulations for the goal-directed reaching will aim to simulate the goal-directed reaching process with typical effects such as the speed-accuracy trade-off of Fitts' law (Fitts, 1954) and perturbations of target and hand (e.g. Heath, Hodges, Chua, & Elliot, 1998; Saunders & Knill, 2005).

In order to understand the findings of Song and Nakayama (2008b) and other reaching studies I will apply the framework of cognitive robotics. Due to the complexity of the experimental results and the underlying cognitive processes of the human reaching process this modelling approach offers advantages in comparison with the classical psychology. For both the choice-reaching tasks and the goal-directed reaching experiments I am presenting a computational model that realizes a control architecture which suggests a neurologically plausible mechanism. I use a purely closed-loop

approach where sensory information constantly updates the movement parameters such as speed and direction of a robot arm in a feedback-based manner. In order to demonstrate that this approach yields a human-like performance I will simulate numerous experiments and discuss how my model can explain cognitive processes such as target selection and motor planning/control during the reaching process with its single-process architecture in respect to existing models or theories.

1.2. Goal-directed reaching

This section aims to lay the foundation for the simulations of the experiments in the following chapters by presenting the relevant literature regarding goal-directed reaching. Since the early study of Woodworth (1899) it has been controversial how reaching movements are planned and controlled. Three general approaches haven been suggested: the purely feedback-based closed-loop approach (e.g. Hoff & Arbib, 1993), the open-loop approach that solely relies on planning (e.g. Plamondon & Alimi, 1997) or the hybrid two-component models that combine the other two approaches (e.g. Glover, 2004). Following recent evidence of early online control (Elliott et al., 2010) my model will be based on the closed-loop approach in order to simulate the human reaching process. While I will give a detailed review of these approaches and existing models that apply those in chapter 2.1 here I am going to give a general overview of the research regarding goal-directed reaching.

Crucially for understanding the goal-directed reaching process have been experiments regarding the speed-accuracy trade-off like it is observed in Fitts' law tasks (Fitts, 1954). Fitts' law states that there is a mathematical relation between the movement time of a reach and the target object's size and distance, i.e., larger and nearer objects can be reached faster (see chapter 5.1 for a more detailed review). In the last decades many different explanations have been suggested to give a reason for the

existence of Fitts' law. For instance the popular stochastic optimized-submovement model by Meyer, Kornblum, Abrams, and Wright (1988) suggests that it results from the fact that the body has to strike a balance between force (speed) and precision. Thus, a high force in the initial movement implies a low endpoint accuracy so that additional submovements could be required to successfully reach the target. Vice versa a low force results in a slow movement speed but a higher accuracy. The body balances those constraints in a way that the total reaching time is minimized which depends on the target distance and width, hence Fitts' law can be explained. However, recent evidence from Elliott et al. (2010) and colleagues found that online control is used much earlier in the movement than previously thought, even during the initial movement phase. This questions Meyer et al.'s (1990) model which is a hybrid model that strictly separates the initial (pre-planned) movement and the online-controlled submovement phase. Hence, new explanations arose to account for those findings. The model I present will simulate numerous goal-directed reaching experiments. Its closed-loop architecture offers an alternative explanation for the long time accepted view of a strictly separated planning and online-control phase like in Meyer et al.'s (1988) model. I investigate how Fitts' law and other typical effects are explained with the framework of my model.

In chapter 5 I will present the goal-directed reaching model in detail and simulate typical experiments for goal-directed reaching: Two experiments regarding the speed-accuracy trade-off (e.g. a Fitts' law task) and two with a target and hand perturbation paradigm will be simulated. While the first group of experiments shows the relation between speed and accuracy of reaching movements and how kinematic markers change with different target properties the second group gives further support for my model by dealing with situations in a dynamically changing environment. Combining the evidence of both kinds of experiments I give an alternative interpretation to two-component models and the question how humans achieve goal-directed reaching.

The framework for my model is the dynamic field theory of Erlhagen and Schoener (2002) which will be introduced in greater detail in chapter 1.5. The dynamic field theory assumes that movement parameters are topologically represented in the brain and therefore possesses a neurological plausibility. Moreover it postulates that the dynamic neural processes of competition are crucial for understanding human behaviour albeit for the preparation of movements. My model implements the competition processes within the model's modules with the mathematical formalism used in the dynamic field theory.

1.3. Choice-reaching tasks

The choice-reaching tasks will play a major role in this thesis. Here I am going to introduce empirical findings on evidence for visual attention from reach movements in several choice-reaching tasks (e.g. Song & Nakayama, 2006, 2008b). Therefore the relevant literature regarding visual attention in visual search tasks in general and choice-reaching tasks in particular will be reviewed here. Later in chapter 2 I will present my model and in the chapters 3 and 4 the simulations of various experiments. In contrast to the goal-directed reaching tasks in a choice-reaching task several objects compete for action and attention. A classical assessment of visual attention is the visual search task (see J. M. Wolfe, 1998; for an introduction). In this task participants see a number of items on the screen and are asked to indicate whether a pre-defined target item is present or absent by pressing a designated button on a keyboard. Typically the speed with which they produce this response (reaction time) is seen as a signature for the way selective attention is influenced by visual characteristics of such displays. For instance, a red bar among green bars is faster detected/attended than a red bar among green and yellow bars (see J. M. Wolfe, 1998; Muller & Krummenacher, 2006; for reviews). In the last decade choice-reaching

tasks have been developed to investigate such effects. In a choice-reaching version of the visual search task participants are asked to reach for the target object and the reaching trajectory is recorded. These tasks offer the advantage that the whole time course of the movement (trajectory) is available to be analysed.

The choice-reaching tasks have been used to analyse a broad range of cognitive abilities (see Song & Nakayama, 2009; for a review). Here I present several examples. The first example concerns the representation of numbers (see Feigenson, Dehaene, & Spelke, 2004; for an overview). Pivotal evidence for this representation comes from tasks in that participants have to decide which of two simultaneously presented numbers is larger. This decision is faster/more accurate the larger the difference between the numbers is ("numerical distance effect"). Song and Nakayama (2008a) examined this effect in a choice-reaching task (see Figure 1.1). They presented three boxes on a screen with a number in the central box. Participants were asked to reach for the box on the left if the number is smaller than five and for the box on the right if the number is greater than five. The results showed that the closer the number is to five the more the reaching trajectories are shifted towards the centre box. Song and Nakayama (2008a) interpreted this as direct evidence for a spatial representation of numbers in the brain as the numerical difference directly influenced the spatial nature of the reaching trajectory.

The second example concerns language processing. In Spivey, Grosjean, and Knoblich (2005) participants saw two pictures of objects on the screen and after hearing an the name of one of the objects they were asked to click with a computer mouse on the corresponding picture. The results showed that the more phonological similar the non-target object was the stronger the mouse trajectory deviated towards the non-target picture. This was seen as direct evidence for a dynamic decision process, often termed competition process, occurring in the phonological processing of words.

The third example is the odd-colour task of Song and Nakayama (2006, 2008b) which

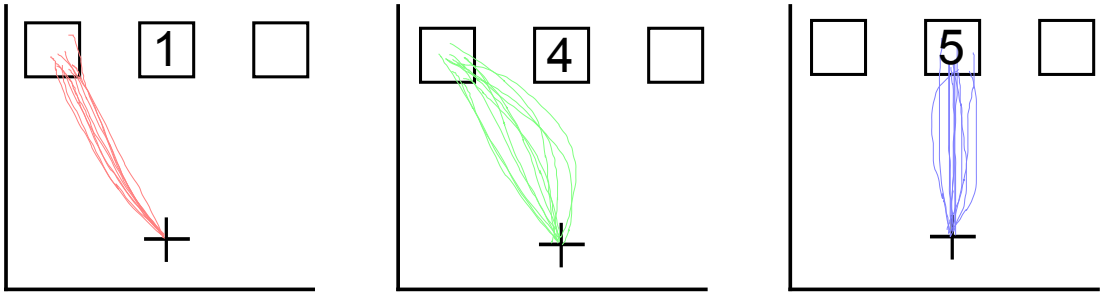

Figure 1.1.: Evidence for spatial representation of numbers from the choice-reaching task of Song and Nakayama (2008a). Participants were instructed to reach for the box on the left if the number is smaller than five and for the box on the right if the number is greater than five. The value of the number influenced the curvature of the reaching trajectory which suggests a spatial representation of numbers in the brain. Figure adapted from Song and Nakayama (2008a).

concerns visual attention and forms the basis for my computational model and the experiments in this thesis. Song and Nakayama (2006, 2008b) published a series of experiments in which they investigated the target-selection process. In their choice-reaching task different objects competed for attention and action and participants were required to make rapid reach movements toward the search target. The search displays consisted of a green square among red squares and vice versa and the participants' task was to reach for the odd-coloured square. Note that the target could be easily reached with straight trajectories. Despite this, Song and Nakayama found that in a high number of trials, movements were initially directed toward a distractor and only later were adjusted toward the target (see Figure 1.2). These "curved" trajectories occurred particularly frequently when the target in the directly preceding trial had a different colour and differed significantly from "straight" trajectories in the other conditions.

Song and Nakayama's explanation of these findings can be summarized as follows. They stipulated that the selection process operates in parallel to the execution of the movement and that the selection process is implemented as a dynamic competition between search items. Hence, in curved trajectories initially the target colour from

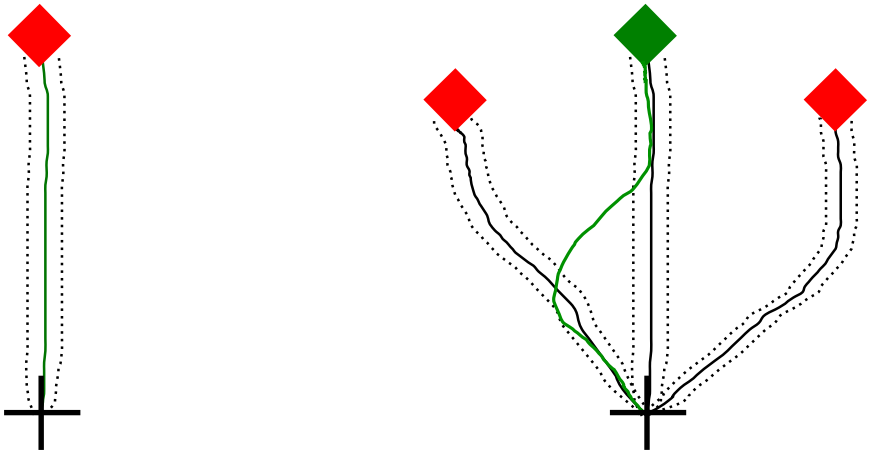

Figure 1.2.: Reaching trajectories of the odd-colour task of Song and Nakayama (2008b). On the left hand side a straight trajectory of the single-target condition is displayed. On the right side the search display of the choice-reaching task with the three objects can be seen. Participants had to reach toward the odd-coloured object. The reach trajectories were often initiated toward a distractor object and corrected in flight. Example trajectories are displayed in green, straight baseline reaches in black and their standard deviation with dashed lines. Figure depicted from Song and Nakayama (2008b).

the preceding trials preactivates or primes distractor objects directing the competition toward the distractors. Consequently the reach movement is guided toward a distractor. Their interpretation was supported further by the fact that the reaction time (or initial latency, the time between search display presentation and start of the movement) was shorter in curved trajectories compared to the initial latency in trials with straight trajectories. Hence because the movements started earlier they are influenced by the erroneous selection due to the priming effect.

The curved trajectories did not have additional costs in terms of total time compared with straight trajectories. However, they had shorter reaction times but longer movement durations. Participants traded reaction time for movement time as quicker target decisions increased the probability of a wrongly selected target which has to be corrected in-flight. Therefore, the authors suggested, the reaching process can be divided in a target selection and a movement coordination sub-process. Both

sub-processes operate in parallel, so that a target re-selection can take place during the movement. The model presented in the the second chapter will follow Song and Nakayama's interpretation of their findings. In fact, Song and Nakayama's view of the selection process as a dynamic competition process is also held by one of the most popular theory on visual attention (e.g. Chelazzi, Müller, Duncan, & Desimone, 1993; Desimone & Duncan, 1995; Duncan, 2006).

Another choice-reaching task example is the experiment of Chapman et al. (2010a, 2010b). There participants had to initiate reaches towards a different number of potential target objects while the final target object only was revealed after movement onset. Their main finding was that the reach trajectory initially pointed towards a location in between the potential targets and later changed the direction towards the final target object. Moreover, the initial pointing direction was not just directed arbitrarily in between the potential target objects but an average of those objects and very sensitive towards changes such as shifted locations of the potential targets to the sides or different numbers of potential targets. In a second set of experiments Chapman et al. (2010b) showed that this so-called spatial averaging effect also is influenced by short-term experience of previous trials. They demonstrated that a series of repetitions on one target side leads to a biased trajectory towards this side. They suggested that overlapping hills of neural activity are responsible for the observed averaging effects. These activations can be weighted depending on the trial history or number and location of the objects producing the averaging effect.

The last example of the choice-reaching tasks presented here regards the Simon effect which is an interesting effect for investigating perception, attention, and action planning. In a classical Simon task participants are required to press a button (on the left or the right side) whereas the target button is encoded by the colour of a cue object. A response conflict arises as the cue's location (which can also be on the left or the right side) has to be ignored (see Simon, 1990; for a review). There exist a

few recent experiments applying the choice-reaching paradigm to the Simon effect. Hereby a setting of the Simon task is combined with a task required visually guided reach; e.g. a coloured cue object is placed on either the left or the right side, whereas the cue colour encodes the to-be-reached side.

I will briefly present the choice-reaching task of Scherbaum et al. (2010) in the following. They conducted a choice-reaching experiment of the Simon effect where a visual guided reach was required. In their study they analysed the trajectories of mouse movements as a whole in order to explore the trial-to-trial influence on the Simon effect. Scherbaum et al. (2010) were able to separate the influences of location and congruency of current and previous trials on the trajectory. With this technique they found an influence of the response in the previous trial early in the trajectory of the current trial as well as an influence of the congruency of the previous trial on a later stage of the reaching process. Their choice-reaching task setup and the measured movement trajectories allowed them to separate those influences which would not have been possible with a standard button press task.

In this section I presented numerous examples of choice-reaching tasks from the literature that demonstrated that those tasks are a useful tool to investigate various cognitive effects. Due to their paradigm and the fact that the whole movement trajectory is recorded otherwise hidden processes can be revealed and give further insight on how the human brain selects target objects and executes reaching movements.

1.4. Neurobiological evidence

My model will utilize a neurologically plausible framework which will be introduced in the following section. In order to discuss the predictions of my model in this area I am going to introduce the recent neurobiological research regarding the reaching process here. Research of brain imaging studies brought further insight about the

human brain and its encoding and processing of reaching movements. Several brain areas were found to be important for the reaching process namely the posterior parietal cortex (PPC), the primary motor cortex (M1, broadmann area 4) and the premotor cortex (PM, 6) (see Kalaska, Scott, Cisek, & Sergio, 1997; for a review). These areas receive sensory input from the parietal occipital visual area (PO) and transform its preprocessed visual information together with further sensory input such as proprioceptive feedback into a motor signal.

The PPC has been suggested as an area responsible for linking sensation and action and plays a major role in goal-directed reaching (Buneo & Andersen, 2006). It consists of many functional subdivisions: amongst others the superior parietal lobule (SPL, 5), the inferior parietal lobule (IPL, 7), intraparietal cortex areas (LIP, MIP, VIP), the parietal reach region (PRR) and the medial dorsal parietal area (MDP). Target representations in different coordinate systems (eye-, head-, shoulder- or hand-centred) were found in many of the sub-areas of the PPC (e.g. SPL, VIP, LIP) (Kalaska et al., 1997; Desmurget & Grafton, 2000). Moreover, this area appears to be the location where movements are planned and prepared. However, it still remains unknown in which coordinate system or space the planning of the movement takes place. Also it remains unclear if the PPC plays a major role for the online control of movements or if this takes place at a later stage in the motor and premotor areas (Buneo & Andersen, 2006).

Areas within the PPC which seem to be important particularly for reaching are the PRR and the MIP. The PRR is suggested to transform visual information into movement plans for reaching (e.g. Scherberger & Andersen, 2007). Also it is assumed that this area represents limb movements in eye-centred coordinates (Andersen & Buneo, 2002). The MIP also seems to be involved into arm reaching as it represents targets in a hand-related space by combining hand and target-related information and is interconnected with the motor areas (Cisek, 2007).

Further areas which are important at later processing stages when a motor signal has to be generated are M1 and PM, however, there are multiple hypotheses about their exact functionality. The premotor areas were found to process a wide range of signals such as proprioceptive, visual and motor command signals. It is assumed that these areas integrate the information about the position of arm and hand (proprioceptive and visual). Furthermore visual stimuli were found to influence PM cell activity as well as motor and attention-orienting instruction. This suggests that the PM areas are involved in the processing of visual, attentional, and motor signals (see Wise, Boussaoud, Johnson, & Caminiti, 1997; for a review). Also the PM often encodes similar potential target related information than the PPC (Cisek, 2007). The motor cortex M1 shows also similar responses and representations of stimulus and target locations, but appears to be involved more in generating movement directions and limb movement signals whereas the PM areas shows more target related responses (see Wise et al., 1997; for a review). Another brain area that could be involved in the goal-directed reaching process is the cerebellum. This area is suggested to be the location of a forward model that can make use of outgoing motor signals and estimate their consequences, i.e., the expected future position of the limb (see Miall & Wolpert, 1996; Desmurget & Grafton, 2000; for reviews). In chapter 6.4 I will come back to neurobiological evidence and will discuss above evidence in the context of the control architecture of my model.

1.5. Neural field theory

The mathematical framework of my model is the dynamic neural field theory (DNFT) of Erlhagen and Schoener (2002) and Erlhagen and Bicho (2006). The model itself will be introduced in chapter 2.3, but in order to gain a better understanding of its modules the qualitative and quantitative assumptions of the DNFT will be presented here.

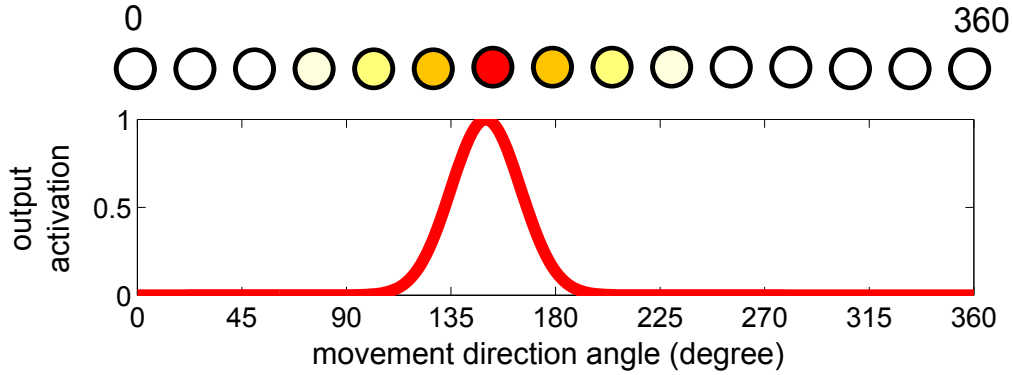

Figure 1.3.: Example of a dynamic neural field. The top graph shows the topological encoding of a movement direction in degrees of heading (0 to 360). The bottom graph illustrates a possible output activation (see also neuron colours in top graph) that could be the result of the neural field dynamics. In this particular case the output activation represents a movement heading of approximately 150° as the neuron corresponding to this direction has the highest output activation.

The DNFT stipulates that the brain topographically represents movement parameters in a neural layer (or field). In such a representation, similar parameter values are encoded in a spatial neighbourhood whereas very different values are represented at locations that are far apart in the neural field. The output activation of the neural field indicates a probability on how likely it is that a particular parameter value influences the movement. Figure 1.3 illustrates this for encoding the direction of movements.

There is biological evidence that parameters are encoded in a similar way in the human or animal brain. For instance there exist motor cortex cells representing the movement direction in monkeys (Bastian, Schoener, & Riehle, 2003) or the head-direction cells in rats (see Taube & Bassett, 2003; for a review). Such cells typically have their *preferred direction* meaning they increase their fire rates when for instance the movement is performed to a certain angle.

Schoener (2008) mathematically described the dynamics of a dynamic neural field (DNF) in a generic form as:

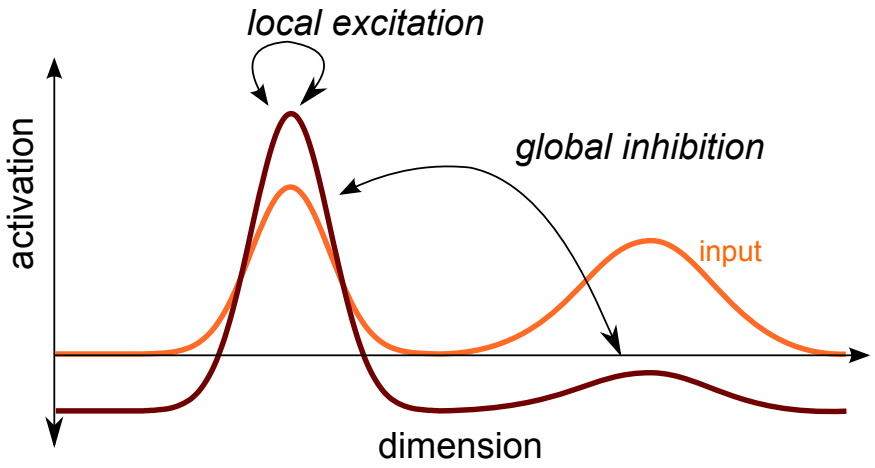

Figure 1.4.: The basic principles of dynamic neural fields (DNFs) are local excitation and global inhibition. While the first process strengthens the input signal (orange) and supports local peaks, the latter one is able to suppress smaller input values such as competing peaks or noise. Hence DNFs are able to select and sustain solutions and filter noise in their field activation (dark red). Figure depicted from Schoener (2008).

$$\tau \dot{u}(\boldsymbol{x}, t) = -u(\boldsymbol{x}, t) + input + resting\ level + interaction \tag{1.1}$$

where $\tau > 0$ defines the time scale, u the internal field activity and $(\boldsymbol{x}, t)$ represents the positions of neurons in the neural field and time respectively. Without the interaction term, which defines the interaction between neurons within the field, the field activation would drift towards its input. However, the interaction can be chosen in a way that the DNF follows the neurologically plausible principles of local excitation and a long range (global) inhibition (see Figure 1.4). These principles base on the fact that cortical cells receive most of their input from cells in their neighbourhood. Such a recurrent structure is able to filter noise and to increase the strength of the input signal (Erlhagen & Bicho, 2006). A mathematical model for DNFs was initially proposed by Amari (1977). While he dealt with a DNF as a continuous field I will discretise the DNF into separate neurons. An arbitrary number of those neurons can form a single DNF. In his model it is assumed that the interaction strength between two points in the field (neurons) only depends on the difference of the values

of their encoded parameter (e.g. the preferred direction). Amari (1977) defines the field dynamics with the following equation:

$$\tau \dot{u}(\boldsymbol{x}, t) = -u(\boldsymbol{x}, t) + s(\boldsymbol{x}, t) + h + \int w(\boldsymbol{x} - \boldsymbol{x}') f\big(u(\boldsymbol{x}', t)\big) dx' \tag{1.2}$$

Hereby, f is a sigmoidal output function (originally a step-function in Amari, 1977), s an external stimulus or input, $h < 0$ the resting level of the field, and $w(x)$ the field's interaction kernel which is defined as follows:

$$w(x) = w_{\text{excite}} \cdot \exp \frac{-(x)^2}{2\sigma_w^2} - w_{\text{inhibit}} \tag{1.3}$$

where w_{excite} defines the strength of excitatory connections and σ_w how far they spread into the neighbourhood of a single neuron within the DNF. w_{inhibit} parametrises the strength of the inhibition between neurons. Erlhagen and Schoener (2002) showed that with DNFs it is possible to model a broad range of empirical findings on movement initiation, e.g. stimulus uncertainty effect, Simon effect, etc.

For the purpose of my model there are three points to note. First, my model employs DNFs for several purposes such as motor control and target selection. Second, a DNF can also encode two-dimensional parameters, e.g. speed in x- and y-direction in planar space, by using a two-dimensional layer. Such two-dimensional DNFs play an important role in my model (more technical details on the implementation of the DNFs can be found in the Appendix). Third, the exact behaviour of the DNF depends on the parameters of the kernel $w(x)$ (see Amari, 1977; for a mathematical analysis). For instance, the kernel can be chosen so that with little or no external input, the DNF drifts towards the resting level h. With a large enough input activation at a certain location (or neuron), the field can establish a single activation peak at this location which can be maintained even after the input is removed. Moreover, if there

are many regions with input activations, a DNF with the appropriate parameter setting chooses the largest region. Although, with an adequate parameter setting the field could also activate multiple regions. Finally and most important for my model, Amari (1977) showed that DNFs can exhibit a "*moving blob*" behaviour. In this type of behaviour an already-established activation peak can move around in a layer in a continuous fashion. The movements of the peak are guided by the gradient of the input activation. The direction of the peak's movement at a specific location is given by the direction of the steepest gradient in the input activation at this location. The speed of the movement is proportional to the steepness of the gradient. The moving blob behaviour will be used in the motor control stage of my model to ensure jerk-free arm movements.

Furthermore it is important to note that the dynamic field theory typically assumes a linear relationship between the spatial representation of a parameter value and the value itself. For instance for the difference of a movement direction of 10 degrees the two corresponding peaks should be 10 neurons apart (in a discretised field, if we assume a spatial resolution of a neuron per degree) at all locations in the dynamic field. In the first experiments it will be demonstrated that the arm movements improve if a non-linear encoding schema for the encoding of the velocity is applied. Such an encoding also is a more natural implementation as in the human brain non-linearities are more common (e.g. the cortical magnification factor of the eye, see also chapter 3.1).

1.6. Cognitive robotics in psychology

I aimed to develop a computational model that accounts for the empirical evidence that has been introduced in the previous sections. The model is connected to a real-world robot arm in order to simulate the human reaching process. Hence, I

will follow a cognitive robotics approach in order to deepen the knowledge about the ongoing cognitive processes during the reaching process. This section gives an introduction to the methodology of this approach.

The cognitive robotics emerged in the last decades with the developments within the field of computations. Hereby, mathematical and computational models for simulations of brain and body parts are developed. With the help of such models experiments and their outcome can be generated to prove or reject theories.

As D'Mello and Franklin (2011) state the cognitive robotics approach differs from the classical (experimental) psychology in some important points. In the classic psychology theories are created or improved with the help of behavioural experiments. Theories can make predictions about the outcomes of experiments. When experiments had an unexpected outcome (e.g. the result was not predicted fully by the existing theory) the existing theory has to be adapted or substituted by a better one. The then (improved) theory makes new predictions that again can be tested in new experiments and so on. These theories are often functional models that in the best case can explain both functionality and psychological processes, however often can not give insight in the underlying cognitive processes.

In contrast, the cognitive robotics follow a slightly different approach: Here models or robots need to be fully integrated from the beginning in order to process all required incoming sensory information and to eventually create an action. Therefore the robot requires an implementation of all underlying mechanisms that are required to solve the desired problem. Moreover, the robot's architecture should be derived from the cognition of humans or animals in order to theorise about the findings and to increase our understanding of the brain (D'Mello & Franklin, 2011). In this fashion cognitive robotics "rebuild" small parts of the brain and with their simulations it is possible to theorise about the cognitive processes that are required to create a human behaviour. The area of my research is the human reaching process. Here perception and action

form a system that produces a complex behaviour as it was demonstrated in chapter 1.3. In order to understand the behavioural evidence of the odd-colour task of Song and Nakayama (2008b) and the other presented reaching experiments often abstract theories are developed. However, due to the complexity of the underlying mechanisms of the reaching process a cognitive robotics approach seems to be appropriate to extend the knowledge in this area. Moreover, with the framework of the neural field theory which I am going to utilise I will be able to implement cognitive processes such as target selection and movement control in a neurological plausible way. Hence, the cognitive robotics approach offers advantages over abstract or purely mathematical models.

There already exist plenty of cognitive robotics models to investigate different aspects of human or animal cognition. Examples for this are Webb (2009) with her cricket robot and Ziemke (2011). My research follows the animat approach of Webb (2009). An animat is a simulated animal or animal-like robot whose sensors, actuators and control architecture are as closely inspired by those of animals as possible. Webb (2009) distinguishes between simulations of robot and environment and real-world robots. In a simulation, the environment and the animal are simulated virtually, while a real-world robot can be used to directly observe its behaviour. However, Webb (2009) suggested that there is no significant difference between these two approaches, if the mechanics of the robot do not limit the feasibility (e.g. flying).

As there are no such engineering limitations for the human reaching process, I will utilise a real world robotic arm. This has several advantages in comparison with a pure virtual simulation: Experiments can possibly be performed by the robot analogously to reaching experiments with humans. This will be the case for numerous experiments in the chapters 3 to 5 where I apply often existing paradigms to simulate experiments with my model. One more advantage of real world simulations is that they must be able to cope with with challenges that do not exist in purely computational simulations

(e.g. handling of different kinds of noise) and therefore reduce the gap between human and simulated experiment. Furthermore real world robots must implement cognition itself and are not able to deal with only isolated facets of cognition (Morse, Herrera, Clowes, Montebelli, & Ziemke, 2011).

Due to above facts cognitive robotics complements the classical psychology as it is able to "participate or replicate a psychological experiment" (D'Mello & Franklin, 2011). Furthermore, cognitive robotics broadens our knowledge of theories of cognition as it can show gaps, assumptions of parameter values and improves details of the theories (see Morse et al., 2011). In the following chapters I will demonstrate how the different versions of my model can contribute to the existing theories of the human reaching process. Hence, in my opinion a cognitive robotics approach is a useful tool to extend the knowledge in the area of the human reaching process.

1.7. Contribution of this thesis

This section is thought to give a summary of the contribution of this thesis to the existing literature. As mentioned before in the following chapters I am going to present a model that simulates a complete perception-action cycle for the human reaching process. My control architecture includes an implementation of all necessary subprocesses (e.g. image processing, inverse kinematics), however, my model focuses on how the human brain plans and executes movements. Moreover, with the dynamic field theory my model possesses a neurological plausible structure and encodes movement parameter which also have been suggested to be encoded in the brain such as location of arm and target and the hand's speed.

In order to simulate various experiments of the choice-reaching and goal-directed reaching tasks I present different versions of my model that account for the task specific requirements. The simulations of the choice reaching tasks show that my

model can simulate and explain human behaviour in those tasks. For some of the simulated experiments to my knowledge my model is the first attempt to simulate their outcome (e.g. the odd-colour task of Song & Nakayama, 2008b). For some of the experiments models and simulations exist already (e.g. the Simon effect), however, the successful simulations of my model demonstrate that the general structure of my model is able to simulate a broad range of different tasks.

For the simulations I make use of different mechanisms such as priming maps and thresholds between different neural layers in order to explain various results. Also I show how the use of non-linear encoding structures (similar to the cortical magnification factor in the eye) in the velocity map can improve the velocity profile of the movement substantially. Hence my model helps to understand experimental results and complicated relationships of various measures.

A novelty within my model is the "moving blob" a permanent activation within a neural field that is able to move smoothly within the neural layer and encodes direction and amplitude of the hand's speed. With this mechanism it is possible to generate jerk-free movements and it enables the robot's endeffector to move in a human-like fashion with a bell-shaped velocity profile. Moreover, the goal-directed reaching model of chapter 5 extends the functionality of the moving blob. The model there can be interpreted as a concrete implementation of an internal model that makes usage of all available information at a point in time to generate a movement under the constraints of a visual delay (see also Miall & Wolpert, 1996).

Finally, my model utilises a single feedback-based mechanism in order to explain the human reaching behaviour. Hence with its closed-loop architecture it also offers a more natural single-process explanation for the long time accepted view of a strictly separated planning and online-control phase like in Meyer et al.'s (1988) model.

1.8. Organisation of the thesis

In this section I am going to conclude the introduction and give an overview of the structure of this PhD. Until here I gave a review of the most important relevant background regarding the human reaching process, the choice-reaching tasks and the frameworks that I will apply to develop my model. The next chapter will present more details of the existing knowledge of the human reaching process and the theoretical assumptions of my computational model to the choice-reaching tasks. Also, there I will give a detailed explanation of the inner working of my computational model. Subsequently chapter 3 presents simulations of several choice-reaching tasks with my model. The model and the simulations of chapter 3 have already been published in Strauss and Heinke (2012). Chapter 4 presents further choice-reaching experiments that required modifications of the original model. Here one of the experiments (the odd-colour irrelevant feature experiment of chapter 4.1) will be published soon in Strauss, Woodgate, and Heinke (2013) (in preparation). Chapter 5 focuses on goal-directed reaching and introduces a modified model which differs in some aspects from the choice-reaching model to prepare it for the simulations of the goal-directed reaching experiments. The main parts of this chapter also will be published shortly (Strauss & Heinke, 2013; in preparation). Finally, the results of all experiments will be summarised and discussed in the final chapter which contains the general discussion. Detailed descriptions of the mathematical details and the parameters of the model can be found in the Appendix.

2. Modeling Choice Reaching Tasks

In this chapter I present the empirical background, theoretical assumptions and the control architecture of my model for simulating the choice-reaching tasks. The model was developed to simulate the odd-colour task of Song and Nakayama (2008b) in a human-like fashion. Hence, the first part of this chapter deals with the existing models and empirical evidence regarding the human reaching process. Subsequently, I will summarise this evidence before presenting in detail my hardware setup with the real world robot arm and the control architecture of my model with its modules. Note that the model has been published in Strauss and Heinke (2012) where we also simulated the choice-reaching tasks of chapter 3.

2.1. Human reaching: existing models and evidence

2.1.1. Planning and online-control

In this section I am going to describe the underlying processes of the reaching process. A reach for an object obviously requires at least two processes: First some sort of *planning* has to take place before the *execution* of the movement can be initiated. However, it is less clear what exactly the two processes entail. On a high level, planning can be described as a process where a target object is selected and the trajectory of the movement is planned. Furthermore, it can involve the selection of an

appropriate movement plan and the timing of movements as well as the determination of acceleration and velocity parameters (Glover, 2004) but also the magnitude and timing of muscular forces on a lower level (Elliott et al., 2010). Such a movement plan can also be influenced by past experience so that even function or fragility of the object can play a role (so called non-spatial characteristics; see Glover, 2004). However, I want to focus on what Glover defined as spatial characteristics such as location and size.

To our knowledge it is not yet known in what space and on which level of representation the planning process takes place. Whether planning only involves the hand or includes the whole limb, whether only future hand positions or also velocity values are planned and whether this also involves the timing of muscular forces remains unknown. However, there is evidence that an integration of a broad range of different information takes place (Glover, 2004; Desmurget, Pelisson, Rossetti, & Prablanc, 1998).

Only when the planning process has terminated the reaching itself can be executed. The most important process that influences the execution of the movement is *online-control*. Online-control assumes that humans make use of a closed-loop of sensory feedback where incoming information is processed to adapt an ongoing movement. In order to deal with motor noise or unexpected changes in the environment online-control can be necessary, thus, it can explain perturbation experiments where hand or target position changes during the reach. When no visual information is available during the reaching process, the error rate typically increases while the accuracy decreases (Elliott et al., 2001; for a review) which suggests that an online-control component that makes use of visual feedback is important for the reaching process.

An important factor for online-control is the fact that humans have a "visual delay" to react towards changes in the environment. This delay is caused by the fact that it takes time to process the incoming visual information by the brain and to generate

an appropriate response by the muscles. There is experimental evidence that visual feedback can be used in a time as short as 110-260 ms (see Elliott et al., 2010; for a review). This time is needed to process the visual information, to update the movement plan and to change the movement of the arm. For this reason some time is needed to adapt an ongoing movement after a perturbation occurred. For very fast movements there even might be insufficient time to react on such a perturbation.

2.1.2. Existing models

As already mentioned in chapter 1.2 there have been three general approaches to explain goal-directed reaching: closed-loop (e.g. Adams, 1971; Hoff & Arbib, 1993), open-loop (e.g. Plamondon & Alimi, 1997) and a mixture of the two (e.g. Glover, 2004). In the following I present these approaches in more detail, explain how they apply the principles of planning and online-control, and discuss their advantages and disadvantages. An overview of the principles can also be found in Figure 2.1.

Open-loop models

In the open-loop approach the reaching process is planned as a whole before its execution. Visual feedback is not used, hence, online-control does not play a role in this approach.

Examples for open-loop models are the *minimum commanded torque change model* (Nakano et al., 1999) which follows the *minimum-jerk models* of trajectory planning (see Desmurget et al., 1998; for a review). In these models the trajectory is pre-planned by minimising a movement parameter such as the torque change of the limb or the angle jerk of the endeffector. These models investigate different strategies on how reaching trajectories are generated and in which space the movement is planned rather than simulating behavioural phenomena such as the introduced experiments or

the goal-directed reaching process with effects such as the speed-accuracy trade-off observed in Fitts' law with a real-world robot.

A model that attempts to explain the latter is the *delta-lambda model* of Plamondon and Alimi (1997). They developed an physiological plausible open-loop model based on a kinematic theory with antagonist muscles. Their model simulates very well velocity profiles and the experimental results of the Fitts' law task, however lacks explanations how it deals with motor noise and perturbations.

An open-loop model that uses neural implementations is the *vector-integration-to-endpoint* (VITE) model of Bullock and Grossberg (1988). This model plans hand movements by comparing the positions of hand and target; the movement then emerges through interactions in the underlying neural network. In its simplest form the model can be described with two differential equations to control the speed and the direction of the movement. The VITE model can be interpreted as a dynamical system with attractor points which has similarities to the dynamic neural field framework of my model (see also chapter 1.5). It is able to simulate straight reaches towards a target while generating a bell-shaped velocity profile. Moreover, the VITE model can explain a wide variety of behavioral and neural data and similar to the delta-lambda model it is able to explain the movement times in a Fitts' law task. A more recent variation of the VITE model by Petreska and Billard (2009) has been utilized to model three-dimensional curved trajectories.

Generally, models based on the open-loop approach have problems to explain some characteristics of the reaching process. Due to the lack of a visual feedback loop, reactions towards perturbations are only possible by introducing special mechanisms that adapt the existing movement plan. Hence the open-loop approach is not parsimonious in explaining the reaching process. Furthermore this approach cannot explain recent evidence for early online-control mechanisms by Elliott et al. (2010) which will be introduced later.

Hybrid models

Hybrid models apply both principles of goal-directed reaching - open-loop and close-loop. The most important type within these models are the two-component models. This type of models goes back more than 100 years to the pioneering work of Woodworth (1899). In two component models the reaching process is divided into two distinguished components: The first component is a pre-planned initial impulse phase in which a ballistic movement is performed in order to transport the limb in the vicinity of the target. The initial impulse is executed in an open-loop fashion and therefore requires a planning process before the movement can be initiated. Due to noise and variations after the initiation of the movement the movement plan of the first component will most likely not be executed without errors. Thus, a second component - the control phase - can be necessary to correct the initial movement with the help of visual feedback. In this phase the hand position is compared with the target position and the reaching is adapted appropriately in order to eventually land on the target. The homing of the second phase occurs if time permits and if the accuracy constraints make it necessary (see Elliott et al., 2001; for a recent review). Since Woodworth's (1899) publication, numerous variations and extensions of the two-component model were suggested to account for the newer empirical evidence of Fitts and other researchers like the model of Meyer et al. (1988) which was mentioned earlier in chapter 1.2.

The *planning-control model* of Glover (2004) is the most recent variation of the two-component models. Glover reviews evidence from behavioural and brain imaging studies to develop his model. He investigates the role of planning and control in the reaching process and postulates that planning and (online-)control are two separate processes that serve different purposes. Moreover, they are physically separated as they are located in different brain areas. In fact his model is the first to postulate

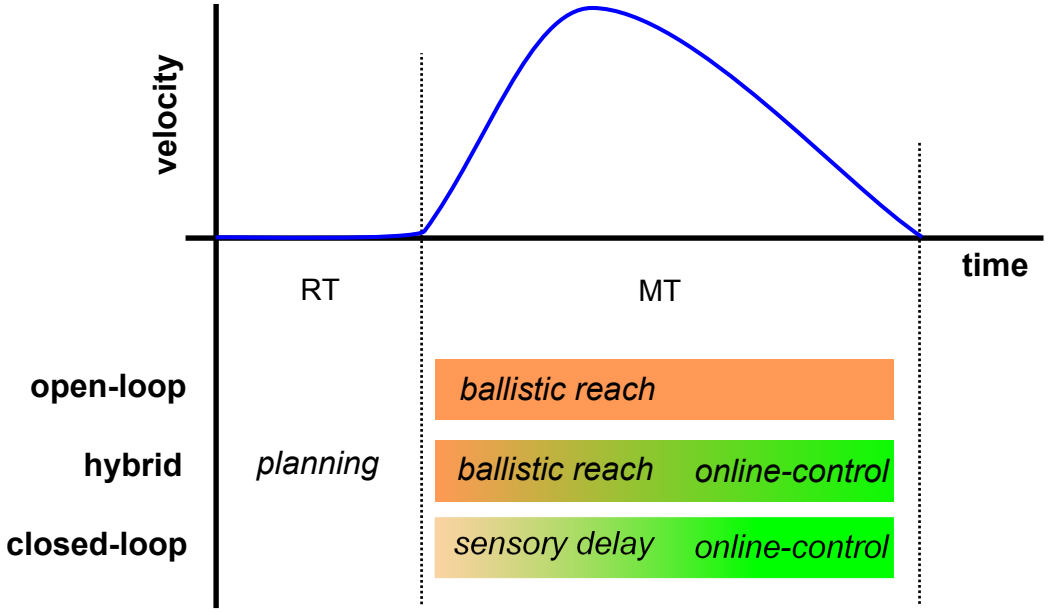

Figure 2.1.: Typical velocity profile of a human reach with common measures: The Initial Latency or Reaction Time (RT) is the time between trial onset and movement initiation. The Movement Time (MT) consists of an acceleration phase and a deceleration phase. The peak velocity is typically reached at around 40% of the movement. Under the velocity profiles the principles of the main types of goal-directed reaching models are shown. While all three types require some sort of planning their interpretation of the reaching movement is very different. For details see the surrounding text.

separate visual representations for the both processes. According to Glover's model planning is a slow and complex process prior to the movement which selects the initial kinematic parameters of the movement while control is only active during the movement execution and is a fast and flexible process with the aim to minimise the spatial error between hand and target. The control process also includes feedback loops of proprioceptive feedback and the use of efference copies (internal copies of the movement plan) to increase its efficiency. Furthermore he suggests that planning is influenced by a large array of available information about the target whereas control only utilizes spatial characteristics of the target including size, shape and position. Glover's model predicts that the speed-accuracy trade-off which can be observed in a Fitts' law task results solely from the planning processes that go on before

the movement. Moreover, the model suggests that perturbations of spatial target properties such as location or size can be detected quickly with the control process. Generally, the two-component models include both processes, planning and online-control, that are involved in the goal-directed reaching process to a significant extend. The first component involves a planning process similar to the open-loop approach and causes the initiation of a ballistic movement towards the target object in the first half of the reach. In contrast, the second component applies the principle of online-control and guides the hand to the target in the second half of the movement. Hence, perturbation experiments where target location or size changes can be easily explained as the online-control component is able to detect changing target properties quickly.

However, human reaching movements are normally smooth and they are able to switch seamlessly between different targets. This fact supports the view of a single underlying mechanism and such a strict separation into two sharply distinguished components does not seem parsimonious. Furthermore, similar to the open-loop models the traditional two-component models cannot explain the new evidence that even in early stages of the movement (which belong to the first phase of the two-component models) online-control can be observed. Thus, new mechanisms as extensions are necessary to explain those findings (Elliott et al., 2010).

Closed-loop models

In contrast to the mentioned open-loop and two-component models, the closed-loop approach mainly applies the principle of online-control to execute the movement. Typically, an error signal is continuously decreased until the target is reached. In an early work Adams (1971) developed a motor learning strategy based on this approach. Hoff and Arbib (1993) presented a control theory based model that works in a feedback-based manner and generates movements by minimising the jerk of the trajectory.

Their model yields good results for reach and grasp perturbation experiments but does not account for different target sizes or the properties of the neural substrate. Another example is the computational model of Flanagan, Ostry, and Feldman (1993) which they developed around their physiological plausible equilibrium-point hypothesis. This hypothesis works well for single joint movements, however, it has been challenged by newer empirical findings in multi-joint movements (see Desmurget et al., 1998; for a review).

For my model I will also follow the closed-loop approach. Thus, there is no need for an extensive pre-planning. The reaching process is executed simply by updating movement parameters such as movement direction and speed throughout the whole movement. Although the visual delay is a constraint of this approach, it has been shown previously that the brain can deal with the delay by using efferent copies and forward models (e.g. Miall & Wolpert, 1996; Elliott et al., 2010).

My approach to model the reaching process is inspired by Elliott et al. (2010), however my interpretation of their recent findings differs from their explanations. They found evidence for a very early utilisation of online-control in experiments with different kinds of perturbations. For instance Grierson and Elliott (2009) investigated the effect of a moving background on mouse pointer movements. This perturbation caused a misperception of the velocity of the cursor and more interestingly also influenced the very early stages of the movement which are part of the ballistic phase in the two-component models. It could be shown that at least three distinguished and independent online-control mechanisms influence the reaching process in very early stages of the movement (Elliott et al., 2010; for a review). Besides the visual online-control, where the limb position is compared with the target position like the second phase of the two-component model, there is evidence for an early efferent control mechanism where a copy of the current movement plan is compared with the outflowing signals. The third mechanism is an early afferent control where the

expected visual and proprioceptive sensory consequences are compared with the actual feedback. While this mechanism is slower than the mentioned efferent control, both, efferent and afferent control, are faster than the standard visual delay discussed earlier which enables corrections in very early stages of the movement. Thus, it is possible to adapt an ongoing movement with very little delay.

This evidence suggests that the early stage of a movement is more online-controlled as previously thought. While Elliott and colleagues developed their *multiple process model* around the introduced two-component model and extended it by an *impulse control* component which is thought to influence the ballistic phase of the two-component model, I want to simulate the goal-directed reaching with a single online feedback-constrained process without strictly separated planning and control phase. The closed-loop approach offers some more advantages: By applying the online-control principle for the whole trajectory it is not necessary to determine and store extensive movement plans before the movement is initiated. My model simply makes use of all available information at one point in time to generate a movement vector. This is done during the whole reaching process until the target object is reached. Summarising above facts I postulate that applying the principle of the closed-loop approach by using visual feedback loops seems to be a natural way to implement a goal-directed reaching process, to deal with unexpected events and to simulate the choice-reaching tasks.

2.1.3. Distractor influence on the reaching process

In chapter 1.3 I have reviewed various choice-reaching experiments and their findings in the area of visual attention. One common feature of those tasks is that whenever a target object is presented with distractors they interfere in the target selection process and can alter measures such as the reaction time or the movement trajectory.

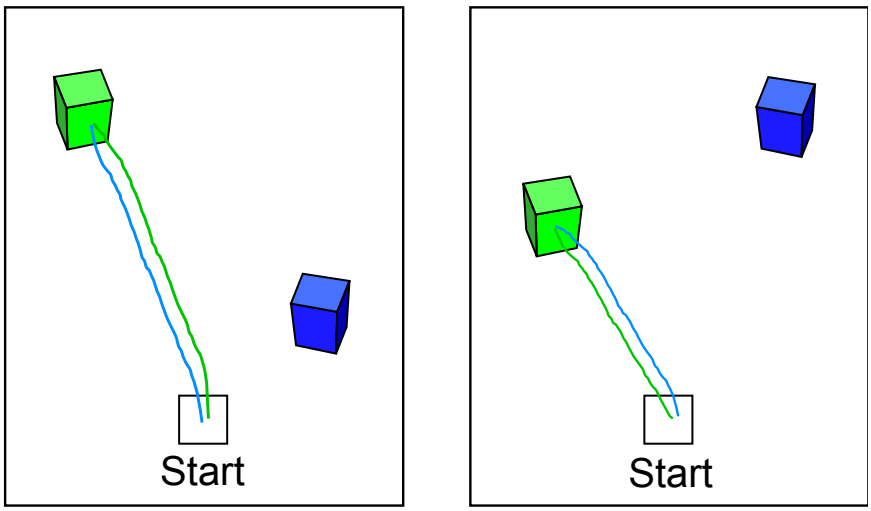

Figure 2.2.: The influence of distractor objects on the reaching path in the experiments of Tipper et al. (1997). In the illustration the green cube is the target while the blue cube is the distractor (in the experiment the target colour was chosen randomly). The green line is the mean trajectory of reaching for the green target cube without the blue distractor cube, while the blue line were the resulting mean trajectory with a present distractor. According to Tipper et al. (1997) close distractors have a repulsion and far distractors have an attraction effect.

In this section I am going to present more behavioural evidence for such distractor interference effects.

Already before the recent choice-reaching experiments (e.g. Song & Nakayama, 2008b) the influence of distractor objects on visual attention and reaching was thoroughly investigated. In fact, when placed in a natural environment a target object usually is surrounded by multiple distractors (non-target) objects. In order to reach successfully, the target needs to be attended and identified whereas distractors have to be ignored. Finally, the movement has to be planned to interact with the selected target object. There is plenty of experimental evidence of visual guided reaching tasks of the last decades that distractor objects significantly interfere in ongoing movements toward targets. Depending on the exact experimental conditions the distractors (non-targets) were found to have a repulsion effect (Howard & Tipper, 1997), an attraction effect (Welsh, Elliot, & Weeks, 1999) or both (Tipper, Howard, & Houghton, 1998; Tipper

et al., 1997) on the reaching trajectory. The relevant literature regarding these effects will be reviewed in a greater detail in the following.

The first evidence I present is the study of Tipper et al. (1997). They found evidence for distractor influence in a choice-reaching experiment. Participants had to reach towards arbitrarily coloured wooden cubes under the presence of different coloured distractor objects (see Figure 2.2). The distractor objects were found to influence the reaching path, however, the effects strongly depended on the position of target and distractor. For near targets and far distractors an attraction effect by the distractor was observed, while for far targets and near distractors the opposite effect (repulsion) was found.

In another reaching experiment with red coloured LED target lights and yellow distractor LEDs, Tipper et al. (1998) found that reaches to near objects (in relation to the hand's position) were initiated faster than to far objects. The reaching process was also significantly slower with distractors close to the hand's position.

To explain the effects, Tipper et al. (1997) suggested the *response vector hypothesis*. This hypothesis suggests that the spatial information about the distractor location is represented in a hand-centred coordinate system and objects close to the hand's position cause a greater activation and hence a stronger respond. Moreover both, target and distractors induce a neural activation. In an early stage of the target selection these activations are combined which explains attraction effects, while after some time an inhibition of the distractor is added. This model could sucessfully explain the experimental outcome e.g. the close distractors of the experiment of Tipper et al. (1998) have a greater effect of interference on the hand's movement than the far distractors which results in slower movement times.

More experimental evidence for the influence of distractors came from Welsh et al. (1999) and Welsh and Elliot (2004). They performed reaching experiments and found no distractor influence in the reaction times. In their reaching experiment

the movement trajectories deviated towards distractors when target and distractors become visible at the same time. In different conditions the distractor appeared before the target stimulus was visible (from 250 ms up to 750 ms). Only in the latter case (750 ms) the effects of the experiment of Tipper et al. (1998) were replicated as here the target-oriented trajectories deviated away from the distractor.

Welsh and Elliot (2004) explained their results of the 750 ms condition with the temporal delay of the inhibitory effect of the distractor. The inhibition is already active by the time the target stimulus appears. For the other conditions where the trajectory deviated towards the distractors they suggested that a dual-response activation mechanism is responsible. Thus both stimuli - target and distractor - are programmed in parallel and for both possible trajectories are prepared, which results in a combined vector. Later during the movement a rapid online adjustment takes place and the internal race between the two movement responses for activation is decided for the target. However, if there is enough time to complete the inhibitory process for the distractor as in the last experiment the trajectory veers away from it similar to the response-vector hypothesis of Tipper et al. (1997). Welsh et al. (1999) suggested that the difference to the results of Tipper et al. (1997) in the conditions with no or little delay between distractor and the target onset are caused by the design of the experiment. Tipper et al. (1997) used physical objects as target and distractor which could have influenced the movement in some way. So the repulsion effect of close distractors (see Figure 2.2) could be a result of a possible obstacle avoidance mechanism. Welsh et al. (1999) followed from their results, that distractors always have an attraction effect, if they are not a potential physical barrier or could cause a collision with the hand.

Summarised it can be said that distractors influence the target selection process. This fact also was confirmed by the already introduced choice-reaching tasks of chapter 1.3. Due to their design these tasks can make the target selection process and the

competition of target and distractor object visible in the movement trajectory. Hence, I will follow their paradigm to investigate the distractor influence on visual attention with my model in the experiments.

2.2. Summary of the empirical evidence of the human reaching process

The purpose of this section is to summarise the empirical evidence of goal-directed reaching and choice-reaching tasks introduced in the first chapter and in the previous sections. The model I present in the following section will base on these theoretical assumptions in order to simulate the human reaching process. The following findings can be considered as commonly accepted:

- The outcome of the choice-reaching tasks (e.g. Song & Nakayama, 2008b; see chapter 1.3) suggests that responses to target and distractor are prepared in parallel and that the final decision of the target location can be made after the movement initiation. This is a strong evidence that the movement planning and control operates in parallel to attentional cognitive processes, such as target selection and distractor inhibition. Visual information can influence both sub-processes in any time of the movement.

- Distractors influence the reaching path. While trajectories can deviate from them in some cases, distractors can have an attraction effect when they are considered as possible targets in particular. Moreover, a spatial averaging effect can be observed when there is not sufficient time to inhibit distractor objects. Thus, the movement can be initiated towards a location in between target and distractor (e.g., Chapman et al., 2010a).

- Besides the influence on the trajectory competing distractors also can influence traditional measures such as the reaction time and the movement time (Song & Nakayama, 2008b) .

For the human reaching process in general the evidence from goal-directed reaching experiments can be summarised as follows:

- Goal-directed reaching movements of humans are typically straight with a bell-shaped velocity profile (e.g. Jeannerod, 1984).
- When visual information is provided during the whole reaching movement the accuracy increases and the movement can be adapted to a changing environment. However, humans have a visual-delay which is needed to update an ongoing movement (Elliott et al., 2010; for a review).
- Characteristics of the cognitive processes are reflected in the reach trajectories. In other words, a dynamic systems approach in which the various processing stages operate in parallel and interactive with each other seems an appropriate approach.

2.3. The choice reaching model

This section presents the model that I developed to simulate various choice-reaching tasks. The model was originally designed to simulate the odd-colour task of Song and Nakayama (2008b), however, later extended to cover a broader range of choice-reaching tasks. First, the hardware setup will be introduced. Subsequently, the control architecture of the model with its modules will be presented. Note that this section gives little details on the mathematics of the model. Instead we will focus on a qualitative explanation of the inner working. The mathematical details of the model

can be found in the Appendix in chapter A.1.

As mentioned before in order to mimic visually guided movements, I embedded my model in a closed-loop control of a robot arm. Finally to link the selection process with the control of the robot arm I integrated the dynamic field theory by Erlhagen and Schoener (2002) into my modelling approach. The dynamic field theory assumes that movement parameters are topologically represented in the brain and was introduced in chapter 1.5. In fact, for the sake of simplicity, my model implements the competition processes in both stages, the attention stage and the motor control stage, with the mathematical formalism used in the dynamic field theory.

2.3.1. Setup

Figure 2.3 shows the experimental setup. As the main effects of the targeted experiments occurred in a horizontal plane I used a planar robot arm with two joints. The robot arm was built with the LEGO Mindstorms NXT kit and the LEGO Education set. The sensors, motors and the programmable brick of these kits offer a flexible and inexpensive way to design programmable robots. I tested several robot designs inspired by Bagnall (2007) and eventually settled for the construction shown in the photos in Figure 2.3. The configuration is mechanically very stable and the joints have only a little slack. The total length of the arm is approximately 36 cm (forearm 19 cm, upper arm 17 cm). I use the Java leJoS API (Bagnall, 2007) to interface with the programmable brick.

The robot arm and its environment is filmed with the Bumblebee XB3 stereo camera (using only one camera) from a birds-eye view (see top right corner in Fig. 2.3a). The distance between camera and table is 90 cm. The photo also shows that we used a normal desk light (gray object next to the camera) to keep the lighting roughly constant. For an easier detection of the robot arm blue markers are attached to the

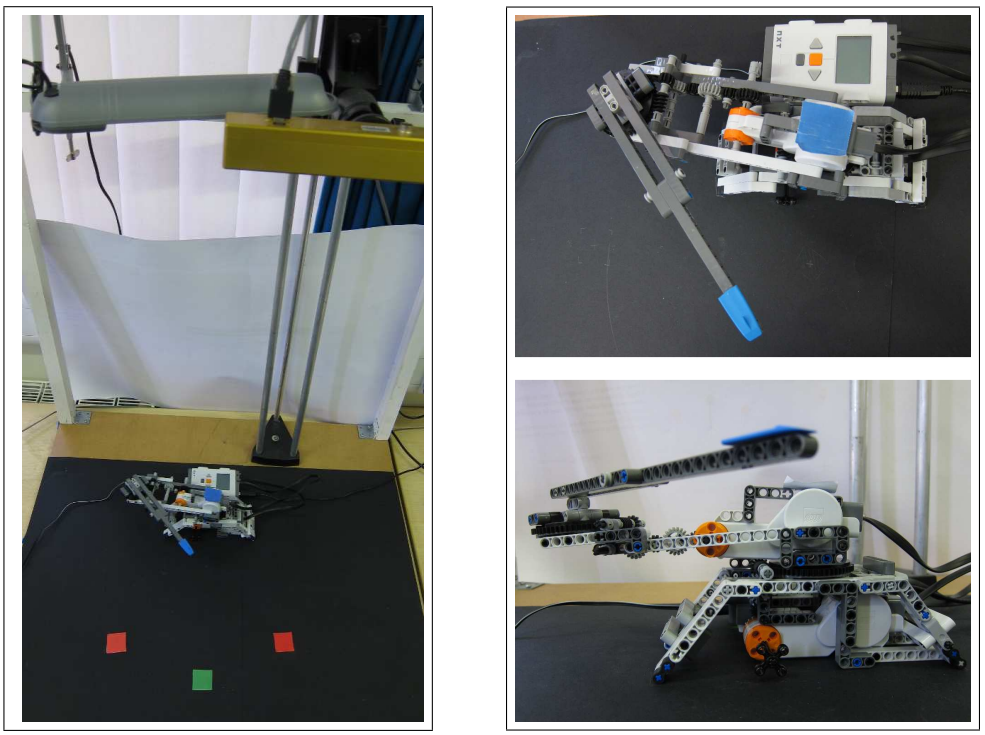

(a) (b)

Figure 2.3.: (a) Lego Mindstorms NXT robot arm with the environment consisting of camera (the golden object, top right), lamps (grey object, top left) and the experimental setup (here the odd-colour task). (b) Details of robot arm with the motors (orange/white), the attached blue markers, and the programmable brick (top picture, above the arm).

arm base and to the end effector. For the search items red and green coloured markers are used (see bottom of the photo in Fig. 2.3a).

2.3.2. The control architecture

Overview

The model is designed to be able to simulate choice-reaching tasks. Therefore, the correct target object of those tasks must be determined and the robot arm must be able to perform human-like movements towards those targets.

Figure 2.4 gives an overview of the control architecture. The input to the control architecture are the images from the Bumblebee camera. The outputs set the speed

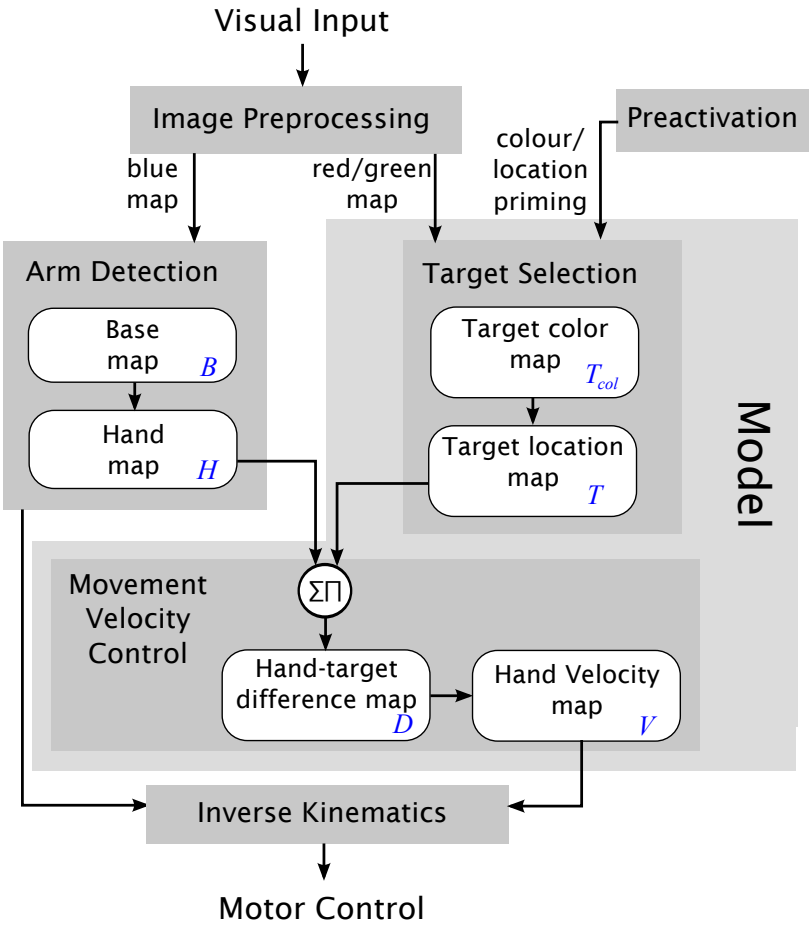

Figure 2.4.: Overview of the control architecture. The light grey box contains the model. Dark grey boxes are the modules of the model. White boxes symbolize Dynamic Neural Fields (DNFs) and the arrows show the flow of information. In the text the blue abbreviations are used for the respective DNFs.

values of the robot arm joints. In the control architecture cartesian speed values are updated continually based on the input images so that the robot arm is controlled in a feedback-based closed-loop fashion. Finally the angle speed values are calculated with a transfer function. The control architecture is made up of five modules. The module *Image Preprocessing* detects the blue, red and green markers in the camera images. The *Arm Detection* determines the location of the arm's end effector by using the blue markers. The *Target Selection* finds the odd-colour marker. The *Movement Velocity Control* combines the location of the end effector with the target location

and determines the speed and direction of the movement for the arm in cartesian coordinates. These movement parameters are then converted into the speed of the robot arm joints in the *Inverse Kinematics* module.

It is important to note that the modules fall into two categories. The first type of modules (Image Preprocessing, Arm Detection and Inverse Kinematics) implement technical solutions which were necessary for successfully controlling the robot's behaviour. However I do not claim that the implementations of these modules model human behaviour. Moreover, these modules are not crucial for the implementation of the theory I fleshed out in the previous section nor for modeling the experimental data of choice-reaching tasks. The second type of modules (Target Selection and Movement Velocity Control) constitutes "the model" implementing the theoretical assumptions explained earlier. These assumptions are: The processes in the target selection stage and the motor control stage use competitive and excitatory interactions between neurons. These are implemented with Dynamic Neural Fields (DNFs). Both stages, the motor stage and the selection stage, operate in parallel. In fact, all modules operate in parallel but this is not of theoretical significance. In the following sections I explain the functionality of all modules of the control architecture in a greater detail.

Image Preprocessing

The Image Preprocessing detects the three markers, blue, red and green (see Figure 2.3) in the camera images and encodes their location in the respective colour maps: the blue map, the red map, and the green map. This is achieved by first transforming the camera image from the RGB colour space to the HSV colour space. In the next step the Hue (H-dimension) is used to detect the markers' colour. Note that the usage of Hue improves the robustness of the control architecture against changing lighting conditions. The detection is illustrated in Figure 2.5 and is implemented by testing each pixel if it falls into an interval around a pre-set H value. If this is true,

(a) (b)

Figure 2.5.: Illustration of the functionality of the Image Preprocessing module. From the camera image (a) three colour maps are generated to detect the location of the robot (blue colour, b) and the objects (red and green colour, not shown). Note that the detection of the arm is facilitated by using two blue markers of different sizes for base and endpoint.

the colour map is set to one at the corresponding location. The pre-set H value takes on a different value, a "blue"-, "green"- or "red"-value, for the different colour maps. But if the pixels have an extreme saturation or brightness the activation is set to zero in order to avoid the detection of white or black areas. Finally, an erosion filter is applied to the maps to decrease the likelihood of isolated pixels by removing artefacts like undesired reflections (Jähne, 2008).

Arm detection

The detection of the robot arm encodes the locations of the arm's base and the end effector (hand) in two separate DNFs. It exploits the fact that the marker on the base is slightly larger than the one on the end effector (see Figure 2.5). So the first DNF (base map) receives the blue colour map as input and selects the larger marker, as the DNF's parameters ensure that an activation peak is only formed at the larger region. The output of the base map is topologically subtracted from the blue colour map. The subtraction leaves activation at the location of the end effector but removes activation

at the arm's base. Subsequently a second DNF (hand map) detects the location of the end effector with this combined map as input. The parameters of the end effector map are set so that the output peak follows the movements of the end effector with only a slight delay. The delay is caused by the neural field dynamics which need some time to adapt to a changed input (depending on their time parameter τ). However, the delay in the hand map was insignificant in relation to the movement time of the arm.

Note that the arm detection implements a technical solution for the simple fact that humans need to keep track of the arm position. Hereby the base location is needed to have a reference point for the hand. Alternatively or in addition we could have used proprioceptive information (joint angles). However, how humans determine the arm position is not relevant to the current research question. Therefore I simply used the camera images as they were necessary for the central research question anyway.

Target selection

This module is designed to detect the target objects of the choice-reaching tasks. For the tasks simulated in this thesis two characteristics are important to determine the target: colour and location. Hence, the module consists of two DNFs, encoding target colour (T_{col} map) and target location (T map).

In the following the Target Selection module will be described for the odd-colour task of Song and Nakayama (2008b) to begin with. In this task the odd-coloured object must be detected amongst three objects. The T_{col} map uses two neurons representing the two possible object colours, red and green. As input, the T_{col} map receives the total activations (sums) of the red colour map and the green colour map. The DNF parameters of the T_{col} map ensure that the neuron with the higher input is activated while the other neuron is deactivated. Consequently the T_{col} map establishes a high activation in the neuron representing the more frequent colour which is equivalent

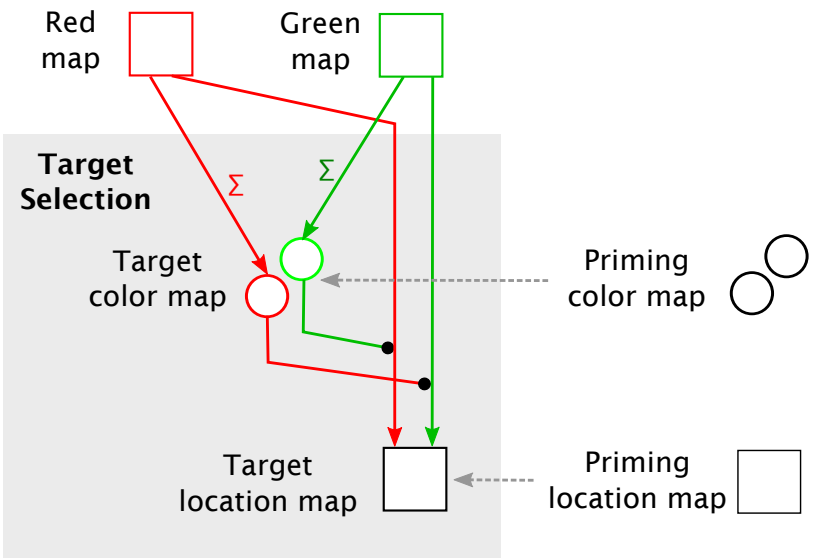

Figure 2.6.: Illustration of the functionality of the Target Selection module. The module consists of two DNFs: the target colour map and the target location map. The added activations of the red and green colour maps are the input for the target colour map. The colour maps also feed directly into the target location map. The weights of these inputs are influenced by the activation of the neurons of the target colour map. In this way it is assured that the odd-coloured object is selected. Note that priming maps can influence the activations in both DNFs.

with the non-target colour (see also Figure 2.6).

The T map is a two-dimensional DNF representing the target location from a birds-eye view. The input to the T map is the topologically added activation from the green and the red colour map. The summation is weighted by the output of the T_{col} map whereby the colours are swapped to implement the odd-one detection. Thus, the T map eventually will establish an activation at the location of the odd-coloured object. The Target Selection module will be modified for the simulation of different choice-reaching tasks in chapter 4. These modifications will be explained in the appropriate sections there.

Preactivation

Priming effects play a big role in choice-reaching tasks. Hence, all DNFs in the Target Selection module can receive a priming activation (see Figure 2.6). When the simulation requires a colour priming effect, the T_{col} map in the Target Selection module can receive an external input that activates the maps before the robot arm starts moving. After the movement initiation of the robot arm this external input is switched off and the map receives the normal colour input as described in the Target Selection module. Nevertheless, the external input preactivates the T_{col} map thereby influencing the early phase of the reaching process. Hence the preactivation can potentially decrease the initial latency as found in Song and Nakayama (2008b). In addition I also implemented preactivation for the T map as there is also evidence for spatial priming from standard visual search tasks (e.g. Maljkovic & Nakayama, 1996). The priming in the T map works in a similar way.

Movement Velocity Control

The aim of this module is not only to generate arm movements towards the selected target item, but also to achieve this with in a human-like manner with a straight path and a bell-shaped velocity profile. These aims are achieved with two DNFs. The first DNF (D map) represents the target in end-effector-centred (hand-centered) coordinates. This representation is generated through a spatial correlation between the birds-eye target information of the T map of the Target Selection module and the hand map which is the output of the Arm Detection module. The spatial correlation is performed in a way that the origin of the effector-centred coordinates are in the centre of the D map. This spatial correlation is implemented in a neurologically plausible way using sigma-pi units. Sigma-pi units were first proposed by McClelland, Rumelhart, and Hinton (1986) (see Heinke & Humphreys, 2003; for another example

of an application). Now with the hand-centred coordinates the D map can encode how far the arm is from the target and what direction the movement should take. Therefore the D map could successfully direct the robot arm to the target (with the Inverse Kinematics module).

However, if the D map was directly used to encode the arm's velocity the movement would be jerky, as the selection of the target would result in a sudden encoding of a high speed (proportional to the distance from the target). Therefore I introduced a second DNF (V map) that converts the representation of the movement direction in the D map to an encoding of movement velocity. The D map feeds in a one-to-one mapping into the V map. This mapping leads to a "proportional" relationship between encoding of distance from target and arm velocity. Zero distance (endeffector at target) corresponds to zero velocity whereas large distances relate to a high movement speed (see also Figure 2.7). However if the parameter set-up of the V map had been allowed to produce an output activation in a standard way, this dynamic would have led to an implausibly high acceleration of the robot arm. Instead, in order to achieve more smooth, human-like movements, without sudden jumps in the velocity the V map realises a *"moving blob"* behaviour in the following way. At the beginning of a reach movement the V map has a peak at its centre, thereby encoding zero speed (see top of Figure 2.7). Then the peak moves towards the direction of the target (as encoded in the D map), ramping up the arm's speed in the direction of the target. This is the acceleration phase of the arm and can be seen in the middle of Figure 2.7. While the arm is getting closer to the target the activation peak in the D map is moving closer to the centre of the map, eventually aligning its location with the output peak of the V map and moving in parallel. Once this situation is achieved the V map guides the arm to the target with closed-loop control (see bottom of Figure 2.7). To be more specific, the arm moves closer to the target and subsequently the peaks in the D map and the V map move closer to the centre, thereby lowering the speed of the arm. This

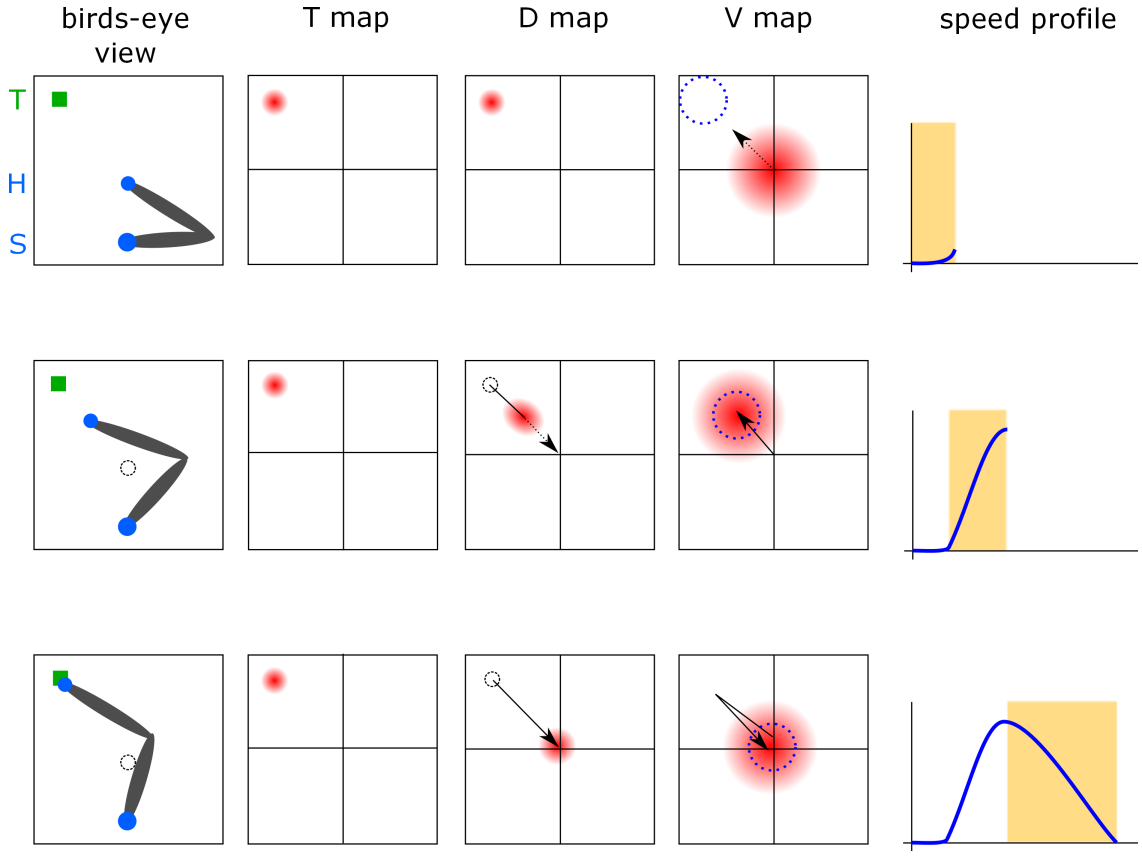

Figure 2.7.: The model is able to move towards target with a bell-shaped velocity profiles with the "moving blob" in the V map which encodes movement velocity and direction. The figures show three stages of a simulated movement: After trial onset (top row) the representations of arm (hand H and shoulder S) and target (T) location are established in the appropriate DNFs. The D map receives information from the T and the H map and encodes the position of the target in relation to the hand which happens to be almost identical to the birds-eye view in the above example as the robot's hand is located close to the centre of the environment. The D map is directly connected to the V map and induces a movement of the broad activation (the moving blob) which rests in the centre of the V map when there is no target present. As the moving blob moves away from the centre towards the target location (blue dotted circle) the arm starts to accelerate and reduces its distance to the target. When the locations of the activations of D and V map meet the point of peak velocity is reached (middle row). Now both activations move back together which induces a deceleration until eventually the target is reached and the arm stops moving (bottom row). Therefore, during a trial the activation of the D map starts at the target location and moves toward the centre of the map while the activation in the V map starts at its resting point in the centre, moves away from it just to return to its origin at the end of the trial.

process continues until the arm reaches the target and stops.

To realize this behaviour the gradient in the input activation had to be designed appropriately as the gradient determines the moving blob behaviour. I created an input activation that is made up of two parts. One part is the output of the D map but convolved with a Gaussian function with a large sigma. Note that this convolution is a biologically plausible operation as it models how spatial activation diverges when travelling from one neural layer to the next neural layer. The purpose of the large sigma is explained at the end of this section. The second part is the "*zero map*" which constitutes a Gaussian-distributed activation around the centre of the V map where zero velocity is encoded and is added to this activation. Without a target selection influence (before the start of the reach movement) the zero map induces a peak at the centre of the V map which encodes zero speed (see top of Figure 2.7). Once the target selection begins the first part of the input activation forms a gradient directing the peak towards the target location. Hence the peak moves and subsequently the arm smoothly increases its movement velocity towards the target.

A final important point of the moving blob behaviour is that the speed of the peak's movement is proportional to the steepness of the gradient, as mentioned in chapter 1.5. Now since the input activation of the V map is based on a Gaussian distribution with a large sigma, the gradient is steeper when the arm is far away from the target compared to when the arm is closer to the target. Hence, when the arm is far away from the target the acceleration of the arm is high while when the arm is getting closer to the target the acceleration is getting lower in a continuous fashion until the peak velocity is reached and the deceleration begins. Eventually, the hand slows down and stops at the target. In general this implements a good control strategy, since on the one hand it is efficient to move the arm as fast as possible when the hand is far away so that it reaches the target as fast as possible, while on the other hand if the target is close the hand should slowly manoeuvre towards the target so that it

does not overshoot it. Moreover and interestingly this qualitative description is also reminiscent of the left part of the bell-shaped velocity profile. Hence it is conceivable that the arm exhibits this bell-shaped velocity profile. However as the Movement Velocity Control is embedded in a control-loop, ultimately this needs to be tested in experiments, e.g. is it successful in a noisy environment; what happens when the arm gets close to the target, will it reach the target, etc. Hence, the first experiment will simulate reaches to single target objects to test and optimise this setup.

Inverse Kinematics

The output of the V map in the Movement Velocity Control module encodes an upcoming speed vector of the end-effector in cartesian coordinates. In order to generate the actual movements of the robot arm, the cartesian speed needs to be transformed into the speed of the robot arm joints. Here I follow the standard approach of using an approximation of the inverse of the Jacobian matrix (e.g. Siciliano & Khatib, 2008; see the Appendix A.1.6 for details). Essentially, the Inverse Kinematics module consists of a transfer function that generates the motor commands out of the hand's speed vector.

2.4. Conclusion

In this chapter I presented the theoretical background, the hardware setup and the control architecture of my computational model. The model was developed with the aim to simulate the findings of the odd-colour task of Song and Nakayama (2008b) and to exhibit reaches in a human-like manner. Hereby, the Target Selection module should be able to select the odd-colour target object and to apply priming to colours and locations. The Movement Velocity Control module with its moving blob was designed to generate bell-shaped velocity profiles when reaching. Moreover, all modules work in

a parallel fashion as suggested by Song and Nakayama (2008b). The following chapter will present experiments that will test the performance of my model in appropriate tasks.

3. Model Simulations

This chapter presents the experiments performed by my model which was described in the previous chapter. In the first experiment I demonstrate that the my model successfully guides the robot arm to a target in a single target setup. This also shows that the motor control stage produces human-like trajectories, i.e., the trajectories are straight and have bell-shaped velocity profiles (e.g. Jeannerod, 1984). The second experiment shows that my model can mimic Song and Nakayama's (2008b) findings in a setting similar to their odd-colour task. The third experiment will compare two possible mechanisms of how distractors influence the reaching movements in the odd-colour task. After each of the simulations I will discuss the performance of my model and its theoretical implications to the current research. All experiments of this chapter also have been published in Strauss and Heinke (2012).

3.1. Single target experiment

The single target experiment aimed to demonstrate that the control architecture is able to successfully reach for objects in a noisy real world environment. I also wanted to show that the model generates human-like reach trajectories. As mentioned before numerous papers show that when reaching for a single object, humans exhibit a roughly bell-shaped velocity profile with peak velocity roughly at the mid-point between starting point and target position (see also Figure 2.1 and Jeannerod, 1984;

Rosenbaum, Cohen, Meulenbroek, & Vaughan, 2006; for reviews). However the profile often is skewed with faster increase at the beginning of the movement and slower decrease when approaching the target. Moreover this single target experiment also provided a baseline for the odd-colour and the remaining experiments. Hereby, only one target object was presented and the target colour did not play a role, hence the T_{col} map was removed and the input for the T map consisted of the combined red and green map (see also Figure 2.6).

3.1.1. Methods

The target objects were square coloured markers (red or green) with a size of 3.5 cm $\times$ 3.5 cm. Targets were located on a virtual circle with the radius of 22 cm at 0°, 45°, 90°, 135°, and 180° (from left to right). The center of this circle was the starting position of the robot arm's hand (see also Figure 3.1). The starting position was located 9 cm in front of the arm's base (shoulder). Before the experiment began the parameters of the Image Preprocessing were adapted to the current lighting conditions. After starting a trial the position of the end-effector was recorded until the target was reached. The arm was considered to have reached the target when it was in a 6 cm $\times$ 6 cm area around the center of the target (see shaded area in Figure 3.1) and when its speed was less than 0.7 cm/s. Detailed model parameters of the experiment can be found in the Appendix. For each possible target location five trajectories were recorded. The location of the endeffector was obtained directly from the hand map. Since the sampling rate varied during each trial the data points for each trajectory (50–80 data points) were not recorded at the same points in time. In order to obtain an averaged trajectory I pre-processed each trajectory with the following steps. A spline function was fitted to each trajectory, then the resulting function was sampled with 100 equal time steps. Since the trajectories were fairly noisy, I smoothed the

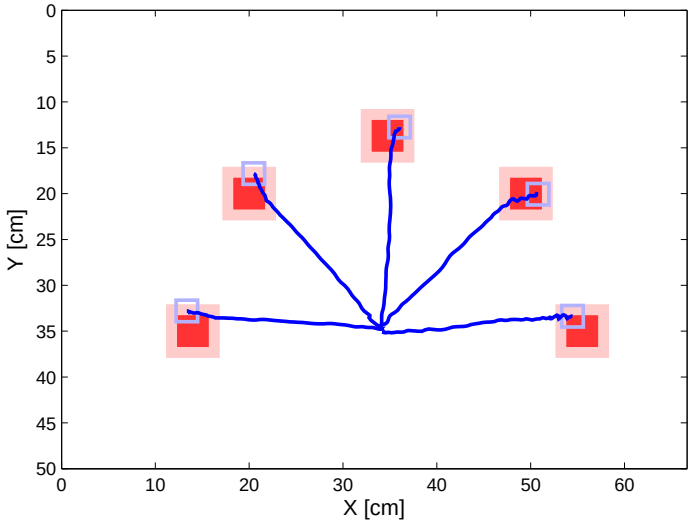

Figure 3.1.: Trajectories of the single target experiment (blue lines). Targets of the reach movements are shown in red. When the arm reached at least the shaded area around the targets it was deemed to have reached the target. The grey square illustrates the size of the tip of the end-effector when the movement stopped. The base of the robot arm (shoulder) was positioned approximately 9 cm under the starting point of the end-effector. The end-effector itself was located in the origin of the trajectories (35 cm, 35 cm). The result showed that the robot arm was able to follow a straight path to the target. All trajectories are mean trajectories of five trials.

result with a moving average over 10 time steps. Finally, the averaged trajectory was obtained by averaging across the same time slice.

3.1.2. Results & Discussion

The first experiment with the robot arm showed that, in principle, the arm exhibited the desired straight trajectories and the bell-shaped velocity profiles. This was expected from the design of the Movement Velocity Control. However the behaviour turned out to be fairly unstable and noisy. For instance, even though the arm was able to move close to the target it had problems fully reaching the target. I therefore chose to modify the V map. Originally the V map followed the linear encoding schema commonly used in DNFs. In the new version the neural layer is mapped onto

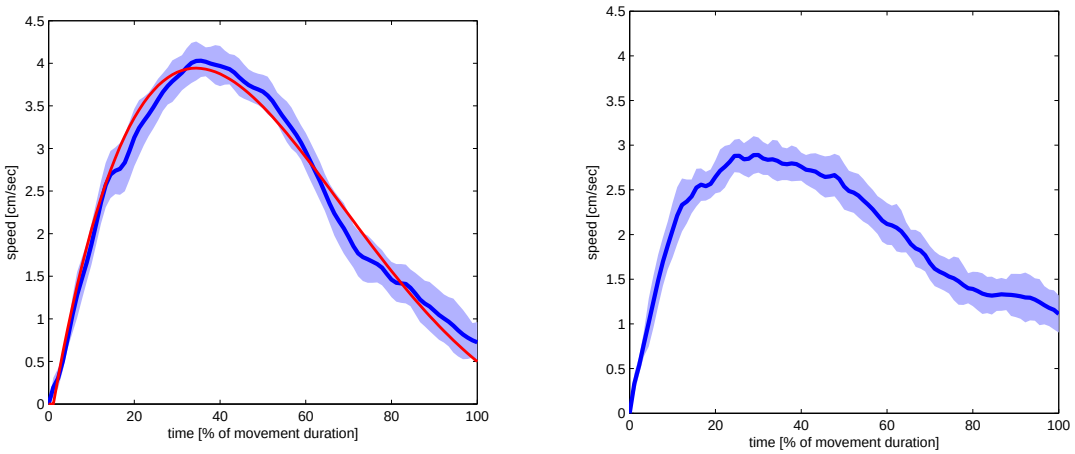

Figure 3.2.: Velocity profiles of the simulated movements to the top centre position of Figure 3.1. The profiles are shown with their standard deviation (light blue area). The dark blue line represents the moving average of 10 time slices of the movement. (b) shows the result of the simulation with with a standard topological encoding in the V map of the Movement Velocity Control module. Due to the relative high speed at the end of the trajectory the arm tended to overshoot the target here. For (a) a non-linear encoding was used and this encoding schema led to better reaching movements. The red line documents the outcome of the VITE-model fitted to the robot arm behaviour (see main text for a detailed discussion).

the parameter space in a non-linear fashion (exponential function with power 1.5) in which many neurons map onto low speeds whereas only a few neurons map into high speeds. I expected that this encoding should lead to a better behaviour of the arm as it represents a good compromise between two objectives. On the one hand it leads to more precise movements when the end effector is close to the target, while on the other hand it allows the arm move more coarsely while it is still far away from the target. Indeed, this encoding schema led to better behaviour of the arm (see Figure 3.2 for a comparison). Overall, the movement was less noisy and more bell-shaped. The peak velocity was higher but in the vicinity of the target the velocity was lower which resulted in a better target reaching behaviour. It is also interesting to note that the maximum speed was reached later in the movement (at around 40%) which fits

better to the experimental findings with humans (e.g., Jeannerod, 1984).

Figure 3.1 shows the mean trajectories toward the five target markers. The trajectories were almost straight with only a little curvature. These results are comparable with experimental findings on humans. For example Haggard and Richardson (1996) found that humans reach with similar (almost straight) paths in different regions of the workspace. Also Desmurget, Prablanc, Jordan, and Jeannerod (1999) support the model's approach that compliant movements in the horizontal plane are planned in the extrinsic space, which results in straight hand trajectories. Taking together the results of this experiment gave support for the implementation of the Movement Velocity Control module.

For an additional verification of our model I compared the arm's behaviour with a mathematical model for velocity profiles. In fact, as already mentioned in chapter 2.1.2 there are several mathematical models for generating human-like velocity profiles such as the Minimum Hand Jerk model, the Minimum Commanded Torque Change model, etc. A recent review by Petreska and Billard (2009) suggested that a modified vector integration to endpoint (VITE) model (Bullock & Grossberg, 1988) yields the best fit to human movement trajectories. Here I used the VITE-model as the reference model for my model. The VITE-model is described with the following equations:

$$y(t + \Delta t) = \alpha - y(t) + x_{target}(t) - x(t) \tag{3.1}$$

$$x(t + \Delta t) = \beta t^v y(t) \tag{3.2}$$

The parameters α, β, and v are real positive constants and control the changing rate of the acceleration. x_{target} and x are the position of the target and the end-effector respectively. y is a secondary variable and related to the speed of the end effector.

To compare the VITE-model with the robot arm's velocity profile I used the average velocity profile shown in Figure 3.2. For each time step in this profile I determined whether the VITE-model produced a velocity value that fell within the one standard deviation interval. Then we calculated that percentage of time steps which fulfilled this criterion. For the following parameters 98% of time steps fulfilled this criterion: $x_{target} = 10$, $\alpha = 0.058$, $\beta = 0.01$, and $vv = 0.0286$ (see Figure 3.2 for the resulting velocity profile). In other words for these parameters the VITE-model and the robot arm's velocity profile were very close in 98% time steps providing further support for my model.

3.2. Odd-colour experiment

After having shown that the model is able to reproduce human reaching trajectories, the next aim was to replicate the odd-colour experiment by Song and Nakayama (2008b) which was introduced in chapter 1.3. Here the aim was two fold: The model should be able to direct the robot arm to the odd-colour target object and second, the model should reproduce the effects of colour priming, i.e., the curved trajectories with longer movement times and the reduction of the initial latency.

As pointed out previously there is also evidence for spatial priming from standard search tasks (e.g., Maljkovic & Nakayama, 1996). Even though there is no evidence from choice-reaching tasks it seems plausible to expect spatial priming effects similar to the colour priming effects. Since the model also allows us to implement spatial priming I will also present these experiments here and compare them to colour priming.

3.2.1. Methods

The setting of this experiment is similar to the single target experiment except that I used an odd-colour display like in the experiment of Song and Nakayama (2008b).

There were three markers placed in the workspace: either two red and one green or two green and one red marker (see Figure 3.3 for an example). Both colours can be easily distinguished by the Image Preprocessing. The possible locations for the marker were at 45°, 90°, and 135°, the three central locations in the single target experiment. All modules of the model were used including the Target Selection module as described in chapter 2.3 and the non-linear encoding of the V map developed in the single target experiment. Moreover, and importantly, the preactivation module should be able to induce the priming effects in the model.

The data analysis followed the same steps as in the last experiment using spline function and moving average to obtain smoothed trajectories. In addition the following durations were extracted from the processed trajectories: the Initial Latency or Reaction Time (RT) was the time between starting the simulation and movement onset. The Movement Time (MT) was the time between movement onset and the end of the movement. Movement onset was determined at the point in time when the velocity was higher than 0.3 cm/s for the first time. These measures allowed us to relate our results to Song and Nakayama (2008b) findings. All parameters of the model can be found in the Appendix.

3.2.2. Results & Discussion

Figure 3.3 shows the trajectories of the robot arm in the odd-colour experiment. To begin with the results demonstrate that the model is able to detect the odd-coloured marker and successfully directs the arm to the target marker. Moreover, with the help of the Preactivation module (priming) we were able to generate the curved trajectories found by Song and Nakayama (2008b). The results also mimic Song and Nakayama's (2008b) finding that the RT was shorter in the priming condition compared to the baseline and that the MT of the curved trajectory was longer. Interestingly, the size

Colour priming

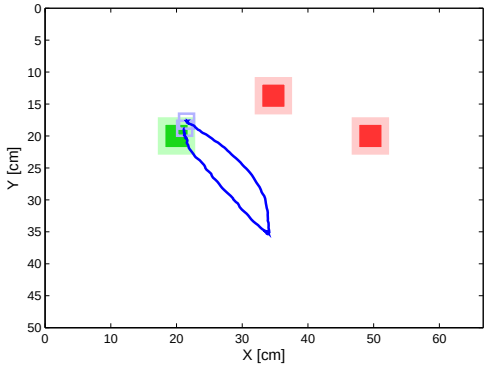

	baseline	curved
MT	11.02 (0.22)	12.79 (0.31)
RT	3.00 (0.12)	2.62 (0.08)

Spatial priming

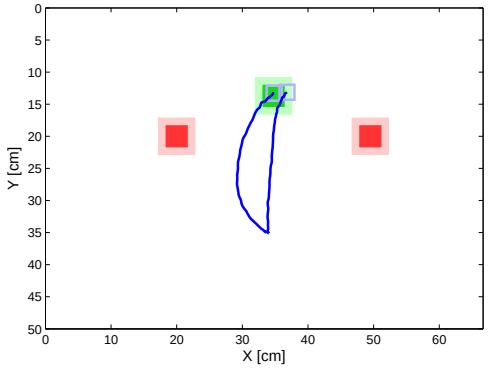

	baseline	curved
MT	11.00 (0.32)	12.39 (0.15)
RT	2.96 (0.27)	1.53 (0.12)

Figure 3.3.: Example trajectories with measured time intervals of the simulation of the odd-colour experiment. In the colour priming condition the red colour was primed while in the spatial priming condition the left target was primed. The trajectories are mean trajectories of five trials. The time intervals are also the average times from five trials in seconds. The figures in brackets indicate the standard deviation. The abbreviations stand for Reaction Time (RT) and Movement Time (MT). The results demonstrate that the model can successfully direct to the robot arm to the odd-coloured target. The "curved" trajectories result from the preactivation of the spatial map (spatial priming, on the right) and the colour map (colour priming, on the left). In both conditions, compared to the straight trajectories the RT decreases and the MT increases matching the experimental data by Song and Nakayama (2008b). Interestingly the effect on the RT is stronger in spatial priming than in colour priming. This effect is discussed in the main text.

of the effect depended on the type of priming, either colour priming or spatial priming. For spatial priming the effect of the RT was larger than for the colour priming. In contrast, the MT was longer for the colour priming than for the spatial priming.

Taken together the results demonstrate that the model can successfully mimic the findings by Song and Nakayama (2008b). In particular the preactivation initially directs the competition in the target selection module toward distractors. In turn, this guides the moving blob in the V map and the robot arm toward the distractors. However after some time the preactivation is overwritten and the moving blob and the

robot arm are directed toward the target. In some way the priming effect in my model can be conceptualized as the distractors first "pulling" the arm toward their direction. I will return to this point in the next experiment. However, it is also worth noting that the response vector hypothesis by Tipper et al. (1997) proposes a similar pulling effect based on a similar mechanism (see also chapter 2.1.3). Their model suggests that the directions of movements toward the target and the distractors are encoded with distributed representations similar to the one postulated in the DNFs. Moreover the model determines that resulting movement direction by calculating the center of gravity of the combined representation of target and distractors. Consequently the resulting movement veers toward the distractors. However, Tipper et al.'s (1998) model does not include a mechanism of how such distorted movement directions are translated into actual movements and how humans eventually reach the target.

Furthermore my model predicts that additional experiments with humans should find a difference between spatial priming and colour priming. Even though the effect found with the robot arm can be due to different parameter settings, e.g., the preactivation is higher in spatial priming than in colour priming (however all other parameters remained unchanged in the different conditions), the difference originates from an architectural difference of how the two dimensions influence the selection process. The spatial priming directly influences the selection map whereas the colour priming affects selection via the weighting of the two colour maps. In addition the difference between colour priming and spatial priming also plays out differently for the RT and for the curved trajectory. For the RT, the structural difference is responsible for the difference. In contrast, for the MT the difference nature of the features is important. In the colour priming two distractors attract movements whereas for the spatial priming only one location distorts movements.

3.3. Odd-colour "continuous" vs. "threshold" experiment

In the previous experiment I pointed out that the curved trajectories in the model are the result of the distractors pulling the arm toward their location. In other words, the activation in the competitive selection does not necessarily need to pass a threshold for it to affect the reaching process ("continuous" hypothesis). This contrasts with a suggestion by Song and Nakayama (2008b). They proposed that the competitive selection first has to reach a threshold before it can direct movements toward an item, e.g., a distractor ("threshold" hypothesis). In fact, this hypothesis can also be simulated with my model by adding a threshold at the output of the selection stage. The current experiment will illustrate the different reaching movements the two hypotheses would predict.

3.3.1. Methods

The settings of this experiment were similar to the odd-colour experiment of the previous section. However, the colour priming activation was increased to make the illustration clearer. To implement the "threshold" hypothesis a threshold between the T map and the D map was introduced so that only high activations in the T map can influence the behaviour of the D map.

3.3.2. Results & Discussion

Figure 3.4 depicts the results based on five trials in for each hypothesis and highlights the differences. As expected, trajectories in the "threshold" setup pointed toward one of the distractors in an early stage of the movement, while trajectories in the "continuous" condition fell somewhere between the two distractors. Hence in order to

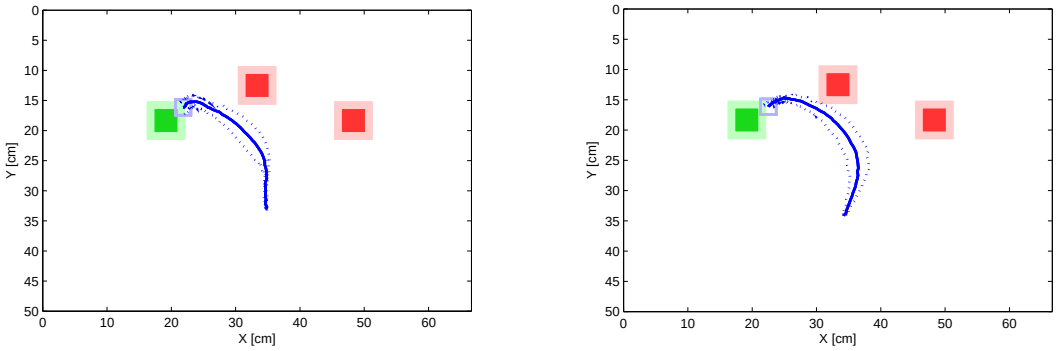

(a) (b)

Figure 3.4.: Comparison of "continuous" vs. "threshold" hypothesis. (a) shows the outcome of the threshold hypothesis. Note that in this setting the trajectory veers towards the middle or the right distractor randomly depending on the noise in the DNFs. For the above figure only the trajectories towards the middle distractor were chosen. The trajectory in (b) is the result of the "continuous" hypothesis (see main text for detail). Each mean trajectory shows the results from five trials. The broken lines document the standard deviation.

distinguish between the two hypotheses it makes sense to determine the orientation of the movements at their early phase. Now for these movement orientations it is obvious that the "threshold" hypothesis predicts a bimodal distribution with the two modes roughly pointing toward the distractors. In contrast, the "continuous" hypothesis predicts an unimodal distribution with a peak roughly between the two distractors. Moreover Figure 3.4 illustrates that the variation of the movement orientation is smaller for the "threshold" hypothesis than for the "continuous" hypothesis. The large variation in the "continuous" hypothesis is due to the fact that the two distractors induce noise onto the movements whereas in the threshold hypothesis only one distractor influences the movements. Note that the latter point implies that we expect a variation around each mode in the order of magnitude of the single target displays.

3.4. Conclusion

Recently Song and Nakayama (2008b) published evidence that the process of attentional selection can influence reach movements towards a target. In this study, the reaching target was given by an object with the odd colour, e.g. a red square among green squares. In the previous chapter I presented a robotics-based approach to modeling the results of this choice-reaching experiment. To take into account that these experiments use human movements the output of model is a robot arm built with LEGO Mindstorms NXT. In order to link the output of this stage with the robot arm we based the motor control stage on the dynamic field theory by Erlhagen and Schoener (2002). Crucially, the motor control stage uses a "moving blob"-dynamics in a neural field to ensure jerk-free (human-like) movements. Overall the model is consistent with Song and Nakayama's (2009) suggestions that there is a direct link between target selection and movement planning, that both processes work in parallel and that the target selection process is implemented in a dynamic competition.

In this chapter three experiments were performed to test the model's abilities. The first experiment demonstrated that the model can guide the robot arm to targets in straight trajectories. Moreover, the trajectories exhibited a bell-shaped velocity profile often found in experiments with humans. Crucial for producing the bell-shaped velocity is the moving blob behaviour in the V map of the Movement Velocity Control module which implements the acceleration and the deceleration of the robots's velocity. This behaviour was theoretically examined by Amari (1977). However, to the best of our knowledge it has never been used to describe human behaviour in a functional model before. It also remains an open question whether the brain employs this behaviour. The second interesting outcome of this first experiment is that I had to introduce an inhomogeneous spatial encoding of the velocity parameter. The inhomogeneity is such that at small velocities the encoding has a high spatial

resolution, whereas at high velocities the encoding is coarse. This divergence from the normal linear encoding schema in DNFs was necessary to achieve a better control of the arm in terms of robustness and higher peak speed, but also made the speed profile similar to human velocity profiles. Importantly the encoding schema is reminiscent of the way the visual cortex represents stimuli, i.e., the "cortical magnifying factor" (e.g., Rovamo & Virsu, 1979). In this representation visual stimuli are represented with a fine grain resolution in the foveal region, while in the parafoveal region stimuli are represented with a coarse resolution. Hence it is not inconceivable that the brain has reused this mechanism in the motor cortex as suggested by my model. However, as with the moving blob behaviour, this prediction remains to be tested in physiological experiments.

The second experiment demonstrated that the model performs the odd-colour search task by Song and Nakayama (2008b), i.e., the robot arm successfully reached the object with the odd-colour. This success also included the reproduction of their finding of curved trajectories. Moreover, the curved trajectories showed a lower reaction time while the movement time increased due the longer length of the trajectories, again mimicking Song and Nakayama's (2008b) findings. The model also predicts that these priming effects not only occur for colour but also for space (see Maljkovic & Nakayama, 1996; for spatial priming effects in a standard visual search task). Moreover the model suggests that the priming effects are stronger for space than for colour. This prediction is in part due to the different way the two dimensions are processed in the model and in part due to how the two dimensions are differently reflected in the visual search display. The latter point refers to the fact that spatial priming may affect a single distractor whereas colour may affect a group of distractors. This prediction remains to be tested.

The third experiment illustrated the subtle but important difference in the way Song and Nakayama (2008b) explain the priming effect and in the way the model realises

this feature. In both explanations it is assumed that the priming effect is the effect of residual activation from the target in the preceding trial misdirecting the reach movement. However, while Song and Nakayama (2008b) suggest that the competitive selection reaches a threshold in order for it to cause reaching toward a distractor ("threshold"-hypothesis), my model suggests a different mechanism. It suggests that the competitive selection does not necessarily need to pass a threshold for it to affect the reaching process. Instead, items during the competition process pull the reaching movements toward their position and the strength of the attraction is related to how much they are selected ("continuous"-hypothesis). The experiment makes predictions for the directions of "curved" movements at their early stage. The "threshold"-hypothesis predicts that the distribution of the directions should be bimodal with the two modes at the directions of the distractors. In contrast the "continuous" hypothesis suggests a unimodal distribution with a peak roughly falling between two distractors. Future experiments with humans will have to test these predictions.

4. Three Simulations with Modified Versions of the Model

The experiments of the previous chapter have shown that the model is able to simulate single target reaching and the odd-colour choice-reaching tasks of Song and Nakayama (2008b). In this chapter I present a second set of experiments with further simulations of the model of a wider variety of choice-reaching tasks. First I aimed to simulate a variation of the odd-colour task of Song and Nakayama (2008b). There the design of the experiment was extended by an irrelevant feature. This experiment and its simulations will be published shortly in Strauss et al. (2013). Afterwards, two further choice-reaching experiments were simulated that required few modifications to the Target Selection module. These tasks will be presented here to show that the control architecture of the model is very flexible and easy to modify to the requirements of different choice-reaching tasks. The first of these experiments dealt with the spatial averaging effect while the final experiment aimed to simulate the Simon effect. Behavioural experiments already were introduced in chapter 1.3, but I will review the relevant results here in a greater detail. Similar to the previous experiments regarding the odd-colour task both tasks apply the choice-reaching paradigm to make ongoing target selection processes in the movement trajectory visible.

4.1. Odd-colour irrelevant feature experiment

This experiment dealt with a variation of the odd-colour experiment of chapter 3.2. In the standard odd-colour experiment of Song and Nakayama (2008b) colour is the relevant feature to distinguish target and distractors so that the objects differ along the colour dimension, but are identical otherwise. This paradigm has been extended by Philip Woodgate, a PhD student in my laboratory, who included an irrelevant feature dimension - the size of the objects. Now all objects could occur in a smaller size which was the object size in the original odd-colour task (see chapter 3.2) or in a larger size.

Before I present the empirical results of Philip Woodgate's experiment (Strauss et al., 2013; in preparation) I will review the typical effects of irrelevant features that were reported in the literature. Subsequently, I will discuss the behaviour of my model in a similar task. It turned out that modifications of the model of chapter 2.3 were necessary which will be introduced in the following. Finally, the simulation results of the modified model will be presented and discussed.

4.1.1. Behavioural evidence

Influence of irrelevant features

The influence of irrelevant feature dimensions in visual search tasks has been investigated in numerous experiments. For instance, Yantis and Egeth (1999) ran a series of experiments to investigate whether irrelevant object features influence the target selection process and how this influence is manifested in search performance. The stimuli of their experiment consisted of bars with different colours and orientation whereas the orientation was the target determining feature and the colour the irrelevant feature. Their results suggest that the degree to which attention is

deployed to Irrelevant Features (IFs) depends upon the extent to which they provide task-relevant information e.g. when the target always has a different colour than the distractors even though orientation is the relevant target feature. There were, however, some exceptions, with size and brightness singletons capturing attention more readily; RTs were significantly faster when the target was also a size or brightness singleton. Similarly, in an inefficient search task (where performance decreases with increasing distractor numbers) Proulx and Egeth (2008) and Proulx (2010) observed expedited RTs when the target was larger/brighter and longer RTs when a distractor was larger/brighter where a non-predictive relationship occurred between target and singleton location. In summary, one would expect that the differently sized objects in the odd-colour task influence the reach trajectories and the reaction times. Also larger objects should catch attention more easily.

The odd-colour IF experiment

As mentioned before the odd-colour IF experiment was conducted by Philip Woodgate. Here I am going to summarise his experiment and findings; the details of his statistical analysis can be found in his thesis. As mentioned earlier he introduced differently sized objects to the odd-colour task of Song and Nakayama (2008b) so that besides the smaller sized objects also larger objects occurred in the search display. In total six conditions could be distinguished depending on the size of the target and the distractor objects. The conditions were: (1) All small (tdd), (2) Small target, 1 large distractor, 1 small distractor (tDd), (3) Small target, 2 large distractors (tDD), (4) Large target, 2 small distractors (Tdd), (5) Large target, 1 small distractor, 1 large distractor (TdD), and (6) All large (TDD) (see also Figure 4.4). Like in the original odd-colour experiment the Reaction Time (RT) and the trajectories of the movement were recorded. As an additional measure also the Maximum Curvature (MC) was obtained from the trajectory of the reach movement.

The results are shown in Figure 4.1 and showed a significant main effect of condition in both measures. The results of the RT are as follows: In the small target conditions the RT decreased with larger distractors. Hereby the condition tdd took significantly longer to initiate than reaches to tDD and showed a borderline significance with tDd. A similar effect but to a less extend was found for large targets. Here TDD was borderline significantly faster than Tdd. There was no significant overall effect between small and large target conditions, however, some more borderline significances could be observed: tdd was slower than TDD and the RT for tDD was lower than in Tdd and TdD.

For the MC a similar result pattern was observed, however, more significant results were found: Tdd and TdD showed the largest curvature. These both conditions were significantly more curved than the conditions with the lowest curvatures (tdd, tDd, tDD and TDD). tDD showed the least curvature; as well as differing from Tdd and TdD it was also significantly less curved than tDd, and tdd, with a borderline difference to TDD (see Figure 4.1). Overall, large targets showed a significant higher curvature than small target objects.

The results showed significant effects of condition in both recorded measures. The resulting graphs for RT and MC were fairly similar, however, overall we found more significant effects between individual conditions in terms of maximum curvature which suggests that underlying mechanisms affect this measure more strongly.

The similar pattern of the results of latency and curvature is not consistent with the results of the original odd-colour tasks where a smaller latency induces a higher curvature and vice versa (see also chapter 1.3 and Song & Nakayama, 2008b). In contrast both measures were affected quite similar by the different conditions: small target conditions showed smaller RTs and MCs than large target conditions (however, not significant in the RTs). Within the conditions of similar target size larger distractor objects caused smaller values of RTs and MCs. Interestingly, large target objects did

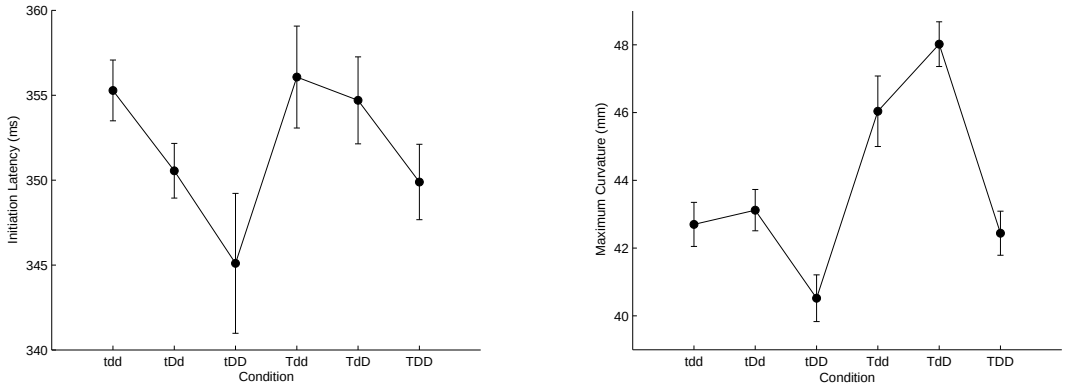

(a) (b)

Figure 4.1.: (a) Reaction time and (b) maximum curvature results of the odd-colour irrelevant feature experiment by Philip Woodgate (Strauss et al., 2013; in preparation). Error bars represent ± 1 standard error averaged within-subjects per condition as in Cousineau (2005).

not facilitate the task in terms of RT costs as normally observed in such tasks (e.g. Proulx & Egeth, 2008). However, the curvature effects differed slightly from the RTs. In the conditions with one large and one small distractor the curvature was increased in comparison with the pattern of the RT. In the following section I will discuss how my model of section 2.3 simulates the experiment. Subsequently, I will discuss the results and possible explanations in a greater detail.

4.1.2. Simulating the experiment with the original model

In the first set of experiments in chapter 3 I simulated the odd-colour task of Song and Nakayama (2008b). The model there was able to simulate the two different types of trajectories and their latency and movement time properties. It turned out that the original model is not able to simulate all aspects of the present target-distractor size experiment. Here I am going to discuss the reasons for that fact. Modifications that improve the model will be presented in the following section.

The main reason why the original model is not able to simulate the experiments is the

continuous information flow in the control architecture that was used to simulate the original odd-colour task in chapter 3.2. There, a low RT caused a high curvature and vice versa as observed in the experiments of Song and Nakayama (2008b). In contrast, in the odd-colour IF experiment both measures show a similar behaviour (i.e. RT and MC are either both high or low). However, with the original model it would be possible to simulate the effects in either RT or in MC depending on the threshold parameter between the T and D map. This threshold parameter acts as a switch so that only activations of objects in the T map above its value are getting passed onto the movement control stage and thus influence the movement. In this way a high threshold allows the DNFs to determine a correct target before the movement is initiated. Thus, no effect in the curvature can be observed. However, the calculation time of the DNFs creates an effect in the latency as the response conflict in the T map has to be resolved before the movement is initiated. In contrast a low threshold value induces a quicker start of the movement and diminishes differences in the latency, whereas wrongly selected target objects create a large effect on the curvature (and also in the movement time as observed in chapter 3.2 in the odd-colour experiment as the curved trajectory requires more time to reach the target object). Hence, it was not possible to generate results where both measures showed similar effects like it was found in the odd-colour IF experiment where conditions showed high RTs with high MCs and vice versa.

4.1.3. Modifications of the original model

The previous sections presented the results of the behavioural experiment and the reasons why my original model is not able to simulate these findings. In order to improve the simulation of my model I will introduce modifications to its control architecture which account for the findings of the experiment. Besides presenting those

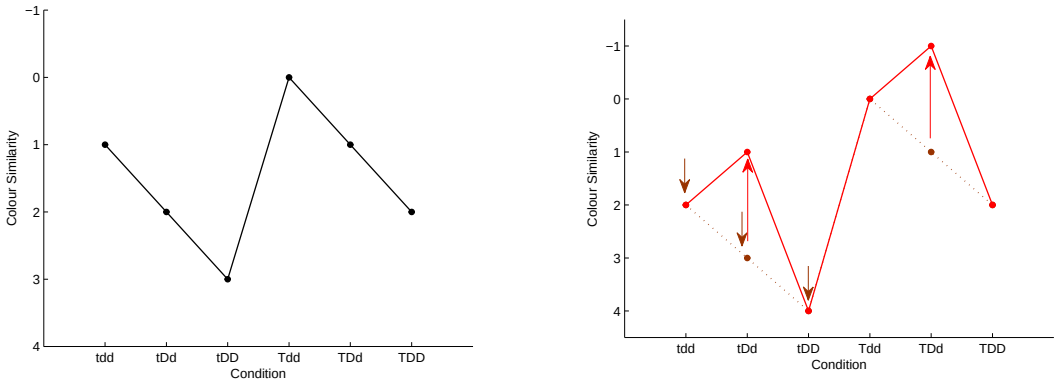

(a) (b)

Figure 4.2.: (a) Colour similarity graph for the experimental conditions. The line shows the difference of the amount of distractor colour and the amount of target colour for each condition as shown in the table. For example, if the target is small the amount of colour equals 1. If this small target is presented with two large distractors the total amount of distractor colour equals 4 (2+2). The results of the RT are already very similar to this graph (compare Figure 4.1). The results of the MC differ from the RT, hence we suggest further mechanisms that affect this measure. The effects of these mechanisms on the colour similarity are displayed in (b). See the text for a discussion of the effects in more detail.

modifications I am also going to develop a theoretical explanation of the behavioural findings.

The first finding to note is that in the behavioural experiment the overall pattern of RT and MC is fairly similar and can be described with the "colour similarity" which is the difference of the amount of distractor and target colour. The simple colour similarity graph in Figure 4.2 (left side, black line) already looks very similar to the RT and MC graphs we see in the results. This suggests that a target selection decision is made at least partly from the discrepancy of target and distractor features – in this case colour. More evidence that the colour difference plays a role in such selection tasks comes from the odd-colour tasks of Song and Nakayama (2006). In their task participants had to reach for the odd-coloured object among a different number (2, 5, or 11) of distractors. One of the main findings was that with a higher number of distractors the task became easier which resulted in lower curvatures and smaller RT

which could also be explained by the colour similarity graph of Figure 4.2. How salient a stimulus is depends, in part, on how strongly it contrasts with the stimuli that surround it (J. Wolfe & Horowitz, 2004). Accordingly, as target-distractor similarity increases the salience of the target decreases and more time is required to select the target (Nothdurft, 1992). Thus, as the contrast between the target and distractors increases along the lines of the target-defining feature (i.e. the "amount" of each colour) target selection is facilitated, and vice-versa.

In my model the functionality of the T_{col} map is very similar to the described colour similarity. Hence, the first modification affects the connection of this map to the motor stage. This is supposed to resemble the similarity of RT and MC of the behavioural experiment without diminishing the effect in one of the measures in the original model as described in the previous section. Essential for the initiation of the movement is the connection from the D into the V map as it causes the moving blob to move away from its resting position. Now this connection is directly linked with the activation level in the T_{col} map as colour is the relevant target feature (see Figure 4.3) which results in the following behaviour: only when the activation of a neuron of the T_{col} map exceeds a threshold (which means that the correct target colour has been detected) the activation from the D map will be passed onto the V map which eventually causes the moving blob to move away from the centre of the map and initiate the movement. In this way the T_{col} map alone is responsible for generating the RT and should resemble the colour similarity graph. Only after the T_{col} map has decided the target colour the distractors can be inhibited in the same way as in the original odd-colour experiment. This allows the T and D map to establish activations at target and distractor positions before movement onset. Due to the new threshold distractors will possess larger activations with a longer RT (as the RT solely depends on the T_{col} map). Hence with this modification the model should be able to reproduce the results of the behavioural experiment where high RTs cause a high MC

and vice versa and the pattern of Figure 4.2 is the expected result of simulations. This modification should already give a good approximation of the behavioural results.

The behavioural results for RT and MC show a similar pattern, however, also still show some differences. A first difference between the measures is the significant effect of target size in the MC. That is, reaches to small targets show less curvature than reaches to their large counterparts. The colour similarity graph shows a small difference in the target object size as well, however, this effect is small and was found to be not significant for the RTs. One explanation for the significant results in the MCs could be that a mechanism independent from the RT-generation is responsible. For instance small targets could be preferred over large targets in the target selection stage. This is in contrast with the finding that large targets capture attention in IF experiments (e.g. Proulx & Egeth, 2008). However, we speculate that such an advantage of small targets may be induced due to the choice-reaching task paradigm. In Figure 4.2 the influence of this effect is shown with the brown arrows and the brown dashed line.

In my model the dynamics of the DNFs offer an easy way to simulate a lower curvature for smaller targets: the parameters of the T map were chosen so that small objects are creating a larger activation than big objects. This was achieved by applying both a high inhibition and an even larger local excitation in the T map. More importantly, the size of the excitation radius was smaller than the (perceived) size of the large items. Hence, small and large items receive a similar amount of excitation, but large objects are influenced to a greater extend by the inhibition. This modification will simulate the small target advantage of the behavioural experiment. Despite the changes the mechanism of the odd-colour detection of Figure 2.6 remains unchanged.

Besides the above small target advantage another difference between the measures in the different conditions was observed: for the MC (but not for the RT) the performance in the conditions TDd and tDd is slightly worse in reality than the prediction of

the introduced target selection mechanisms that are reflected in the adjusted colour similarity graph of Figure 4.2 (black and brown dashed line). Thus, there must be some other factor at play. The likely candidate is the ease with which distractors can be grouped. As colour is the dominant feature this grouping should occur along the colour dimension. The increased curvature in the conditions tDd and TDd suggests that this grouping also occurs along the size dimension, however, this makes grouping in these conditions more difficult as one distractor is the odd-sized object which consequently leads to an increase in the curvature (see Figure 4.2; red arrows/line). This curvature increase was not reflected in the RTs that were primarily influenced by the colour similarity aspect discussed earlier. Therefore we suggest that this effect is caused by a mechanism that is independent from the colour difference and affects only the ongoing movement.

Implementing such a grouping mechanism in my model would require major extensions and further neural fields. For this reason we found it is sufficient to model this finding in a more abstract way. The modification here only affects the two conditions with an odd-sized distractor (tDd and TDd) and decreases the weight on the connection from the T_{col} map to the T map. This mechanism should only influences the trajectory of the ongoing movement as it takes place after the T_{col} map and is independent from the T_{col}-threshold that determines the RT. I will simulate the two relevant conditions with and without this mechanisms to demonstrate its influence on the trajectory.

In the following I present the results of the simulation of the odd-colour IF experiment with the modified model and discuss the possible explanations for the experimental results that it offers.

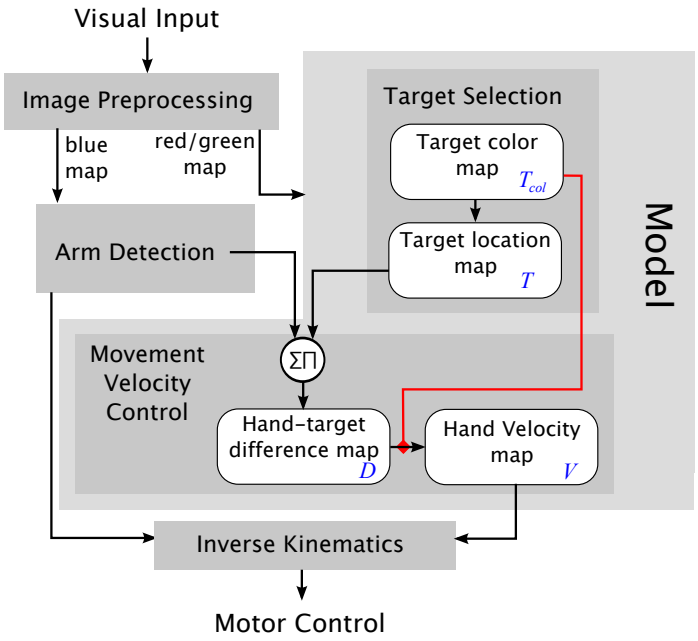

Figure 4.3.: Overview of the modified control architecture of my model to simulate the odd-colour IF experiment. The red line symbolizes the threshold switch of the T_{col} map which has to be surpassed in order to activate the information flow from the D to the V map. This feature has been added to account for the new behavioural evidence. See Figure 2.4 for the original control architecture and Figure 2.6 for the Target Selection module and its description.

4.1.4. Methods

The hardware setup was identical to earlier experiments. The target objects were square coloured markers (red or green) with a size of 3.5 cm × 3.5 cm (small object size) and 4.38 cm × 4.38 cm (large). Targets were located on a virtual circle with the radius of 22 cm at 45°, 90°, and 135° (from left to right). The center of this circle was the starting position of the robot arm's hand. The starting position was located 9 cm in front of the arm's base (shoulder). Like in the behavioural experiment six different conditions were distinguished with the differently sized target and distractor objects (see Figure 4.4). For each condition five trajectories were recorded. However, exceptions were the conditions tDd and TDd where five trajectories for both possible distractor placements (large distractor on the left side or in the centre) were recorded.

Before the experiment began the parameters of the image preprocessing were adapted to the current lighting conditions. After starting a trial the position of the end-effector was recorded until the target was reached. The arm was considered to have reached the target when the encoded velocity in the V map fell under a threshold value of approximately 0.5 cm/sec. The encoded velocity was the distance of the centre of gravity of the neural activation (the moving blob) to the centre of the V map.

For the purpose of data analysis the raw data of each trajectory was pre-processed with the following steps. First, a B-Spline (3rd order) of the raw data points was calculated which reduced noise and normalized the trajectories to 100 data points. Second, I applied a Butterworth filter (2nd order) with a cut-off frequency of $\frac{1}{20}$ of the sampling rate of the camera in order to reduce the noise even more. Note that the data analysis procedure was improved in comparison to the last experiments.

This experiment focused on the Reaction Time (RT) and the Maximum Curvature (MC) of the trajectories, thus these two measures were processed and analysed accordingly. The MC was calculated by dividing the maximum deviation of the data points from a straight line by the length of this line. The straight line was determined by the start and end point of the trajectory. The RT was obtained in a similar way than in the previous experiments. Finally, in comparison with the original model further DNF parameters of the T_{col} and D map were modified (see the Appendix for details). The simulations of the conditions tDd and TDd were performed without and with the abstract distractor grouping mechanism to demonstrate its influence on the measures.

A one-way ANOVA with the factor Display Type (tdd, tDd, tDD, Tdd, TdD & TDD) was conducted with RT and MC as dependent variables. Furthermore, the influence of the target size (small vs large) was investigated in a separate ANOVA. All statistical tests were run twice: once with and once without the distractor grouping mechanism. In order to investigate the influence of the distractor grouping mechanism in the

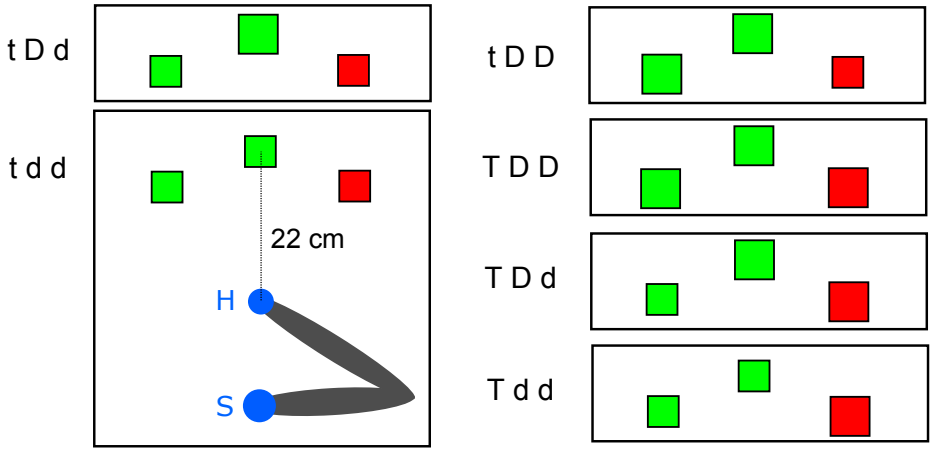

Figure 4.4.: Object placement of the odd-colour IF experiment. The red target object was always placed on the right side. Note that in the conditions with one large and one small distractor the two distractors switched their location in half of the trials.

appropriate conditions (tDd and TdD) the results with and without the mechanism were compared using paired samples t-tests.

4.1.5. Results & Discussion

The results of the experiment can be found in Figure 4.5. The findings of the measures are as follows:

Reaction Time (RT): For the results without the distractor grouping mechanism a significant main effect of Display Type was found ($F(5,34)=12.28$, $p<0.001$). A posthoc Bonferroni pairwise analysis found significant differences ($p<0.05$) between the condition tdd compared with tDD and TDD. The condition Tdd was different to tDd, tDD and TDD. tDD also was different to TDd and TDD to TDd. Also with included distractor grouping mechanism the main effect of Display Type could be observed ($F(5,34)=10.632$, $p<0.001$). The pairwise analysis led to a similar result, however, now tDd was also different to tdd and there was no significance between tdd and TDD anymore.

In the resulting graph it can be seen that the simulation results of the RT resemble

the results of the behavioural experiment. In the model the RT depends on the colour difference of target and distractor objects as the amount of colour feeds into the T_{col} map which has to reach a threshold activation before the movement can be initiated. Thus, the smaller the difference between the combined size of the distractor objects and the target the higher the initial latency. This implies that smaller target objects show a shorter RT than larger target objects and for large distractor objects it is shorter than for small distractor objects. This effect also was found to be significant (without distractor grouping mechanism: $F(1,38)=5.068$, $p=0.03$; with: $F(1,38)=4.604$, $p=0.038$). Both patterns can be found in the resulting RTs which demonstrates that the T_{col} map threshold can explain the behaviour of this measure. Finally, as predicted the distractor grouping mechanism did not alter the RT significantly in the condition tDd ($t(18)=0.921$, $p=0.369$) and TDd ($t(18)=1.1$, $p=0.286$).

Maximum Curvature (MC): Here also a significant main effect of Display Type was found for the model without the distractor grouping mechanism ($F(5,34)=14.073$, $p<0.001$). Here the pairwise analysis found significant differences of the condition tDd with Tdd and TDd. Also tDD was different to all conditions with a large target (Tdd, TDd and TDD). With distractor grouping mechanism there was also a significant main effect ($F(5,34)=12.489$, $p<0.001$). The pairwise results were similar: tDD was still different to all conditions with a large target. Furthermore, tdd was different to TDd and the condition tDd was different to tDD and TDd. Reaches to smaller targets were significantly less curved than reaches to larger targets on both without ($F(1,38)=42.976$, $p<0.001$) and with ($F(1,38)=24.985$, $p<0.001$) the distractor grouping mechanism. The distractor grouping mechanism increased the MC significantly in both, the condition tDd ($t(18)=2.791$, $p=0.012$) and TDd ($t(18)=2.788$, $p=0.012$).

Generally, the MC follows the pattern of the RTs to some extent. The model explains these results through the T map receiving its input from both target and distractor

objects and building up activations over time at all these locations after trial onset. However, the input weightings of the T map are influenced by the T_{col} map so that the distractors are inhibited after the target colour has been chosen. Thus with a small colour difference the T_{col} map needs more time to decide the target colour. This also means that the T map has more time to build up activation at the distractor locations and more time until the distractor inhibition can affect the T map. Importantly, in these maps more than one object can be activated at a time which leads to an increased MC in these conditions. Hence, the longer the RT the more distractor activation still exists upon movement onset and is inhibited only after the movement is initiated which generates the curvature observed in the experiment.

As it was expected the results of the measures followed closely the colour similarity of the objects (see Figure 4.2). However, the colour difference alone cannot explain all of the results, particularly where the graph of the MC differs from the colour similarity graph in the behavioural experiment. The first difference is that conditions with small target objects show less curvature than conditions with large target objects. This behaviour was induced by the T map preferring smaller target objects due to its neural field parameters.

Overall, similar to the behavioural experiment in the conditions with similar target size the effect of the colour difference can be observed, while smaller target objects show a much smaller curvature than large target objects. This effect is smaller in the T_{col} map which was demonstrated by the ANOVA results which were less significant in the RT. This is consistent with the behavioural evidence.

In the behavioural experiment RT and MC also differed in the conditions with an odd-sized distractor. In order to simulate this aspect I introduced an abstract grouping mechanism and performed simulations in both affected conditions (tDd and TDd) with and without this mechanism. The results are shown as red and black data points in Figure 4.5. The results of the modified model without the mechanism did not

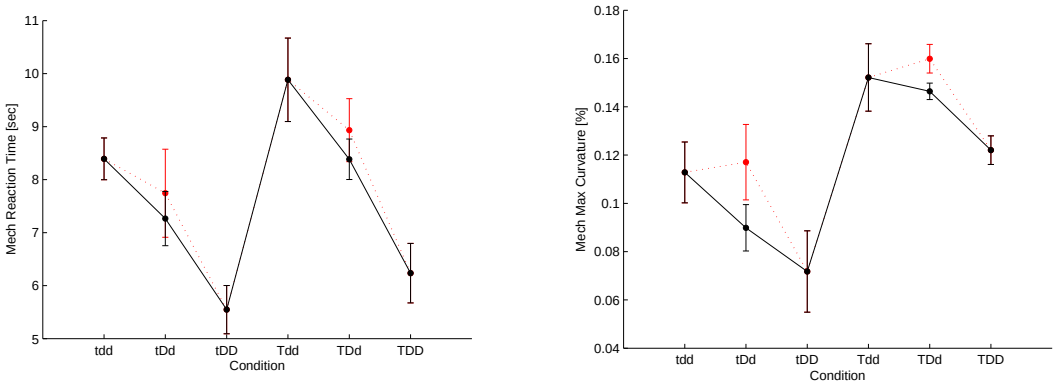

(a) (b)

Figure 4.5.: Results of the odd-colour IF experiment: (a) Mean reaction time and (b) mean maximum curvature values of the simulations in the different conditions. Error bars represent the standard error. The black line shows the results for the simulations of the modified model. The red line shows the influence of the distractor grouping mechanism that is supposed to resemble the results for the conditions with an odd-sized distractor (see text for details).

account for this finding. However, with the mechanism the results of the increased MC in these conditions could be replicated. This was underlined by the significant difference of the MCs and the not significant difference in the RT.

In the following I am going to discuss possible explanations for the observed results in the simulations and implications for the interpretation of the results of the behavioural experiment. The finding that small target objects have an advantage over large target objects can be explained simply due to the fact that smaller target objects are preferred in the target selection stage which leads to a smaller curvature in these conditions. Interestingly, in standard responding tasks larger targets have an advantage over smaller targets (e.g. Proulx & Egeth, 2008). However, as mentioned before in chapter 4.1.3 we suggest that small targets seem to have an advantage in this task as colour is the relevant feature.

Another explanation for this finding could be that large target objects induce a shorter latency. Thus, the smaller latency of large targets induces an increased curvature in

those conditions. Moreover, this explanation is in line with the findings of Song and Nakayama (2008b) and the original choice-reaching model where a shorter RT leads to an increased curvature (see also chapter 3.2). Consequently, also the higher MC with larger target objects can be explained.

4.1.6. Conclusion

In this experiment I investigated the influence of variations in target and distractor size on the odd-colour choice-reaching task of Song and Nakayama (2008b). The behavioural experiment which was conducted by Philip Woodgate showed that the object size influences the latency and the curvature of reaching movements towards the target object. I simulated the experiment with the choice-reaching model of chapter 2.3. In the first experiments of chapter 3, the model had shown its ability to replicate the basic findings of the standard odd-colour task of Song and Nakayama (2008b) and was now tested in this more general setting of the odd-colour task with varying object size. It turned out that the original model required modifications in its control architecture in order to show effects in both measures. Thus, I introduced an additional pathway, modified the parameters of the DNFs, and introduced the abstract distractor grouping mechanism to account for the new findings. The modified model was able to simulate the results of the reaction time very well. Furthermore with the abstract distractor grouping mechanisms also the curvature results could be simulated in detail. Hence, overall the control architecture was able to simulate this variation of the odd-colour task that showed different behavioural results. This gives further support for my model as only minor modifications were necessary to reproduce the behavioural findings.

4.2. Spatial averaging experiment

This experiment aimed to simulate the spatial averaging effect (see chapter 1.3; for an introduction) with an modified version of the original model of chapter 2.3. My experiment consisted of two parts: The first experiment followed closely the rapid reaching experiments of Chapman et al. (2010a). In the following section I will give a more detailed review of their findings. The second part of the experiment aimed to test the model's ability to simulate priming effects in the spatial averaging effect to replicate the results of Chapman et al. (2010b) with the priming maps that were already applied in the experiment of chapter 3.2. Hereby I will show that my modified model is able to replicate their results and that the control architecture based on the dynamic neural field theory is consistent with their theoretical explanations of the effect. Subsequently the results of the model and their implications will be discussed.

4.2.1. Behavioural evidence

As reviewed in chapter 2.1 distractors have shown a clear influence on the reaching process such as an attraction effect (e.g. Welsh & Elliot, 2004). In some experimental setups it has been observed that the endpoint of the trajectory lands in between the target and the distractor objects. This effect has been named "global effect" or "spatial averaging effect" (see Findlay, 1982; Lee, 1999; for reviews).

Recently, Chapman et al. (2010a) designed and performed various experiments to investigate the spatial averaging effect in a choice-reaching task. This allowed them to see how visuomotor decision unfold in real-time similar to the odd-colour task of Song and Nakayama (2009). In their experimental paradigm reaches had to be initiated towards multiple potential target objects under strong time constraints so that the final determination of the target object only took place after movement onset. Hence participants had to select the final target after the initiation of their reach so that

the target selection process occurred during the movement and was visible in the movement trajectory.

Chapman et al. (2010a) found clear indications for a spatial averaging effect in the movement trajectories when one potential target object was placed on the left side and another one on the right side. In an early stage of the movement the movement trajectory pointed towards a location in between the two potential targets. Moreover, the effect was sensitive towards changes of the potential target locations e.g. when the left potential target was placed further left then the initial movement direction accounted for this change. Also different number of potential targets on each side of the display influenced the trajectory: Hereby, more potential targets on one side "pulled" the trajectory towards their side.

In a similar setup Chapman et al. (2010b) also found an influence of previous trials on the spatial averaging effect. There the reach trajectories showed a bias towards the repeated target side. This effect was stronger with more repetitions. So called trial history or priming effects have been observed for a wide variety of movement task. For instance also the introduced odd-colour task of Song and Nakayama (2008b) is influenced by priming of previous trials.

The results of the experiments were consistent with the suggestion that the visuomotor system plans multiple motor plans in parallel (Chapman et al., 2010a). The movement then is an average of those activated motor plans. Evidence for this explanation comes from Cisek and Kalaska (2005) who found brain cells in the premotor cortex encoding possible target locations in a reach experiment with monkeys. Chapman et al. (2010a) suggested that due to their paradigm the visuomotor system was forced to represent all objects as potential targets during the planning process. Subsequently, the following execution of the movement is an probabilistic weighted average plan towards the potential targets. After movement onset, when the target had been defined, the movement was adapted towards the target object.

Attraction effects of distractors have been reported before (e.g. Welsh et al., 1999) and were reviewed in chapter 2.1.3. As explanation for the spatial averaging effect has been suggested that this effect can be observed due to the fact that the internal representations of target and distractor objects can overlap especially when they appear in spacial proximity (Chapman et al., 2010a). Thus, the representations of two objects or their appropriate motor plans could join when they are close and form a larger combined activation that results in a movement to the spatial averaged location. This effect also has been observed for both, arm and eye movements (Georgopoulos, Schwartz, & Kettner, 1986). In this way target and distractor objects initially are encoded as potential targets and distractor objects have to be inhibited over the course of time. However, in a rapid reaching task there might be insufficient time for those processes to complete and the reach is initiated towards an average location.
I attempted to simulate the experiments of Chapman et al. (2010a, 2010b) regarding the spatial averaging effect with my model. I will show that the model is able to replicate above effects with its control architecture based on the dynamic neural field theory.

4.2.2. Modifications of the model

In order to be able to perform the following experiments the original model (without the modifications of the previous experiment) had to be modified within the Target Selection module (see chapter 2.3.2 for the original setup). Unlike the previous experiments colour did not play a role in this experiment; thus the T_{col} map was deactivated. The colour maps for green and red colour were topologically added and fed as input into the T map. However, the object colour was used to distinguish between (green) non-target and (red) target objects after movement onset (see Figure 4.6). Note that this is a technical implementation to determine the final target object

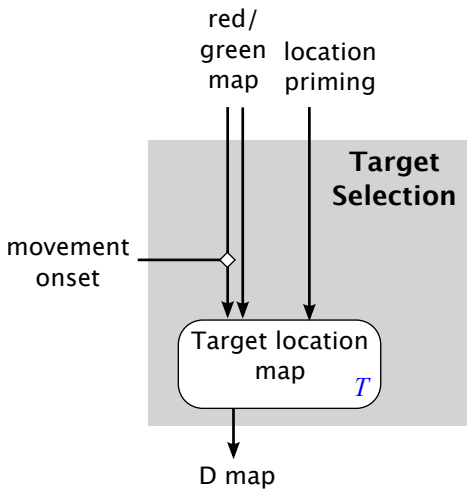

Figure 4.6.: Overview of the modified Target Selection module for the spatial averaging experiments. The topological sum of the two colour maps is fed into the T map as input. However, after movement onset the input from the green map is blocked in order to distinguish between potential target objects and the final target object. For the second part of the experiment location priming was applied in some conditions similar to the odd-colour experiment. For a complete overview of the control architecture I refer to Figure 2.4.

after movement onset. In the experiments of Chapman et al. (2010a) this was realised with empty circles (for potential target objects) before movement onset and filled circles (for final target objects) after movement onset. The mathematical details of the technical implementation can be found in the Appendix in chapter A.1.4.

In first test simulations it turned out that the time the model needs for processing the changes of the target after movement onset is too short so that the model immediately moved towards the final target object and no effect in the measures could be observed. Therefore, the processing time was artificially extended by introducing a *dead-time* parameter which simply extended the information processing of the T map and gave direct control about the processing time. Note that this is similar to the visual delay of humans which was reviewed in chapter 1.2. The dead-time parameter will also be applied in the goal-directed reaching model in chapter 5.

In order to apply the priming effect some sort of short time memory module is

necessary. My model has shown before that the application of priming maps can lead to a similar effect (see the odd-colour experiment of chapter 3.2). The technical implementation of the priming effect in this experiment is similar to the odd-colour experiment. The priming took place in the T map of the model which received a priming map as an input signal before the actual trial took place (see Figure 4.6). This priming effect was implemented by adding a Gaussian activation to the location of the potential target object which had to be primed. With this method the T map already contained some activation before it received the input from the colour maps.

4.2.3. Methods

The hardware setup of this experiment was similar to the first series of experiments (see chapter 3). The target objects were square coloured markers (red or green) with 3.5 cm length of the edge and were placed in front of the robot arm depending on the experimental condition.

The experiment was divided into two parts. First, several conditions were performed which based on the setting of Chapman et al. (2010a): A single-target baseline (BL) condition was performed to see the trajectories without influence of distractors (similiar to the setting of chapter 3.1). Furthermore, the spatial averaging effect was simulated in different settings with two potential target objects arranged in a symmetrical fashion (1-1) or shifted to the left (SL) or the right side (SR). Also conditions with three (2-1, 1-2) potential target objects were performed. Figure 4.7 shows details of the arrangement of the markers in the different conditions.

For the priming conditions in the second part of the experiment only symmetrical two target displays (similar to condition 1-1) were conducted. Two different levels of priming (low - P1 and high - P2) were applied towards either on the left or on the right side. Only trajectories towards the primed target side were recorded so that the

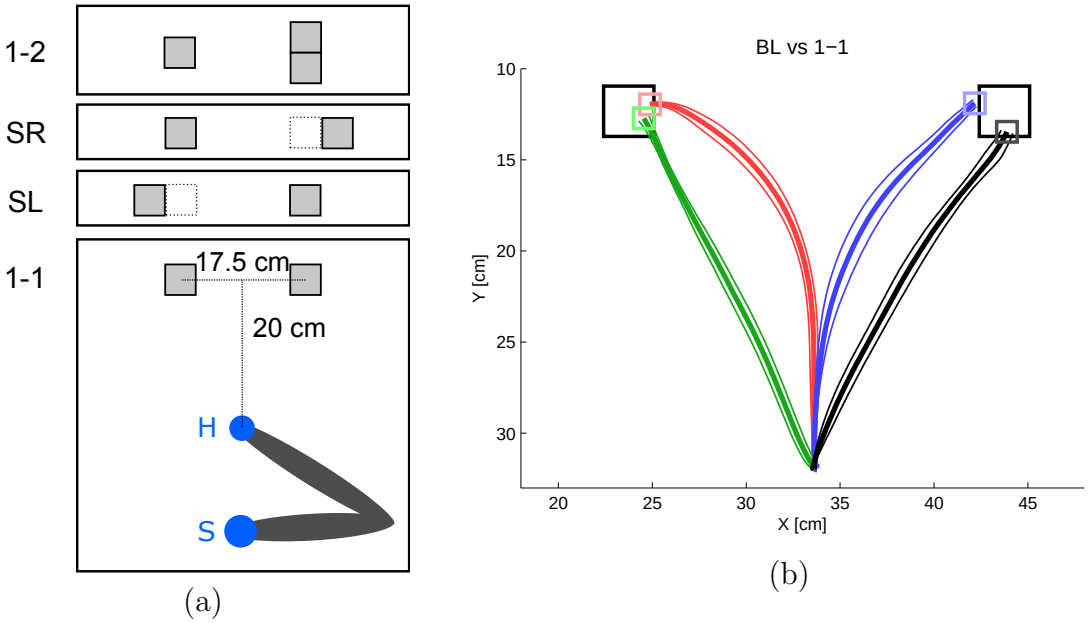

Figure 4.7.: (a) Object placement in the spatial averaging experiment in the different conditions. The abbreviations of the conditions mean: two target displays (1-1), shifted left/right (SL/SR), three target displays with two targets on the left (2-1; not shown) or right (1-2) side. (b) Resulting trajectories of the single target baseline (BL) condition (black and green) and of the two target displays (1-1, blue and red). The trajectories (bold lines) are averaged trajectories of five trials and shown with their standard deviation (thin lines). The two target displays have a much higher curvature than the single target displays. Moreover, they initially point to the midpoint in between the two potential target objects in the early stage of the movement which is clear indication for the spatial averaging effect.

final target always was on the primed side. These two conditions were compared with the two target display (1-1) and the single target condition (BL) of the first part of the experiment.

As mentioned before the determination of the target object occurred after movement onset which was considered as the point in time when the peak activation in the V map (the moving blob) reached a distance of a least two neurons away from the centre of the map. In each condition five trajectories were recorded.

The data processing was similar to the previous experiment: a B-Spline (3rd order) and a Butterworth filter (2nd order) were applied on the raw data points. As the experiment focussed on the trajectories and their Maximum Curvatures (MC), these

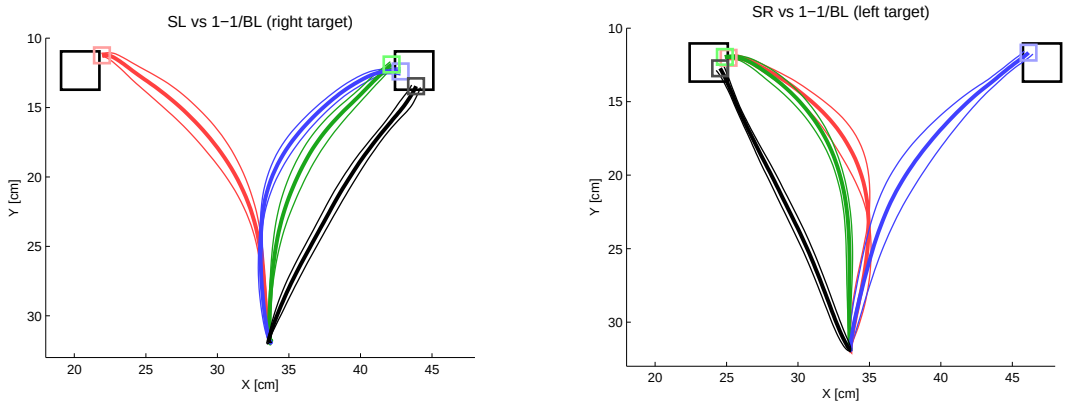

(a) (b)

Figure 4.8.: Trajectories of the shifted two target displays (red and blue; (a) SL and (b) SR) of the spatial averaging experiment compared with the symmetric two target (green; 1-1) and the one target displays (black; BL). In the shifted conditions the midpoint of the two objects is slightly further away from the target of the not shifted side which increases the curvature of the trajectory even more in comparison with the trajectory of the 1-1 condition.

two measures were recorded and obtained from the raw data similar to the previous experiment. The detailed values of all parameters of the simulation of this experiment can be found in the Appendix in chapter A.2.7.

4.2.4. Results weighted spatial averaging effect

In this section I am going to present the results of the first part of the experiment. The results of the different conditions will be presented separately. The detailled values of the MCs can be found in Table 4.1.

Single target displays (BL): When only one target was presented, the trajectory was fairly straight and the maximum curvature was very low with values lower than 5% (see Figure 4.7). This was independent of the side where the target appeared. This result was expected and is consistent with the earlier single-target experiment of chapter 3.1.

Two target displays (1-1): In the two target displays much higher curvatures were

observed. A comparison of the trajectories of the single target displays with the two target displays can be found in Figure 4.7. By exploring the mean trajectories of the movement it can be seen that this effect can be accounted to a spatial averaging effect: In the early stage of the movement the hand reaches towards a point in between the two potential targets. After the final target has been detected the movement trajectory gradually changes towards it.

This behaviour arises directly from the moving blob in the V map. Due to the broad overlapping input activation in this DNF the movement initially points toward an intermediate location of the two potential target objects and is later corrected towards the final target.

Shifted two target displays (SL, SR): The trajectories of these conditions where either the left potential target object was shifted to the left side or the right one to the right side can be found in Figure 4.8. When comparing the trajectories of the not-shifted side of the SL and SR conditions with the 1-1 condition it can be seen that the shifted object had a clear influence on the trajectory of the movement. Here also the observed curvature values of SL and SR were increased more than the curvatures of the 1-1 condition (see Table 4.1). The reason for this is the shifted midpoint of the two potential target objects. Hence the moving blob and also the trajectories in an early stage of the movement now pointed towards the new midpoint. This shows that the averaging effect is sensitive towards changes in the location of the potential target objects.

Three target displays (2-1, 1-2): Presenting two potential target objects on one side and one object on the other side had a similar effect than the shifted target objects before: The movement direction in an early stage of the movement pointed towards the side with the two targets (see Figure 4.9). Again the trajectories of the 1-1 condition were compared with the unaltered side (the side with one potential target). Here the influence of the opposing two potential targets caused the curvature to increase even

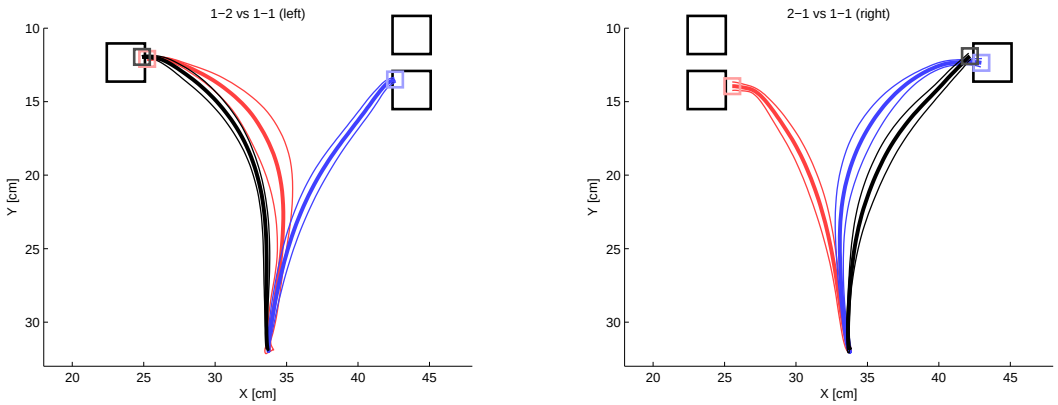

(a) (b)

Figure 4.9.: Trajectories of the three target displays (red and blue; (a) 1-2 and (b) 2-1 condition) of the weighted spatial averaging experiment in comparison with the two object displays (1-1) on the side with only one potential target object (black). The two potential targets pull the trajectory towards their side so that the curvature towards the one-target side is increased.

more, however, the MC was decreased on the other side with two potential targets. This result is a clear indication that the spatial averaging effect is weighted depending on the number of potential target objects.

Overall the results are consistent with the findings of Chapman et al. (2010a). First my model successfully simulated the spatial averaging effect in the two target displays (1-1) which showed a greatly increased curvature compared with the single target displays. Moreover, the effect was sensitive towards slightly changed locations of the potential target objects in the SL and SR condition and a weighted effect in the three target displays (1-2, 2-1) could be observed. In that way all aspects of the spatial averaging effect that were found by Chapman et al. (2010a) could be simulated with the implemented control architecture of my model.

4.2.5. Results primed spatial averaging effect

This section presents the results of the second part of the experiment where the influence of priming on the spatial averaging effect was investigated. The priming

condition	MC [%]	condition	MC [%]
BL		**SR**	
left	3.9 (0.7)	left	25.1 (0.1)
right	3.6 (0.5)	right	13.3 (0.4)
1-1		**2-1**	
left	18.5 (3.3)	left (near)	16.0 (0.4)
right	14.3 (0.7)	right	25.4 (0.3)
SL		**1-2**	
left	15.2 (1.5)	left	28.5 (0.1)
right	24.1 (0.7)	right (near)	10.8 (4.8)

Table 4.1.: Maximum curvature results of the weighted spatial averaging experiment: Displayed are all conditions with their mean values of the Maximum Curvature (MC) with standard deviations (in brackets). In the left column the bold text describes the condition and the normal text specifies the target location. Due to the spatial averaging effect all experimental conditions have a much higher curvature than the one object baseline conditions. For the discussion of the conditions see the text.

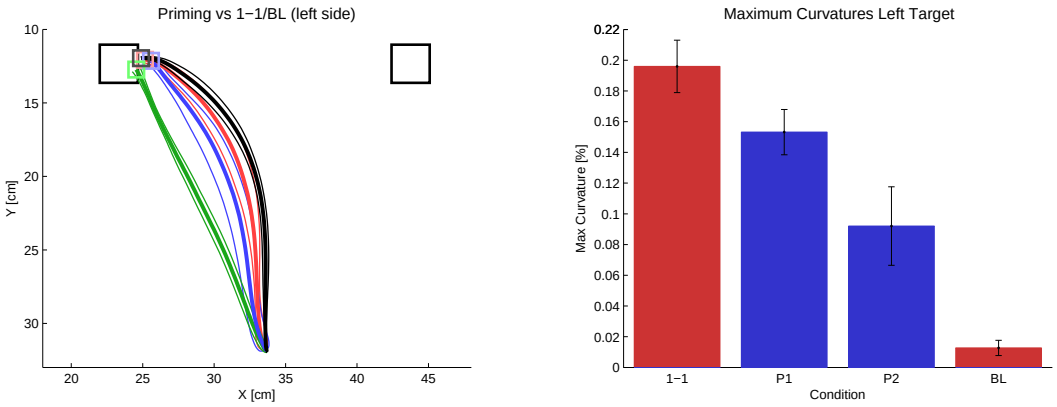

(a) (b)

Figure 4.10.: Trajectories of the primed spatial averaging effect towards the left target side (a) and their maximum curvatures (b). The priming decreases the curvature and shifts the trajectory towards the primed object. This effect is even stronger with a higher priming strength.

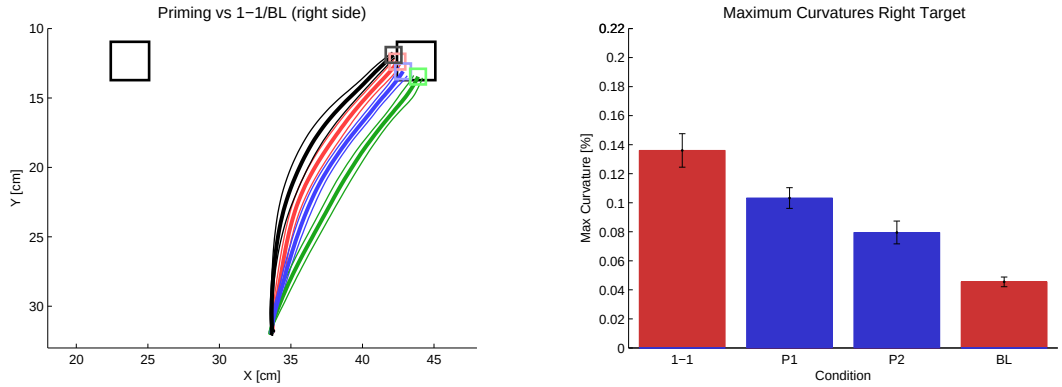

(a) (b)

Figure 4.11.: Trajectories of the primed spatial averaging effect towards the right target side (a) and their maximum curvatures (b). Again the priming shifts the trajectory and decreases its curvature.

had a strong influence on trajectory and curvature. The trajectories of the priming conditions P1 and P2 differ clearly from the two target display (1-1) trajectories as they show a bias towards the primed target side. This bias was stronger with a higher level of priming (see the left side of the Figures 4.10 and 4.11). However, the biased trajectories still differ significantly from the single target trajectories.

This effect is also visible in the MCs. The curvatures of the P1 and P2 condition are in between the high curvature of the two target displays and the low curvature of the single target displays. Moreover, with a higher level of priming (P2) the curvature was even more decreased than in the low level priming condition (P1) compared to the two target display (1-1) (see the right side of the Figures 4.10 and 4.11).

Note that the values of the MCs differed slightly between the left and right target side. As the standard deviations of trajectory and curvature were fairly low this can be explained with different kinematic constraints for the arm's joints when reaching for the left and the right side.

Also in this part of the experiment the behavioural results could be replicated by my model. In the following I will summarise and discuss the findings of the two parts of the experiment.

4.2.6. Discussion & Conclusion

The main purpose of the spatial averaging experiment was to show that the control architecture of the odd-colour model with its underlying framework of the dynamic neural field theory is applicable to a wider range of choice-reaching tasks. In order to prepare the model for the requirements of these experiments, i.e., no colour feature and the technical implementation of potential and final targets the original model of chapter 2.3 had to be modified in the Target Selection stage.

In the first part of the experiment I demonstrated that the modified model is able to reproduce the spatial averaging effect when two potential target objects are presented at trial start and the target only is specified after movement onset. The resulting movement was initiated towards a location in between the two potential target objects and only after the target was detected the movement was adapted. Moreover the spatial averaging effect had a similar sensitivity than in the experiments of Chapman et al. (2010a) which could be seen in the shifted and three object conditions where the initial direction of the trajectory changed with a different placement of the potential target objects or by adding a third object to one of the target sides.

Chapman et al. (2010a) suggested that overlapping activations are the reason for the spatial averaging effect. In my model potential target objects establish separate hills of activation in the T map after trial onset which mainly reflects the input. Then those target activations are passed through further into the model as inputs for the D map and cause the development of activations there. Finally, in the V map the overlapping of the targets happens: Here broad activations are combined in order to perform the moving blob behaviour (see also chapter 2.3). Due to the DNF parameters in earlier processing stages (T, D map) no overlapping occurs unless the spatial difference of the potential target objects is very small. Later, in the V map those activations are broadened and therefore influence the moving blob to move towards a location in

between the targets. The experiment showed that this averaging is sensitive towards changes in the potential target objects' location. Thus, the model confirms that it is applicable to generate the spatial averaging effect in that way.

The second part of the experiment aimed to simulate short-term motor plasticity of the spatial averaging effect with the help of priming maps. Hereby, the model was able to replicate the results of the study of Chapman et al. (2010b). When one target received an initial activation before trial onset from the priming map the resulting trajectory was biased towards the primed target side. Large differences between trajectory and maximum curvatures of the priming, two-target and single target conditions could be found. The primed trajectories differed clearly from the baselines and the strength of the bias varied with the strength of the priming so that the trajectories were straighter with a stronger priming. This biased trajectories were explained by Chapman et al. (2010b) with the "effects of repeated cueing on the attentional landscape". In this way the repetition primes the repeated target and affects the weightings of the motor plans assigned to the potential target objects. These movement parameters are accumulated from trial to trial so that the effect becomes stronger with an increased number of repetitions.

My model implements such attentional landscapes in the two-dimensional DNFs. This is also the location where the observed behaviour is realised. The T map is responsible for the target selection and receives the priming activation before trial onset. Hence the primed location will have a stronger activation here. Then the same mechanism that causes the spatial averaging creates the biased trajectories: While in the Target Selection module (potential) targets establish separated activations they overlap and join in the velocity map to create the moving blob behaviour. When one target side is primed then its belonging activation will be larger thorough all DNFs behind the T map (D and V map). Hence the movement vector has a bias towards the primed target side and only slightly shifts the initial movement direction towards the primed

target which eventually causes the shift in the trajectory.

My model demonstrates that it can be sufficient for a priming method only to affect the target selection stage in order to generate this behaviour as the movement vector is continuously generated in a closed-loop fashion. Thus the execution of the movement only depends on the target weightings and the parameters that direct the moving blob. In this way the parameters that directly control the movement (the moving blob parameters) remain unchanged and only the weightings of the potential target objects are adapted in between trials.

The fact that the modified model was able to simulate both spatial averaging effect experiments gives further support that the control architecture of my model works in a similar way like the attentional and movement preparation processes in the human brain. Note that the model originally was designed to simulate the odd-colour task (chapter 3). Nevertheless, with only minor modifications to the Target Selection module the results in the simulation of the spatial averaging effect are similar to humans. Hence, the model can be seen as an appropriate tool to simulate such choice-reaching experiments.

4.2.7. Further experiments

Recently various related studies of the simulated experiments of Chapman et al. (2010a) and Chapman et al. (2010b) were published. While it was not possible to simulate or discuss all of them more deeply in this thesis I am going to present a short summary about their results and implications for my model here.

The first study of Chapman and Goodale (2008) dealt with perturbation effects (the target jumped upon movement onset) and the influence of physical obstacles. The results showed that physical non-target obstacles can cause an avoidance or repulsion effect in the trajectory of the movement. They also observed velocity reductions when

there was a risk of collision. In my model such a behaviour could be realised with an interplay of negative activations caused by obstacles that push the moving blob away from the obstacles to avoid collisions and the *Onset* mechanism of the goal-directed reaching model (which slows down the hand when the perturbation occurs; see also chapter 5).

In a different setting Wood et al. (2011) tested if the spatial averaging effect is influenced by the saliency of the potential target objects. They found that the movement trajectories were biased to the side of higher salient objects. They suggested that this was due to a possible influence of saccades as they also found that the movements veered towards the position where the participants looked. Moreover they suggested that this effect could be observed due to the fact that a fast direct route prefers the salient objects. Later those preselected salient objects have to be inhibited which takes more time. My model is not designed to simulate saccades, however, more salient objects could receive a larger input activation in the T map leading to a similar result.

In the last experiment that I present here Gallivan et al. (2011) conducted a rapid-reaching task similar to the spatial averaging tasks of Chapman et al. (2010a) with a larger number of objects (up to 16 per side). They found that the spatial averaging effect occurred only up to a number of four presented potential targets objects per side and explained these findings with the fact that only a limited number of objects can compete for attention at a time. Furthermore, they were not able to find a size effect with potential targets of different sizes. Regarding potential simulations of a similar experiment in my model it can be said that it does not have a strict upper limit for target objects which can be encoded. However, due to the mechanism of local excitation and global inhibition the parameters of the DNFs (T, D map) could easily be adjusted in a way that only a limited number of potential target objects can establish activations at a time. For instance a higher inhibition would suppress

smaller inputs and only fewer (and higher) inputs would establish activations in the DNF. Moreover, larger groups of potential target objects might be perceived and encoded with only one activation particularly when the objects are close to each other like in the setup of Gallivan et al. (2011). Regarding the fact that they could not find a bias toward larger potential target objects, this could be simulated with appropriate parameters in the Target Selection module so that the size feature is not passed through onto the motor stage.

To conclude this section it can be said that it would be possible to simulate the mentioned experiments with only minor modifications to the control architecture of my model which gives further support for my approach to explain the choice-reaching tasks.

4.3. Simon effect experiment

This last choice-reaching experiment aimed to simulate the Simon effect. I already introduced the Simon effect and the choice-reaching task of Scherbaum et al. (2010) in chapter 1.3. Here I am going to review more behavioural evidence about the Simon effect before I present the experiment and the simulations of my model.

4.3.1. Behavioural evidence

In experiments regarding the Simon effect stimuli (cue objects) with multiple (at least two) dimensions such as colour or location are presented. One dimension (e.g. colour) determines the to be selected response, while the other stimuli feature (e.g. location) has to be ignored. From measures such as reaction times or movement trajectories the effect of the irrelevant information on the processing of the stimuli can be investigated. In a typical Simon task irrelevant spatial information has to be ignored whereas the non-spatial information (e.g. sound or colour) of the cue encodes the target (see

Hommel, 2011; for a review).

Historically the Simon effect was discovered in keypress experiments (see Simon, 1990; for a review). There, subjects were instructed to perform keypresses to pitched tones of different frequencies. When perceiving a high tone the subjects had to press the right key and with a low tone the left key. The surprising discovery of this experiment was that subjects responded significantly faster when listening to the high-tone with the ear on the (associated) right side than with the other side. This effect of a non-relevant dimension (location) in the stimulus was interpreted as a natural tendency to react toward the source of the stimulation. Consequently, the effect is now commonly known as the Simon effect and has been replicated in numerous experiments (see Lu & Proctor, 1995; Simon, 1990; for reviews). A popular setup to show the Simon effect uses red and green coloured markers as cue objects where each colour encodes a target side. The cue can appear on either the left or right side therefore the trials can be divided into congruent (where the cue location matches the target location) and incongruent (cue on opposite side than the target location) conditions. In congruent trials the cue matches the encoded target side while in incongruent trials the opposite target side is encoded. The strength of the effect is measured with the difference of the reaction times of incongruent and congruent trials (see Figure 4.12).

In the last decades the Simon effect was thoroughly investigated. For instance, it could be shown that under certain circumstances the Simon effect can be reversed (when the target sides are logically re-coded, DeJong, Lian, & Lauber, 1994; for a review). Further it was found that for trials with faster reaction times the effect is stronger than in slower responses. For this reason often the time course of the Simon effect is explored. The typical effect that can be found is a decreasing (even disappearing) Simon effect with increasing Reaction Time (RT). However, the reversed Simon effect tends to increase in slower RT bins.

Recently, the paradigm of the choice-reaching tasks (see also chapter 1.3) was applied

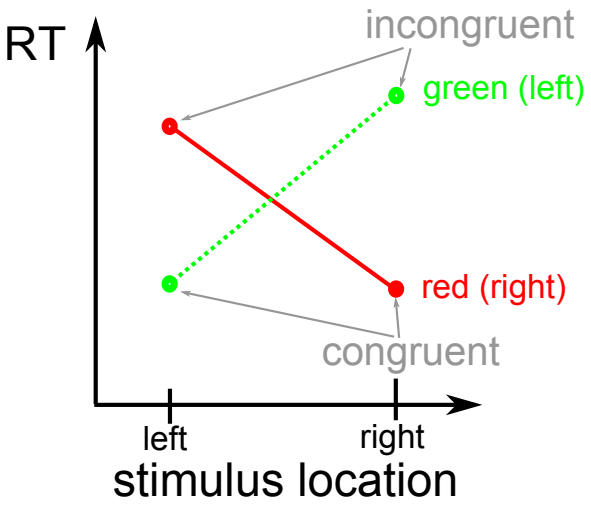

Figure 4.12.: Typical observed Reaction Times (RTs) in a Simon task where the stimulus colour (green/red) encodes the response key location (left/right): In congruent conditions (stimulus location = encoded key location) RTs are faster, in incongruent conditions RTs are slower.

for experiments regarding the Simon effect. One of the first experiments is the work of Rubichi and Pellicano (2004) who investigated the influence of response strategies on the Simon effect. In their experiments they forced the participants to apply a particular response strategy (response with one hand where the movement direction had to be selected versus two hands where the responding hand had to be selected). The Simon effect occurred during the reaction time when the response-selection can be terminated before movement onset and in the movement time when the movement onset occurs before the definite selection of the correct response.

In a similar setup Buetti and Kerzel (2008, 2009) made use of movement parameters of the trajectory: they measured the Initial Movement Angles (IMA) of the movement after 20% of the Movement Time (MT). They investigated the size of the Simon effect in different measures and the influence of different response selection strategies. In their studies they found a Simon effect in the IMAs which decreased the greater the RTs were (Buetti & Kerzel, 2008). This was the case for settings for the introduced visuomotor and cognitive Simon effect what suggests that there is one underlying

mechanism for both. Buetti and Kerzel (2009) confirmed these results with a wider range of experiments: Under time pressure the Simon effect almost disappeared in the RTs but was stronger in the IMAs. In contrast, with advanced movement preparation (i.e. more time before movement onset) the Simon effect was reduced in the IMAs, however, increased in the RT. Buetti and Kerzel (2008) suggested that the Simon effect in RTs is caused by response selection while the effect in the trajectory is caused by the response programming, however, both effects might have a single underlying mechanism.

Interpretations and models of the Simon effect

Different explanations and models came up to explain the observed effects of Simon tasks. It can be considered as accepted that the Simon effect affects the response-selection stage rather than stimulus encoding stage (Simon, 1990). The most popular explanation that accounts for this fact is the so-called *dual-route model* (see Figure 4.13 and Kornblum, Stevens, Whipple, & Requin, 1999; for a review). It presumes that two routes are responsible for producing the Simon effect: a direct route where the stimulus location activates the corresponding response code and an indirect route to determine the correct response with the relevant stimulus dimension. In a congruent trial both stimulus dimensions activate the same response, which facilitates responding, whereas in incongruent trials different responses are activated causing a response conflict that has to be resolved.

A similar explanation was made by DeJong et al. (1994). According to their interpretation the stimulus affects two processes: First, after stimulus onset an unconditional component induces activation at the stimulus location and also primes the motor response toward this location. This activation vanishes quickly over the time and leads to a decreasing Simon effect in slower RT bins. This effect was also described by Hommel (1994) as spontaneous decay of the irrelevant spatial response. Second, the

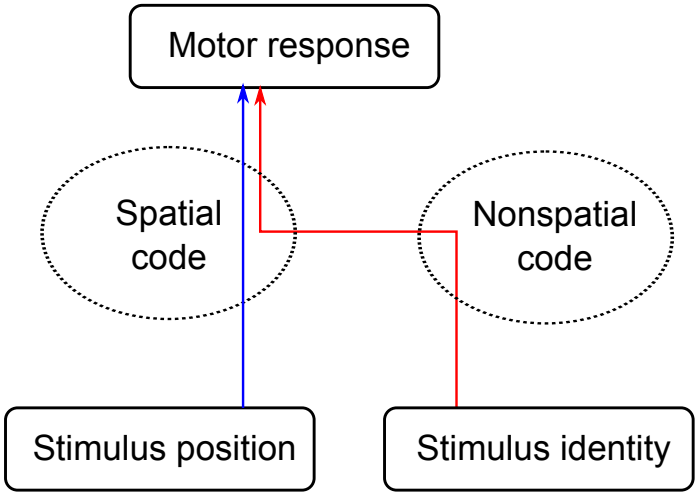

Figure 4.13.: Dual-route model to explain the Simon effect. After the onset of the stimulus its location primes the spatial code on and a motor response towards its location (blue arrow). It takes some more time to process the stimulus identity (and to logical recode it if necessary), thus the non-spatial code influences the motor stage slightly later (red arrow). Congruent trials are faster due to the already existing priming in the spatial code and the motor response, while incongruent trials are slower because a recoding in these areas has to take place. Picture depicted from Metzker and Dreisbach (2009).

conditional component depends on the mapping of the stimuli and does not depend on the RT. Within this process the identification of the nonspatial stimulus feature takes place as well as the transformation rule. The conditional component only depends on the stimulus-response mapping while the unconditional component is able to give an explanation for the time course of the regular (decreasing in slower RT bins) and the reversed Simon effect (increasing).

4.3.2. Modifications of the model

My experimental setup was similar to the studies of Scherbaum et al. (2010) and Buetti and Kerzel (2008). They used paradigms where a cue (an arrow or a coloured marker) appeared on either the left or the right side. This cue indicated the target side which had to be reached. In those experiments the Simon effect could be observed in both the Reaction Time (RT) and the trajectory. However, as mentioned in the

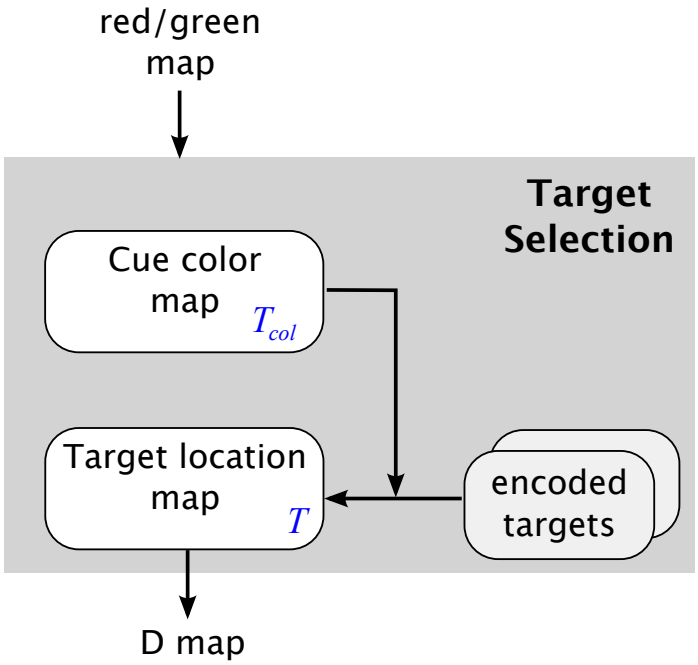

Figure 4.14.: The Target Selection module of the modified control architecture of the Simon task model. For the original model and the complete control architecture see Figure 2.4. The cue colour map works in a similar way than the target colour map of the original model. However, this map now is connected to non-dynamical encoded target maps that already contain activations at the locations of the two possible target regions. In this way the cue colours activate their appropriate target region. The Simon effect results from the fact that the cue location also directly is fed into the T map. This information has to be overwritten by the activated cue colour and its encoded target.

previous section other experimental evidence suggests that with a shorter RT the trajectory tends to be more curved, however then the Simon effect in the RT is diminished. Vice versa with longer RTs the trajectories are straight, but the Simon effect can be observed in the RTs (Rubichi & Pellicano, 2004; Buetti & Kerzel, 2008). Few modifications were necessary in order to implement the experimental setup consisting of cue object and its encoded target position. Similar to the previous experiment these modifications regarded only the Target Selection module and will be presented in the following. Earlier experiments with my model (e.g. chapter 3.3) showed that the RT can be controlled in an easy way by changing the value of the threshold between the T and D map. This threshold parameter th_T controls how

much activation is necessary to initiate the movement, hence two conditions with different values of th_T will be conducted to observe the Simon effect in the RT (high threshold) and the Maximum Curvature (MC; low threshold).

Instead of using arrows that indicate the target side, I use colours to define the side of the target that has to be reached. This is a solution that is closer to the odd-colour experiments and requires less modifications of the model. Note that experimental designs with coloured cues that indicate the target side have been applied before (e.g. Rubichi & Pellicano, 2004).

In order to detect the cue colour and the target side that it encodes the Target Selection module had to be changed. Hence a slightly modified version of the model of the odd-colour task of section 3.2 was used for this experiment (see Figure 4.14). For the Simon task model the output of T_{col} was not connected to the colour maps, but to the weights of two predefined target locations maps (left, right) that feed into the T map. These predefined target maps were non-dynamical maps each containing a Gaussian activation on either the left of the right target location. In this way, the cue location will play a role in an early stage of the simulation as the colour maps serve as a direct input for the T map, however, the predefined target maps will dominate the input activation in the T map once the cue colour in encoded in the T_{col} map as their weightings are higher. This can be interpreted as the non-spatial route in the dual-route models so that the target side solely depends on the cue's colour and not on its location.

4.3.3. Methods

The hardware setup was similar to the earlier experiments. The target locations were located 20 cm in front of the robot arm identical to the locations of the 1-1 condition of the spatial averaging experiment (see Figure 4.7). The cues were red or green

coloured markers (3.5 cm length of edge) which were placed either at the left or the right target location.

The experiment had two factors with two conditions each. The first factor was the congruency of target side and cue. The target side had to be identified by the colour of the cue object. Hereby green encoded the left target while red encoded the right target. In the congruent condition (C) the side of the cue also was the encoded target side while in the incongruent condition (I) the cue appeared on the opposed side. The second factor was the strength of the threshold, which could a low value (*low*; $th_T = 0.2$) or a high value (*high*; $th_T = 0.95$) depending on the threshold th_T between the T and the D map.

The trajectory data and the measures (Reaction Time, RT; Maximum Curvature, MC) were obtained and analysed like in the previous experiment. For each condition five trajectories were recorded. The model parameters can be found in the Appendix.

4.3.4. Results & Discussion

As it was of no significance for the model whether the cue colour is red or green, only the results for red coloured cues for the different conditions (C/I, high/low) are documented here. The results with the green cues were identical, however, mirrored as green encoded the opposite target colour. The results of the RTs and the MCs of all conditions are displayed in Figure 4.15, the movement trajectories can be found in the Figures 4.16 and 4.17.

The effect of the different threshold values were as expected: With a high threshold straight trajectories in both congruent and incongruent condition could be observed (see Figure 4.16). In this condition the determination of the target side had sufficient time to complete before the threshold in the T map was reached and passed along to the D and V map which caused the initiation of the movement. However, the

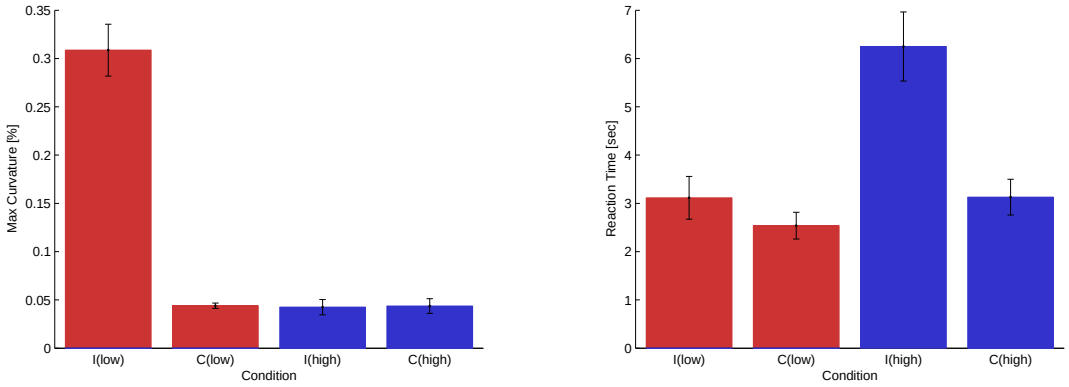

(a) (b)

Figure 4.15.: Maximum curvatures (a) and reaction times (b) of the different conditions in the Simon task experiment. In the low threshold conditions (red colour) the Simon effect occurs after movement initiation during the reaching process as the maximum curvatures are very different here but the RTs are almost identical. In contrast, in the high threshold condition (blue colour) the congruency does not influence the curvature but the RTs of congruent and incongruent trials differ clearly. Moreover, both RTs in the high threshold are higher than the RTs of the corresponding low threshold conditions.

congruency strongly affected the RT so that a large Simon effect could be seen in this measure as the RT of the incongruent condition is much higher than the RT of the congruent condition. The reason for this is the dynamic in the T map; here the cue caused a small activation after it appeared. Hence the correct target side can build up activation much quicker when it got the bonus activation from the cue in the congruent condition.

In the low threshold condition less activation in the T map was needed influence the moving blob in the V map. This had a visible effect on the resulting trajectory in the incongruent condition. Here a significantly higher curvature could be observed. The reason for this is that the activation in the T map caused by the cue object was high enough to surpass the threshold and to initiate the movement. Hence the movement was initiated much quicker and the trajectory pointed initially towards the location of the cue (see Figure 4.17). In the congruent condition no differences could be observed

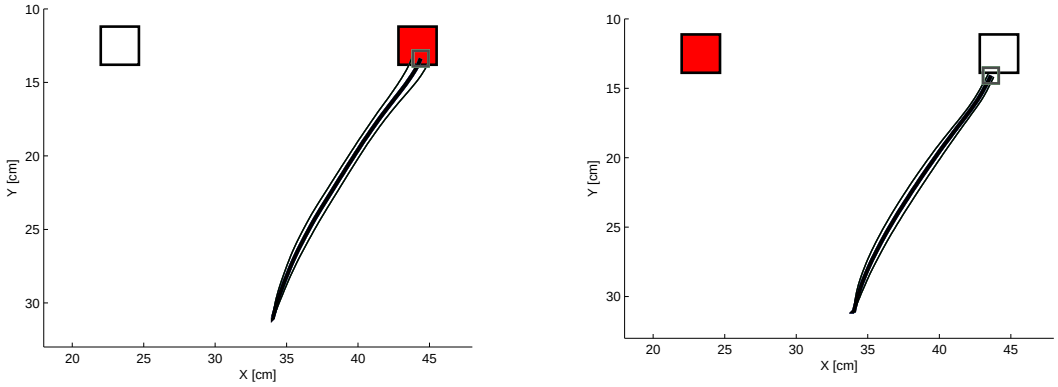

(a) (b)

Figure 4.16.: Trajectories of the Simon task experiment in the high threshold condition. The red colour encoded the right square as target object. (a) shows the congruent and (b) the incongruent condition. The congruency does not influence the trajectories, both reached the right target object with a straight path.

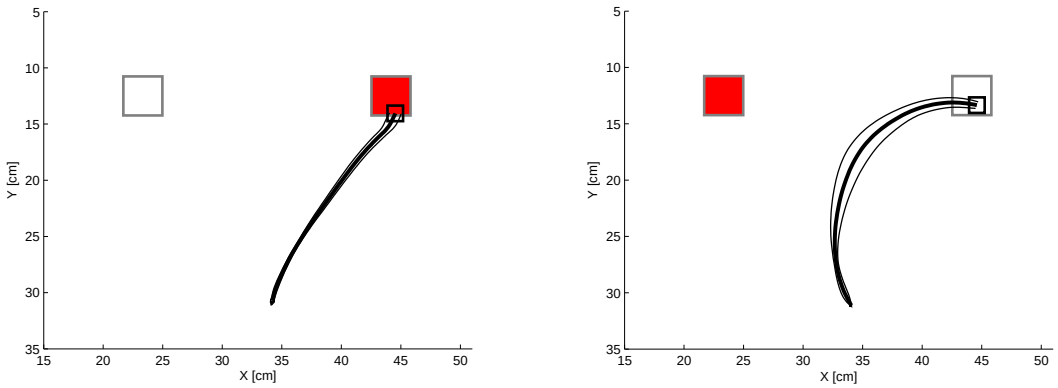

(a) (b)

Figure 4.17.: Trajectories of the low threshold condition of the Simon task experiment. The red colour encoded the right square as target object. (a) shows the congruent and (b) the incongruent condition. Due to the low threshold the movement is initiated towards the cue location. This results in a highly curved trajectory when the cue appears on the non-target side as the movement has to be corrected.

and the trajectory was straight like in the high threshold trials as the cue's location was identical with the target location here. However, the RT here was only slightly faster than in the incongruent condition because the low threshold diminished the difference in this measure.

The results in the low threshold condition are consistent with the experimental evidence of Scherbaum et al. (2010) who also found differences in the movement trajectory depending on the congruency. Moreover, the overall results are consistent with the findings of Rubichi and Pellicano (2004). They performed an experiment with lateral movements and found a similar effect of a strong Simon effect in the trajectory when the RTs are low and no differences in the trajectories but a Simon effect in the RTs when the RTs were high. Their explanation follows the dual-route models which see the Simon effect as a response selection phenomenon. According to this the Simon effect should occur in the RT if the target side is selected before movement initiation or in the trajectory (or curvature/ movement time) if the target side is selected after movement initiation. This view was confirmed by Buetti and Kerzel (2008) in a similar experiment. According to them large trajectory deviations occur for fast responses as the cue directly activates a motor response. With the passing of time this automatic activation is inhibited and overwritten by the encoded target side.

With the architecture in the Target Selection module my modified model follows the dual-route models of the Simon effect as the location of the cue influences the target selection map in an early stage (direct spatial route) and the colour in a later stage (indirect non-spatial route). In my model for the Simon task the direct spatial route is implemented with the direct connection of the colour maps to the T map while the indirect route influences the T map only after the colour of the cue has been processed in the T_{col} map and the existing (spatial) information is overwritten.

4.3.5. Potential extensions of the experiment

The experimental paradigm of my simulations was inspired by the experiments of Scherbaum et al. (2010), however unlike in their experiment not inter-trial effects but the occurrence of the Simon effect in RT and trajectory was investigated similar to the experiments of Buetti and Kerzel (2008) and Rubichi and Pellicano (2004). With only a few adjustments of the Simon task model it would be possible to simulate all aspects of the experiment of Scherbaum et al. (2010). In the odd-colour experiment of chapter 3.2 it was shown that priming maps can be applied to simulate priming effects of colour or location. The Simon task has a different setup, however, the priming effects for the target location were simulated in a similar way.

4.3.6. Simon effect models

Before concluding the Simon effect experiment it should be noted that there already exist numerous models to simulate the Simon effect. I am going to introduce a few computational models here. The first is the model of Kornblum et al. (1999) that accounts for stimulus-stimulus and stimulus-response consistency effects. It assumes that the processing of those effects is divided into the sequential stages of *stimulus processing* and *response production*. Accordingly, the model consists of two layers: an input and an output layer. Each layer consists of modules of neurons which represent stimulus dimensions (in the input layer) and response dimensions (output layer). Another example for a computational model for the Simon effect is the one of Tagliabue, Zorzi, Umilta, and Bassignani (2000) who investigated the role of long and short term memory on the Simon effect in a series of experiments and developed a computational model to explain these findings. Also DeJong et al. (1994) presented a computational model that deals with the Simon effect and its reversion based on the dual-process hypothesis.

All these models are able to simulate the fundamental characteristics of the Simon effect, including its reversal and its time course. However, these models are all isolated and theoretical in the sense that they do not account for the processing of the stimulus information and the execution of the motor response. Colour and location of the stimulus often are the direct input for these models and those information are available immediately after stimulus onset. Only in the model of Kornblum et al. (1999) the processing of the colour can be delayed due to the simulation of the stimulus-stimulus consistency in Stroop tasks.

Note that even though I applied a modified version of my original model of chapter 2.3, all above models could easily be included into my control architecture. The models presented here typically consist of two neurons for encoding colour and location of the cue to determine the target location. By converting the x-y position of cue and target into discrete left/right positions the target selection module could be replaced by one of those models. Those models are able to cover more aspects of the Simon task (e.g. explaining the reversed Simon effect) than my model. However, in my thesis it was not the aim of my experiment to simulate all aspects of the Simon effect rather than to show that the control architecture of my model can be used to simulate a wide range of choice-reaching tasks utilising a complete perception-action cycle. Nevertheless with the potential to apply existing models in the target selection stage my model could be utilised for further Simon effect experiments.

4.3.7. Conclusion

The main purpose of this experiment was to show that the hardware and control architecture of the model can easily be modified to a wider range of choice-reaching tasks such as the Simon task and to simulate important findings of those tasks. It could be shown that my model is able to reproduce typical observed behaviour of

such tasks. In the different conditions of the experiment I showed that the Simon effect occurred either before or after movement onset depending solely on the value of the threshold parameter th_T that already played a crucial role in the odd-colour "continuous" vs. "threshold" experiment (see chapter 3.3). The results demonstrated that the modified model is able to reproduce the experimental findings of existing choice-reaching studies regarding the Simon effect. In the model the Simon effect emerges from the fact that the irrelevant location feature influences the target selection map directly, later the cue colour as the relevant target feature determines the target side and overwrites the irrelevant location information which is consistent with current explanations of the Simon effect. This demonstrates that my model is general enough to simulate a broad range of choice-reaching tasks. Furthermore, my model possesses a control architecture that can utilise existing computational models of the Simon task. Thus, it is possible to use the motor stage of my model together with existing abstract models to simulate experiments regarding the Simon effect.

5. Modeling Goal Directed Reaching

The experiments of the previous chapters demonstrated that my model and its control architecture is able to perform human-like reaching movements in single-target experiments as well as the odd-colour task of Song and Nakayama (2008b) and other choice-reaching tasks. In this chapter I will extend the existing model to simulate a range of goal-directed reaching tasks. The aim hereby is to show that a human-like behaviour in those tasks can be achieved with the closed-loop architecture of my model. This approach differs from the established two-component models and open-loop models that were introduced in chapter 2.1. Four experiments will be simulated: the first two deal with speed-accuracy trade-off and the last two with perturbation effects. Before presenting the experiments I give a detailed overview of the modifications of the original model in the next section. The extended model and the speed-accuracy experiments also will be published shortly in Strauss and Heinke (2013).

5.1. Relevant empirical evidence

Chapter 1.2 and 2.1 already reviewed the current research and models regarding goal-directed reaching. Here I am going to present a detailed review of the most relevant empirical evidence of human behaviour in typical goal-directed reaching tasks. These findings will be compared with the simulations of my model afterwards.

The probably most important and general finding in the area of goal-directed reaching is the already in the introduction mentioned Fitts' law. It goes back to the findings of Fitts (1954) who was the first to provide a functional relation between the movement speed of reaching movements and their accuracy (see also Meyer et al., 1990; for a review). He analysed goal-directed reaching movements towards target objects of different sizes that were placed in various distances where the participants were asked to reach the target as quickly as possible. In such so-called time-minimisation tasks (where participants are asked to minimise their movement time) Fitts found that larger objects have shorter Movement Times (MTs) than smaller objects, while objects with a greater distance have longer MTs than nearer objects. Moreover, he proposed an equation to estimate the "difficulty" (*Index of Difficulty*, ID) of a movement depending solely on the distance D and the width W of the target object which is to be reached:

$$\mathrm{ID} = log_2\Big(\frac{2D}{W}\Big) \tag{5.1}$$

With the ID an estimation of the MT can be calculated using parameters $a, b > 0$:

$$\mathrm{MT} = a + b\ \mathrm{ID} \tag{5.2}$$

Above equations and their linear relation between the difficulty and the movement times were confirmed in many experiments over the last decades and were found to be so general that it is now commonly known as Fitts' law.

Another important fact of the goal-directed reaching process is the already mentioned and simulated (see chapter 3.1) bell-shaped velocity profile. Typically the peak velocity is roughly at the mid-point between starting point and target position (see also Figure 5.1 and Rosenbaum et al., 2006; for a review). The profile often is skewed with faster increase at the beginning of the movement and slower decrease when approaching the

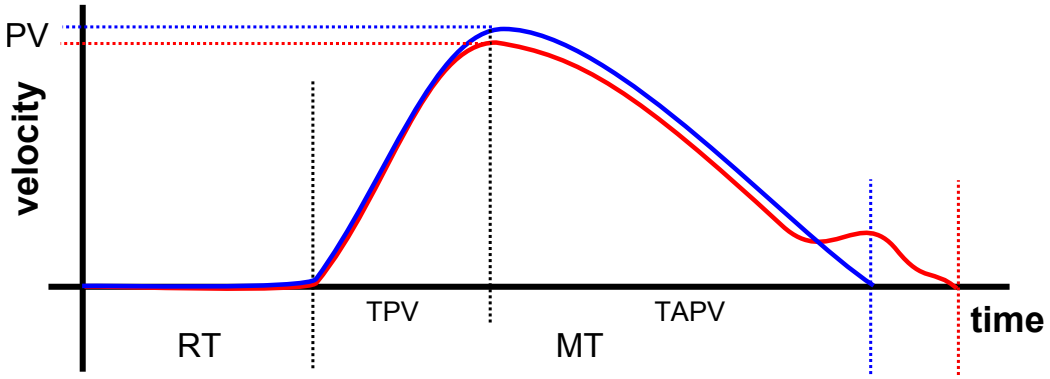

Figure 5.1.: Typical velocity profile of a human reach (blue line) with common kinematic markers: The Reaction Time (RT) is the time between trial onset and movement initiation. The Movement Time (MT) can be divided into an acceleration phase (Time to Peak Velocity - TPV) and a deceleration phase (Time After Peak Velocity - TAPV). With a smaller target size (red line) the TAPV phase usually is extended by a "low-velocity" phase which even could show secondary peaks towards the end of the movement (red). Also other measures change: the PV is slightly lower and the MT increased.

target.

More recent experiments brought further insight in the nature of goal-directed reaching e.g. a relationship between target properties and velocity profile was found. From the velocity profile further kinematic markers such as the Peak Velocity (PV) can be obtained. Moreover, the MT can be separated into a Time to Peak Velocity (TPV) and a Time After Peak Velocity (TAPV) (see Figure 5.1). When size and distance of the target object are varied, then the influence of this variation is not limited on the MT only as described by Fitts' law but can also change the velocity profile and the kinematic markers of the reaching substantially (MacKenzie, Marteniuk, Dugas, Liske, & Eickmeier, 1987; Thompson, McConnell, Slocum, & Bohan, 2007; for experimental evidence and Table 5.1 for an overview). A variation in the target size was found to have a strong influence on the TAPV so that smaller targets have a much longer deceleration phase than larger targets what makes their velocity profile highly asymmetrical. In contrast the TPV mainly is influenced by the target distance and no significant effect of the target size was found here. The PV typically increases with

larger objects and larger distances. These results are often explained with different accuracy requirements of smaller and larger targets. The introduced two-component models suggest that with higher accuracy constraints the control phase requires more time to land on the target. Smaller targets have more precision demand than larger targets which extends the TAPV. Low accuracy requirements due to large objects or the task itself leads to more symmetrical profiles while a change in the distance of target objects does not change the shape of the profile but scales up the whole velocity profile (e.g. MacKenzie et al., 1987; Thompson et al., 2007). This empirical evidence demonstrates that a Fitts' law task that takes into account various kinematic markers besides the movement time can already represent numerous aspects of the goal-direct reaching process.

More findings about the goal-directed reaching process come from the so-called time-matching tasks. In such tasks participants have to reach with different velocities in a similar environment. Hereby Schmidt, Zelaznik, and Frank (1978) found evidence that the endpoint accuracy increases with higher average movement speeds. This fact is also predicted by the optimized-submovement model by Meyer et al. (1988) for the standard deviation of the primary-submovement endpoints. I will investigate the behaviour of my model in a time-matching task similar to Schmidt et al. (1978).

The second group of experiments will focus on perturbation experiments where the target or the hand can change their properties upon movement onset. Typically targets are perturbed in size or location while hand perturbations only affect the location. In contrast to experiments with a Fitts' law setting, the perturbation paradigm focuses on the use of online-control and the processing of visual information during the reaching process. The changing target/hand has to be detected and the movement trajectory adjusted in-flight in order to successfully reach the target under the new circumstances. As the already initiated movement has to be adapted kinematic markers such as MT, TPV and TAPV then can reveal ongoing competition processes

measure	size effect	distance effect
MT	-	+
PV	+	+
TPV	o	+
TAPV	-	+

Table 5.1.: Influence of target distance and size on the Movement Time (MT) and other kinematic markers (PV - Peak Velocity; TPV - Time to Peak Velocity; TAPV - Time After Peak Velocity). A "+" means that with increasing size or distance also the measure increases (respectively a "-" means decrease and a "o" means no change). See the text for a detailed explanation.

in the brain between initial and perturbed target to give a better understanding of the goal-directed reaching process.

In the experiments regarding target perturbations the initial target was found to have a strong influence in the early trajectory of the reaching process and the perturbed one only dominated towards the end. Hence kinematic markers such as PV and TPV should mainly be influenced by the characteristics of the initial target while the TAPV depends more on the properties of the final target. Experimental evidence showed this behaviour in various setting (Paulignan, MacKenzie, Marteniuk, & Jeannerod, 1991; Paulignan, Jeannerod, MacKenzie, & Marteniuk, 1991; Heath et al., 1998). Moreover, the re-planning and adapting of the trajectory typically leads to strongly increased MTs, independent of the kind of the perturbation. This effect is even stronger with a change of the target location in comparison with a change of target size (Heath et al., 1998).

Experiments perturbing the location of the hand focus more on if and how the perturbation is compensated and what time it takes to correct the perturbation. Typically, hand location perturbations are not fully compensated (e.g. Saunders & Knill, 2005; Sarlegna & Blouin, 2010). Moreover, changes in the movement trajectory can be detected earlier when the hand is perturbed towards the sides in comparison with changes in movement direction (Saunders & Knill, 2005).

To conclude this section I am going to summarise the empirical evidence. The aim for my model is to simulate appropriate experiments in order to demonstrate the following findings:

- In time-matching tasks the endpoint accuracy decreases with higher average velocities (e.g. Schmidt et al., 1978).
- In time-minimisation tasks the movement time logarithmically increases with distance and decreases with target size (Fitts' law). Moreover, kinematic markers are also influenced by those variables and need to be taken into account in order to generate human-like behaviour.
- In perturbation experiments time is needed to update an ongoing movement (visual delay). Thus, when the target object changes its properties upon movement onset the beginning of the movement is influenced by the initial target properties while the second half is dominated by the final target. Additionally, the MT is increased when perturbations occur.
- When the location of the hand is perturbed during a movement, humans account for this change with a delay that depends on the direction of the perturbation. However, the perturbations are not fully compensated (Saunders & Knill, 2005).

5.2. The goal directed reaching model

The base for the goal-directed reaching model is the original choice-reaching model of chapter 2.3. The there described functionality (e.g. the closed-loop architecture and the moving blob principle) also plays an important role in the here presented model. The changes and adaptations will be described in the following. A complete overview of the model is displayed in Figure 5.2.

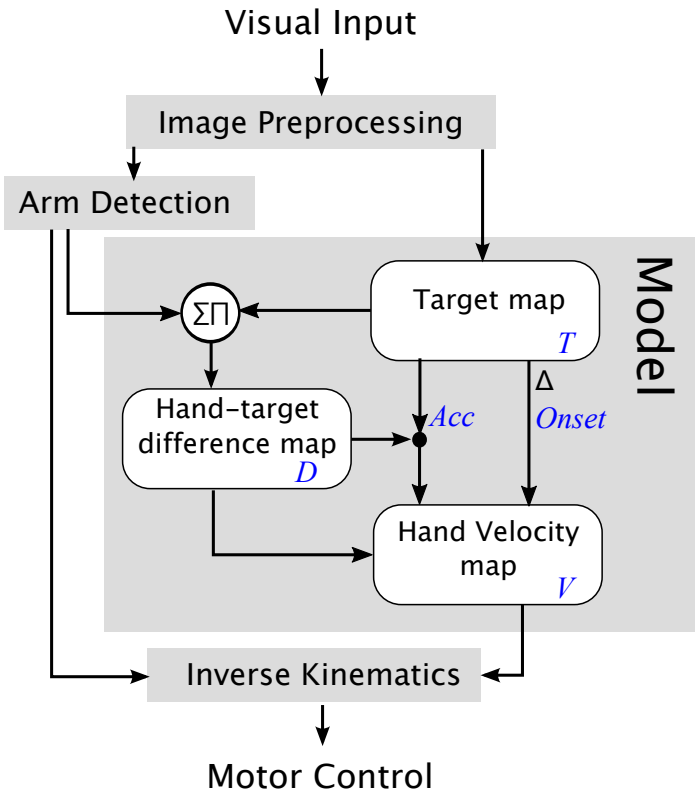

Figure 5.2.: Overview of the control architecture of the goal-directed reaching model. The big grey box contains the model, white boxes symbolise DNFs. In the text the blue abbreviations are used for the respective DNFs or mechanisms. The smaller grey boxes are modules not belonging to the model and are similar to the choice-reaching model (see also Figure 2.4). In comparison with the original model new pathways of the *Acc* and *Onset* mechanism were introduced. These mechanisms influence the reaching movement to account for accuracy and perturbation effects and are presented in detail in the text.

The aim of the new model in this chapter is to simulate experiments regarding the speed-accuracy trade-off of Fitts' law and perturbation experiments where the target object can change its properties during the reaching process. The choice-reaching model already was able to simulate reaches in a human-like manner, i.e., with a bell-shaped velocity profile and a straight trajectory. Moreover, due to the fact that object sizes carry over from the visual input through the DNFs of the model it will simulate an effect of object size influencing the kinematic markers. Hence the model offers a good base for simulating Fitts' law where the object distance and size influence

movement time and kinematic parameters. In early test simulations it turned out that the original model produces fairly good results for the movement time but only a rough approximation of the kinematic markers in Fitts' law. In order to achieve a better fit and to simulate the details of the experimental data the original model was modified in some modules. In the following I am going to present the adaptations and new mechanisms of the model.

Accuracy mechanism

Important for the goal-directed reaching model is the moving blob principle which was explained in detail in chapter 2.3. The first adaptation is the accuracy mechanism (*Acc*) and extends the functionality of the moving blob. This mechanism is necessary to model details of the Fitts' law as it is supposed to control the reaching accuracy in the vicinity of the target object and slows down the hand if the accuracy constraints are high which is the case when reaching for smaller target objects. Hence the *Acc* mechanism causes an increase of the zero map in the centre of the V map when the hand reaches the vicinity of a target. The increase of the zero map is greater in smaller targets as they have higher accuracy constraints and therefore causes the velocity to drop slightly faster towards the end of the trajectory for small targets. This is supposed to resemble the velocity profiles as shown in Figure 5.1. In order to receive information about the target size the sum of the activation in the T map is determined. Furthermore, information about the distance from the target comes from the D map by multiplying the activation of every neuron of this map with a Gaussian-shaped function which is aligned around the centre of the map. Both parts (target size and distance) are combined by a multiplication which contributes to the strength of the zero map in the V map.

Moreover, the non-linear output function of the V map is replaced by a linear function. The non-linear eccentricity now is located in the D map, in an earlier stage of the

model. I found that moving the eccentricity function to an earlier processing stage of the model stabilizes the behaviour of the moving blob. Furthermore it seems to be a more neurologically plausible way as in humans this non-linearity occurs much earlier on the sensory stage with the magnification factor of the eye. From this viewpoint the activation in the D map can be interpreted as the (untransformed) visual information of the hand in the centre of the visual field, while the T map with its birds-eye representation is a corrected version that shows the true proportions of the object.

Onset mechanism

The second modification is the *Onset* mechanism that deals with uncertainty, detects changes in the environment, and regulates the velocity in case of unexpected perturbations. It works like an onset detector and decelerates the hand when changes in the perceived environment (T map) occur. This is consistent with findings in the literature where effects have been observed that cause the movement times to go up in conditions with abrupt object onsets (e.g. Castiello, 2001).
Both mechanisms - *Acc* and *Onset* - include new processing pathways in the model and directly influence the moving blob by controlling the strength of the zero-map of the V map. Hence they do not contradict the claim of presenting a parsimonious model towards goal-directed reaching. The *Acc* mechanism plays a major role in the Fitts' law experiment as it controls the TAPV of smaller target objects. The *Onset* mechanism will be important for simulating the target perturbation experiments.

Further adaptations

Another aspect of the functionality of the model is that it needs time to process the visual information in the DNFs and to adapt the movement speed and direction of the arm accordingly. On the one hand this results from the DNF dynamics but on the other hand this is an important factor that has to be considered when implementing a

closed-loop model. As mentioned before in chapter 2.1, also humans show such a delay in processing information (Elliott et al., 2010). Note that the visual delay plays no such big role in models that plan the movement in an open-loop fashion. In order to gain more control of the processing time I decided to introduce a "dead-time" parameter which reflects a processing time within the T map and which only functionality is to increase the time the model reacts to perturbations to a human-like amount. The dead-time does not interfere with the DNF dynamics as it only adds a time delay for the output information of the T map. Note that the dead-time does not influence the processing of the position of the robot's base and hand. As my model solely relies on visual information I motivate this with the need of a quicker adaptation of the hand's position in order to correctly land on the target. Besides visual information humans possess additional mechanisms to update the internal representation of the hand's position such as forward models and proprioceptive feedback (e.g. Miall & Wolpert, 1996).

Outlook goal-directed reaching experiments

In the first two experiments of chapter 5.3 and 5.4 I am going to present the goal-directed reaching experiments regarding the speed-accuracy trade-off. The first experiment was the time-matching task which investigates the influence of the moving blob parameter on the movement. Here it was required to reach for a target object with different speed values. This speed regulation was introduced in a neurological plausible way. In the second experiment I aimed to simulate Fitts' law with my model. The second group of experiments of chapter 5.5 and 5.6 aimed to simulate perturbation experiments in order to give further support for my model. Two different kinds of experiments were simulated: First, I attempted to simulate target perturbation experiments. Here an aspect of the target (size or location) changed upon movement onset. Second, I simulated a hand perturbation experiment where the perceived

location of the hand changes. Note that all parameters of the model and the DNF were determined before the experiments and remained unchanged in all experimental conditions in this chapter unless stated in the appropriate methods sections.

5.3. Time-matching movement task

This first experiment aimed to test the influence of the moving blob parameters on movement characteristics such as speed and accuracy. In empirical studies participants are usually asked to reach for targets within a specified amount of time (e.g. Schmidt, Zelaznik, Hawkins, Frank, & Quinn, 1979). Hence, they have to adapt their movement speed. In my model a different movement speed can be achieved by changing the weights of the inputs of the moving blob which I am going to explain in more detail in the following (see also chapter 2.3).

The moving blob in the V map receives its input from two sources: First, a constant part (zero map) that assures the presence of a permanent activation in the centre of the map where zero speed is encoded. Second the V map receives an input from the D map in order to push the moving blob away from the centre to initiate the movement toward a target object. While in the modified model the strength of the constant activation also is influenced by the *Acc* and the *Onset* mechanism which were introduced in the previous section, these two mechanisms will not play a role here as only the constant part will vary. It can be expected that with decreasing strength of the zero map the moving blob will be pushed further away from the centre by the input activation from the D map which eventually leads to an increase in the speed so that peak velocity and the speed in general will be increased. With increasing movement speed I expect a behaviour of the robot arm which is similar to the empirical evidence of Schmidt et al. (1978) and the theory of Meyer et al. (1988)

where besides the higher velocity also increased endpoint errors were observed. My experiment aimed to reproduce these findings.

5.3.1. Methods

The target objects were square coloured markers (red or green) with 4.38 cm length of the edge. The size of the target was relatively large so that the influence of the *Acc* mechanism was minimised. As described before this mechanism can influence the constant activation in the V map for smaller target objects. Targets were located in front of the initial position of the robot arm's end-effector in a distances of 20 cm. The starting position of the end-effector was located 9 cm in front of the arm's base (shoulder). Before the experiment began the parameters of the image preprocessing were adapted to the current lighting conditions to ensure a stable detection of arm and target object. After starting a trial the position of the end effector was recorded until the target was reached. The arm was considered to have reached the target when the encoded velocity in the V map fell under a threshold value of approximately 0.5 cm/sec. The encoded velocity was the distance of the centre of gravity of the neural activation (the moving blob) to the centre of the V map. This is a technical solution to estimate the end of the movement. Note that the noise in the V map was fairly low and did not influence this measure.

Three conditions were distinguished depending on the strength of the central activation in the V map: *low*, *mid*, *high*. In each conditions ten trajectories were recorded and processed like in the previous experiments of chapter 4. The following measures were obtained from the raw data: the Movement Time (MT) was the time between movement onset and the end of the movement and the Peak Velocity (PV) was the highest speed value measured. Furthermore the average movement velocity (AvgV) was calculated by dividing the moved distance (endpoint - starting point) by the MT.

condition	MT [sec]	PV [cm/sec]	AvgV [cm/sec]	EP_{err} [cm]	EP x	EP y
low	16.3	1.59	1.27	0.57	40.3	14.7
mid	17.3	1.40	1.11	0.43	40.6	16.5
high	17.2	1.32	1.03	0.29	40.1	18.2

Table 5.2.: Results of the different measures in the time-matching task. Displayed are mean values with their standard deviation in brackets.

Finally, the endpoint error (EP_{err}) was determined as the standard deviation of the distance of endpoints to the mean endpoint of the movement trajectories.

5.3.2. Results & Discussion

The results of the experiment can be found in Table 5.2. As expected PV and AvgV increased with decreasing central activation (from high to low condition). However, when investigating the distribution of the endpoints I found that the robot arm also moved a longer distance with decreasing central activation. Hence, in the conditions with the smallest central activation the target was slightly overshot and in the conditions *mid* and *high* undershot.

Moreover, also the endpoint variation EP_{err} increased with smaller central activation. This finding is consistent with the results of (Schmidt et al., 1979) and Meyer et al. (1988) who also found that the endpoint error increases proportionally with increasing average velocity.

The results show that the moving blob and its determining parameters can influence movement parameters significantly. With a smaller central activation the moving blob is dominated by the target dependent input activation and is pushed out faster and further away from the centre of the V map. This leads to a significant increase of the speed of the robot's hand. Moreover, with the increased speed the noise in the system (especially the noise originating of camera and motor) has a larger influence on the movement which tends to increase the endpoint error as demonstrated.

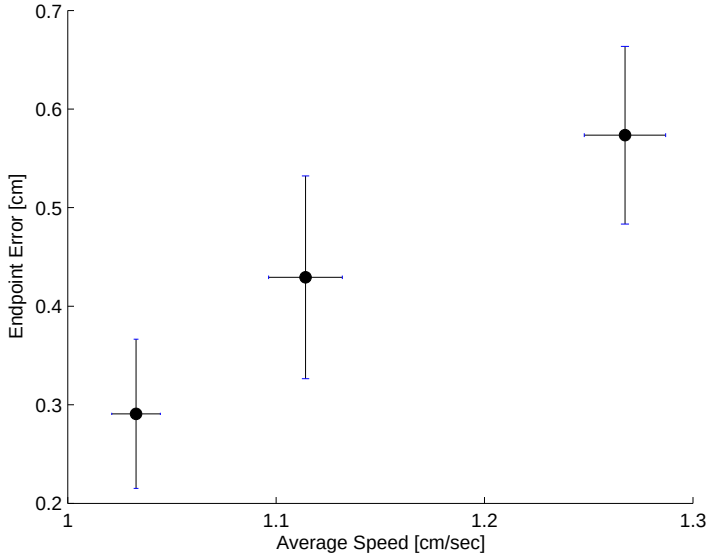

Figure 5.3.: Results of the time-matching experiment. Displayed is the endpoint error against the average movement speed of the different conditions (from left to right: high, mid, and low condition). Error bars represent the standard deviations. It can be seen that with higher speed values the accuracy decreases.

5.3.3. Conclusion

In this first experiment with the goal-directed reaching model the influence of the input parameters on the moving blob and on movement properties was examined. In the different conditions the strength of the constant activation in the V map was varied. The results showed that with smaller constant activation the peak velocity and the average movement speed was increased. Moreover, the endpoint error of the movement was larger and the robot arm tended to overshoot the target object. This is consistent with empirical evidence of Schmidt et al. (1979) who also found increased endpoint errors in similar experiments. In my model this behaviour emerges from the fact that with smaller constant activation in V map the moving blob was more strongly dominated by the target dependent input activation. Hence the moving blob moved further away from the centre of the V map which led to higher speed values and an increased influence of the noise in the system.

This experiment also demonstrated how the general velocity can be controlled on a neurological level. However, future experiments have to prove the existence of a permanent activation that controls movement speed and direction.

5.4. Time-minimisation movement task (Fitts task)

In this experiment I aimed to simulate the speed-accuracy predictions of Fitts' law. Typically, in such reaching tasks the object's size and distance vary in order to show the linear relation of the Movement Time (MT) and the Index of Difficulty (ID) which was introduced earlier in chapter 5.1 (e.g. Heath, Weiler, Marriott, Elliott, & Binsted, 2011). Hereby the model should reproduce this relation of MT and ID in order to simulate the human reaching process. Moreover, the model should be able to generate bell-shaped velocity profiles as before and to mimic the effect of different target sizes and distances on the velocity profiles and its kinematic markers which were reviewed earlier.

5.4.1. Methods

The setup was similar to the time-matching experiment. However, now the target objects had different sizes of 2.63 cm, 3.50 cm and 4.38 cm length of the edge depending on the experimental condition. Moreover, the distance of the targets varied. Targets were located in front of the initial position of the robot arm's end-effector in different distances at 15 cm, 17.5 cm, 20 cm, and 22.5 cm.

For each possible combination of target size and distance five trajectories were recorded. The raw data was processed to determined the following measures: The *Movement Time* (MT) was the time from movement onset until the end of the trial. The *Time to Peak Velocity* (TPV) was the time from movement onset to the time of the peak velocity. The *Time After Peak Velocity* (TAPV) was the time from the time of peak

velocity until the end of the trial. Finally the *Peak Velocity* (PV) was the speed value of the highest velocity during the movement. Movement onset and the end of the trajectory were determined like in the previous experiments.

Within the same condition (same target size and distance) the means and standard deviations of the measures were determined. In order to make the effects and trends of different target size and distance visible, a weighted linear least square fit function was applied for the same target sizes across different logarithmic distances (distance effect) and the same target distances across the logarithmic sizes (size effect) by using the MatLab function "lscov" with a weighting vector that contained the reciprocal variances of the respective conditions. The weighting was applied to decrease the influence of noisy data points. In order to measure the validity of the fitted functions their r^2 values were determined. For the graphs the binary logarithm of target size or distance was calculated to account for the Fitts' law equation that defines a linear relation of movement time and those two conditions.

The data processing was similar to the earlier experiments and the model parameters were identical to the time-matching experiment. The moving blob parameters were similar to the low condition there.

5.4.2. Results & Discussion

Table 5.3 contains the means and standard deviations of all measures and conditions. The detailed values of the slopes of the fitted least square functions and their r^2-value can be found in Table 5.4. Furthermore, the results of the measures are displayed in the Figures 5.4 to 5.8. The results show that the robot arm is able to simulate all major aspects of Fitts' law, however, the measures are more or less influenced by the noise in the system. In the following the effects in the measures will be discussed:

Movement time (MT): The MT shows the characteristic linear increase with larger

condition	MT [sec]	PV [cm/sec]	TPV [sec]	TAPV [sec]
small				
15.0 cm	16.2 (1.2)	1.00 (0.08)	7.3 (1.4)	8.9 (2.1)
17.5 cm	17.4 (1.1)	1.05 (0.11)	6.9 (1.9)	10.5 (2.0)
20.0 cm	18.9 (1.2)	1.17 (0.08)	7.7 (1.0)	11.2 (1.7)
22.5 cm	19.2 (1.7)	1.44 (0.13)	8.0 (0.5)	11.3 (1.3)
normal				
15.0 cm	14.6 (1.6)	1.18 (0.07)	5.9 (0.5)	8.7 (1.4)
17.5 cm	16.1 (0.9)	1.31 (0.12)	6.8 (0.9)	9.2 (1.7)
20.0 cm	17.0 (1.6)	1.48 (0.24)	7.3 (1.6)	9.7 (1.8)
22.5 cm	17.2 (0.8)	1.72 (0.12)	6.4 (0.4)	10.8 (0.5)
large				
15.0 cm	14.3 (1.1)	1.35 (0.15)	6.3 (0.7)	8.0 (1.0)
17.5 cm	14.9 (1.1)	1.52 (0.13)	7.1 (1.7)	7.8 (0.6)
20.0 cm	16.3 (0.9)	1.56 (0.10)	6.7 (0.8)	9.7 (0.7)
22.5 cm	16.9 (0.4)	1.77 (0.04)	6.8 (0.7)	10.1 (1.1)

Table 5.3.: Results of the time-minimisation experiment: All conditions with their averaged measures and standard deviations (in brackets) of five trials.

effect	MT	PV	TPV	TAPV
distance				
size:small	0.97 (5.6)	0.81 (0.7)	0.91 (1.4)	0.87 (3.9)
size:mid	0.93 (4.1)	0.98 (0.9)	0.57 (0.8)	0.98 (3.7)
size:large	0.98 (4.7)	0.98 (0.7)	0.24 (0.6)	0.73 (4.5)
size				
dis:nearest	0.94 (-2.5)	1.00 (0.5)	0.43 (-1.1)	0.89 (-1.3)
dis:near	1.00 (-3.4)	1.00 (0.6)	0.53 (0.3)	1.00 (-3.7)
dis:mid	0.97 (-3.4)	0.99 (0.5)	0.99 (-1.4)	0.88 (-1.9)
dis:far	0.89 (-2.7)	0.96 (0.4)	0.60 (-1.8)	0.89 (-1.5)

Table 5.4.: r^2 values and slopes (in brackets) of the fitted linear trends of the time-minimisation experiment. See the text for the discussion.

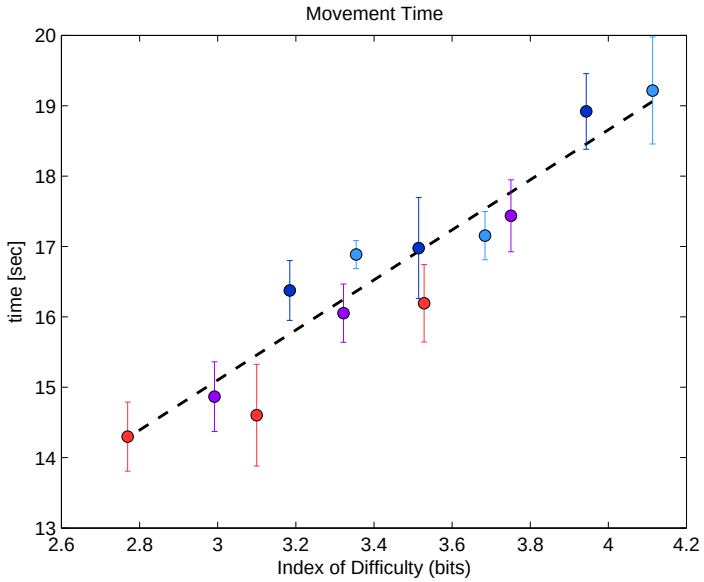

Figure 5.4.: Movement Times of the time-minimisation experiment against their Index of Difficulty according to Fitts (1954). The colours refer to the target distances in the order red, purple, blue and light blue (from nearest to farthest). Each colour has three data points representing the target sizes (leftmost data point stands for the largest target). The experimental data of my model shows a linear increase which is also typical for Fitts' law. The dotted line is the weighted linear least square fit function which shows a clear trend of longer MTs with higher ID.

distances and smaller target objects (see Figures 5.4 and 5.5). Due to the noise the slopes of the least square fit linear functions possess some variety for the size and the distance effects. They vary with changing distances from 4.1 to 5.6 and with changing sizes from -2.5 to -3.4, but all conditions show high r^2 values of at least 0.89 which is a common finding in experiments of this kind (e.g. Heath et al., 2011). Note that contrary to the original Fitts' law (Fitts, 1954, Fitts & Peterson, 1964) but similar to the more recent publication of Heath et al. (2011), the slopes for distance and size differ: Distance has a stronger influence on the MT than size.

Peak velocity (PV): The result for the PV is similar to the MT as it shows very clear trends with fairly little noise (see Figure 5.6). It increases with object size and distance. Moreover, the r^2 values are all high and again the slopes for distance show a stronger increase than the ones of the the size effect. The effects of the PV underline

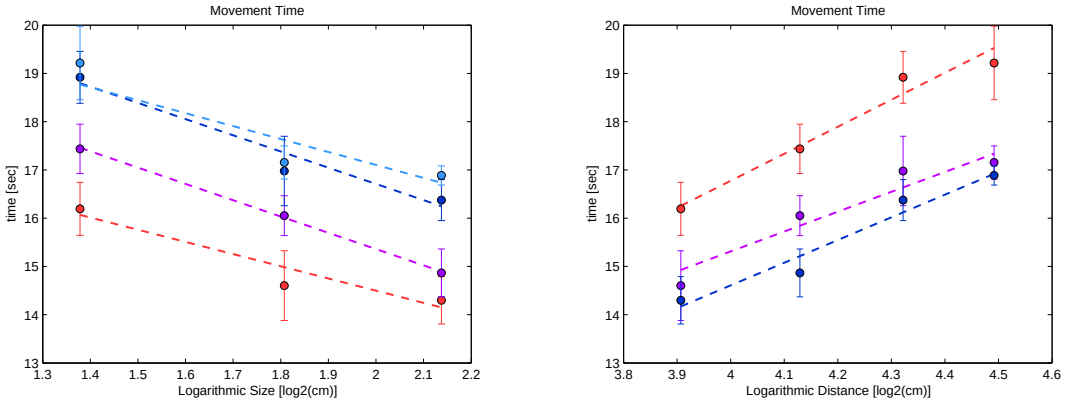

(a) (b)

Figure 5.5.: Movement Times (MTs) of the time-minimisation experiment: (a) The effect of the logarithmic target size: larger targets have shorter movement times. The different colours refer to the target distances (in the order red, purple, blue and light blue from nearest to farthest); all data points are shown with their standard deviation. The dashed lines refer to the weighted least square fit of the appropriate distance (colour). (b) Here the same data points were rearranged according to the logarithmic target distance. The colours blue, purple and red now stand for the target size from the largest to the smallest. Here it can be seen that objects with a smaller distance were reached quicker.

the fact that larger target sizes and distances push the moving blob further away from the centre of the V map.

Time to peak velocity (TPV): The results for the TPV show a more noisy behaviour with higher standard deviations (see Figure 5.7). Although, the results are consistent with typical experimental evidence: With larger distance the TPV also increases while there is no clear trend in the target size (one positive and three negative slopes). Typically there is no significant size effect in this measure (e.g. Heath et al., 2011, MacKenzie et al., 1987).

Time after peak velocity (TAPV): In contrast to the TPV the TAPV shows clearer trends (see Figure 5.8). It decreases strongly in larger objects with high r^2 values and slopes between -1.3 and -3.7. It increases with object distance in a similar pattern with even bigger slopes between 3.7 and 4.5. Those effects are consistent with experimental evidence (e.g. MacKenzie et al., 1987).

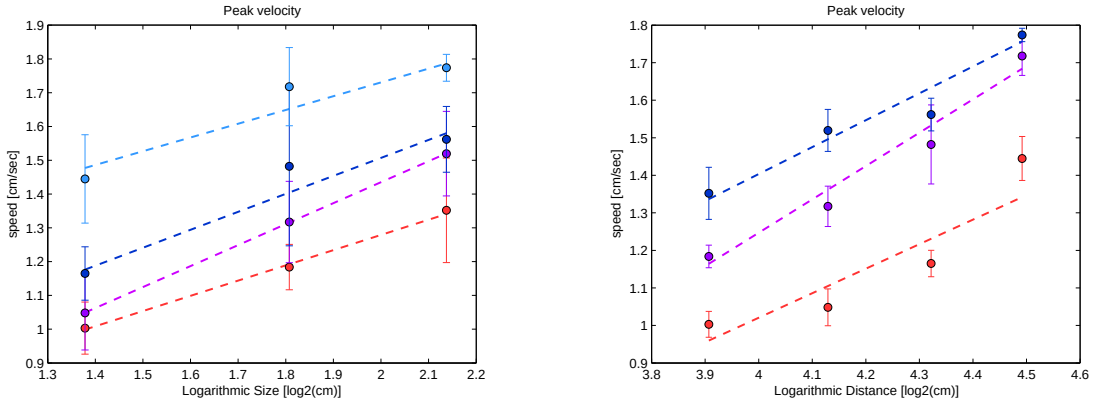

(a) (b)

Figure 5.6.: Peak Velocities (PVs) of the time-minimisation experiment: (a) With larger target size the PV increases. (b) Also with greater distance a higher PV can be observed. The colours and lines have the same meaning as in Figure 5.5.

The results of the measures confirm the theoretical description of the model's behaviour earlier: As the MT is the sum of TPV and TAPV its behaviour depends on these two kinematic markers. The results for TPV and PV emerge entirely from the moving blob behaviour. For larger targets or greater distances the blob will move further away from the centre of the V and therefore the PV increases in these conditions. The TPV increases with greater distances for the same reason, however remains constant for different target sizes which results from the fact the the blob moves not only further for larger targets but also quicker what counterbalances the longer travelling distance of the activation in the V map.

For different target sizes the behaviour of the TAPV mainly can be accounted to the *Acc* mechanism which causes the velocity to drop earlier when reaching smaller targets. Thus, a phase with relatively low velocities towards the end of their trajectories can be observed (see Figure 5.9). Such a "low velocity phase" also has been reported in the literature for human reaching movements (e.g. Jeannerod, 1984). Due to this phase smaller objects tend to have a longer deceleration phase so that these objects show a higher TAPV. Also for longer distances the TAPV is increasing. Here the

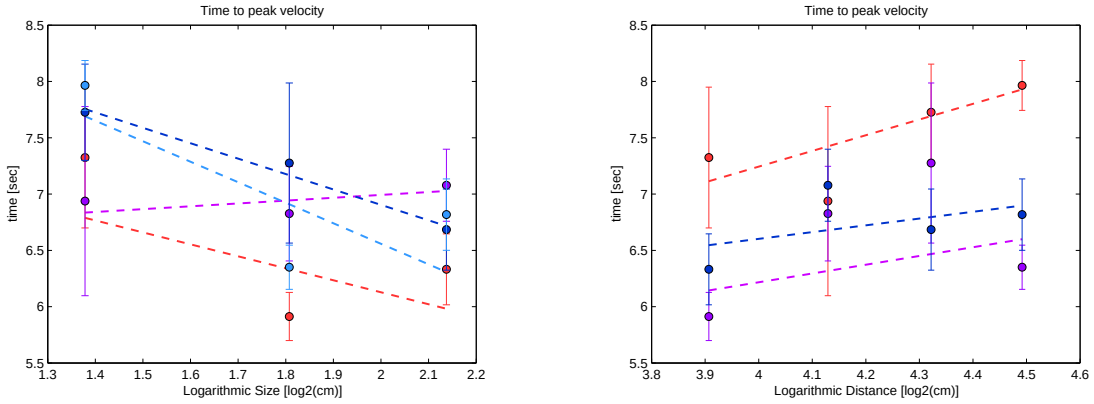

(a) (b)

Figure 5.7.: Time to Peak Velocities (TPVs) of the time-minimisation experiment: (a) No clear trend of the target size on the TPV could be observed. (b) However, with greater target distance the TPV increased slightly. The colours and lines have the same meaning as in Figure 5.5.

travelling distance for the moving blob becomes bigger as the blob is pushed further out of the centre of its DNF. Since the beginning of the trajectory is not influenced by the *Acc* mechanism, it has no effect on the other measures. Moreover, small objects have a tendency towards an undershooting behaviour than large objects which partly can be accounted to the new mechanism but also to the moving blob implementation in the V map. In fact, a similar result was found in the time-matching task only by varying the moving blob parameters.

It can be seen from the results that the TPV was the measure which was the most difficult to balance. This is due to the fact that the point in time when the peak velocity occurs evolves from the dynamic of the moving blob and is not directly controlled by parameters. Thus, the results for the TPV are the poorest and the most noisy ones amongst the measures which equates to the inconsistent slopes that were found.

When looking at the trends of the fitted linear functions it can be said that generally the simulations are consistent with typical results of Fitts' law experiments (e.g. Munro, Plumb, Wilson, Williams, & Mon-Williams, 2007; Thompson et al., 2007;

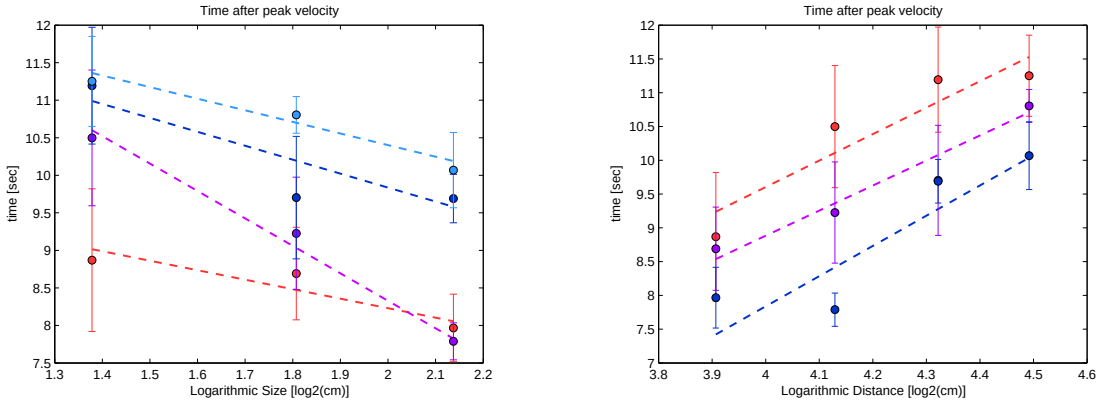

(a) (b)

Figure 5.8.: Time After Peak Velocities (TAPVs) of the time-minimisation experiment: (a) Objects with a smaller size had a higher TAPV which is a direct effect of the accuracy mechanism of the model. (b) A greater target distance increased the TAPV clearly. The colours and lines have the same meaning as in Figure 5.5.

Heath et al., 2011). Humans often achieve r^2 values of the MTs very close to the theoretical implications of Fitts' law (see Plamondon & Alimi, 1997; for a review) - a behaviour that is very well replicated by my model. Moreover, my model can simulate human-like velocity profiles that are bell-shaped and show the typical behaviour for target objects with different sizes/distances. Additionally, the model produced remarkable results for the kinematic markers and could replicate the human performance very well.

All results were achieved despite the noise in the system which caused some variation in the measures. While humans have noise in their neuromuscular system they also have more potential to prevent the effects of it (for instance with a forward model or proprioceptive feedback; e.g. Miall & Wolpert, 1996) while my model solely relies on visual information.

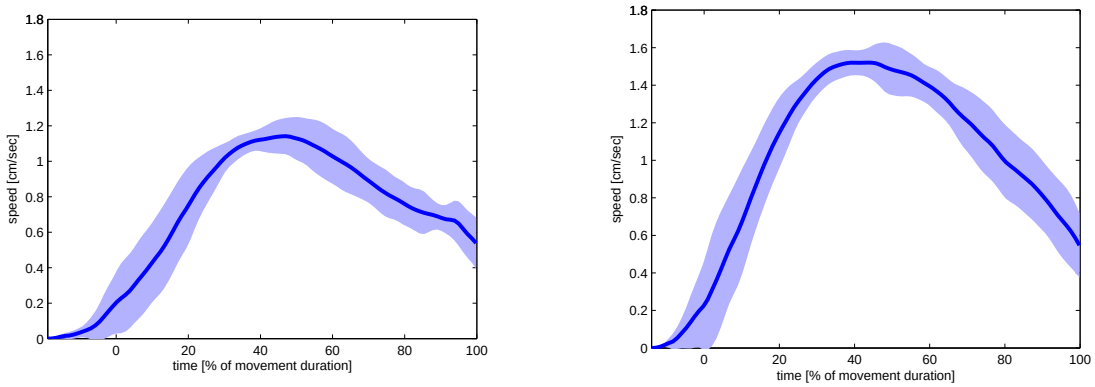

Figure 5.9.: Two examples of velocity profiles of the time-minimisation experiment. (a) Velocity profile of the smallest target size in the longest distance. Towards the end of the movement the velocity decreased only slowly and remained almost constant on a low level to account for the small target size due to the *Acc* mechanism. (b) The velocity profile of the largest target in the longest distance does not show this effect as the speed decreases constantly towards the end of the movement.

5.4.3. Conclusion

This experiment demonstrated that my model is able to reproduce a behaviour that is consistent with Fitts' law. It was shown that reaches for smaller objects and longer distances resulted in higher MTs. This behaviour was expected as the control architecture based on the dynamic neural field theory supports the encoding of information such as the target size or distance directly in the DNFs in the location and/or size of the neural activations. In this way the information about the target is passed through all DNFs until the V map where it influences the moving blob behaviour.

Moreover, the model mimicked successfully the behaviour of several kinematic markers e.g. an increased TAPV when reaching for smaller objects. However, especially for the TPV poorer results were achieved that were more influenced by the noise. Furthermore, I was able to simulate a "low-velocity" phase towards the end of the trajectory in the first experiment. Such a phase is also documented in the literature

and occurs mainly when the accuracy constraints are high as it is the case when reaching for small targets (e.g. Jeannerod, 1984). This behaviour emerges directly from the interplay of the *Acc* mechanism and the moving blob in the V map. The usage of such mechanisms also shows that the model is easily expandable by further processing pathways in order to achieve a more human like performance in different aspects of the movement or the movement itself.

Overall the experiment demonstrated that it is possible to simulate Fitts' law with the closed-loop architecture of my model. As reviewed in chapter 2.1 the goal-directed reaching process traditionally is explained with the two-component models (e.g. Glover, 2004), however, recent findings question the early ballistic phase of those models (Elliott et al., 2010). My model demonstrated an elegant way to simulate Fitts' law with a human-like behaviour in numerous kinematic markers. I will discuss the implications of this finding for the existing models detailed in chapter 6.3.

5.5. Target perturbation experiment

In this first experiment regarding the perturbation effects the target object changed its properties after movement onset. Hereby I focussed on two aspects: the perturbation of the target's location and size. I already reviewed the typical experimental outcome of such perturbation experiments in chapter 5.1. Independent from the kind of the perturbation I expected some of the measures (TPV and PV) being mainly influenced by the properties of the initial target whilst the others (TAPV and MT) should be dominated by the properties of the final target. Especially the introduced *Onset* mechanism and the dead-time parameter will play an important role in this experiment. I will discuss their role and the model's performance with respect to its functionality and compare the results with humans in similar experiments from the literature.

5.5.1. Methods

The experimental setup was similar to the previous experiment, however with the mentioned perturbation effects included. The experiment consisted of two parts. In the first part the target could change its position and in the second part the size. The expected behaviour was that in the first part of the trajectory the kinematic markers depend on the initial target properties (location or size) while in the second part of the trajectory the final target influences the kinematic markers. Target objects were again squared coloured markers.

In the target location conditions the target size was constant with 3.5 cm length of the edge and had an initial distance from the robot's hand of 20 cm. Note that this setting is identical to a condition of the Fitts task experiment (mid sized object in mid distance). After the perturbation occurred the target could jump to a location 3.5 cm in front of the initial target position (*near*), behind the initial target position (*far*) or to a position 7.0 cm right of the initial target position (*side*).

In order to make more general conclusions about the perturbations in the second part the perturbation affected the target size. Here two conditions were conducted: the target's size could either increase (*grow*) or decrease (*shrink*) after movement onset. In order to achieve greater effects, the largest and the smallest target size of the Fitts task were used. The target sizes were 2.63 cm (small) and 4.63 cm (big) length of the edge respectively. In the grow condition the target size changed from small to big, while in the shrink condition the target size changed from big to small. Again the objects were placed 20 cm in front of the robot's endeffector.

Besides the perturbed conditions single target baseline trials were performed. As some of the conditions in the Fitts task were identical to the setting here I did not run simulations with those conditions again but took the results from the previous experiment. This includes the mid distances trials of all object sizes.

In order to simulate the perturbation effect the Image Preprocessing module was extended and two different target colours were used: An initial target colour and a perturbed target colour. The initial target colour was visible for the model at the start of a trial until the the perturbation occurred. Then the input of the model switched to the perturbed target colour which remained active until the end of the trial. Note that this is just a technical realisation of the perturbation effect and that the target colour did not play a role in the experiment. In fact, this implementation is similar to the spatial averaging experiments of chapter 4.2.

The perturbation occurred after movement onset which was considered as the point in time when the peak activation in the V map reached a distance of a least two neurons away from the centre. The target reached conditions and measures were similar to the previous experiment. Moreover, all data processing steps were identical to the previous experiments.

5.5.2. Results perturbation target location

The perturbation of the target location had a big influence on the trajectory and the kinematic markers of the movement. Generally the model was able to achieve results that are consistent with the empirical evidence of humans in similar tasks. The results can be found in Table 5.5 and in the Figures 5.10 and 5.11. An example trajectory and velocity profile of the side condition is displayed in Figure 5.12. The effects of the individual kinematic markers are as follows:

Peak Velocity (PV): The PVs of the perturbed conditions possess some variation, however, they are approximately on the level of the PV of the initial target. In contrast, they are not related to the PVs of the baselines of the final targets, which differ more strongly due to the distance effect that was found in the Fitts task (see Figure 5.10).

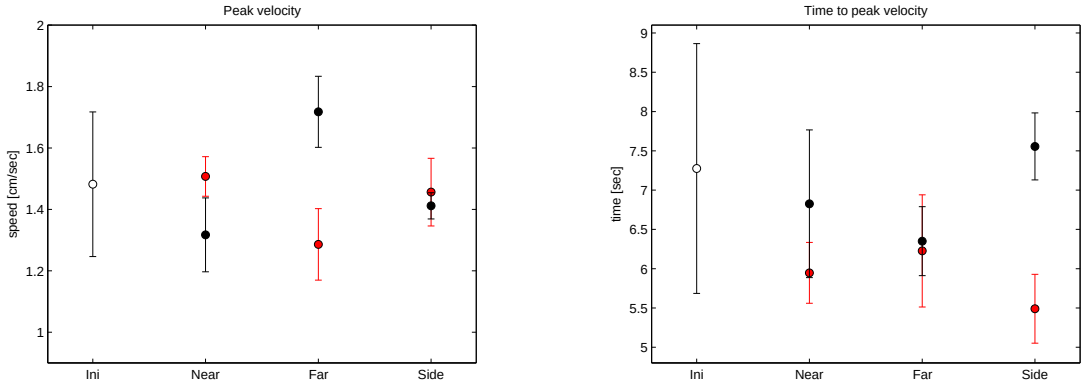

(a) (b)

Figure 5.10.: Results of the target location perturbation experiment. Shown are the mean values of PV (a) and TPV (b) with their standard deviations of the different conditions. The perturbed trials are coloured in red and the baselines in white (initial target location) and black (final target locations). The baseline conditions were unperturbed reaches toward the different locations. In the perturbed conditions both measures were independent from the location of the final target object. The PV values of the perturbed condition were similar to the PV of the initial target location while the TPV of the perturbed conditions was slightly shorter than TPV of the initial target.

Time to Peak Velocity (TPV): Like the PVs also the values of the TPV of the perturbed conditions are roughly similar, however a bit lower than the TPV by the initial target baseline (see Figure 5.10). Thus, the TPV does not seem to be affected by the final target. The fact that the values are lower than the TPV of the initial target can be explained with the decrease of the velocity due to the *Onset* mechanism. The detection of the perturbation occurred at the end of the acceleration phase what caused the velocity to drop. Hence, the PV was slightly lower and the TPV smaller.

Time After Peak Velocity (TAPV): In the perturbed trials the TAPV is strongly increased in comparison with the baselines of the larger distances (far and right) (see Figure 5.11). Only the near condition which is the only condition where the distance to the target is decreased due to the perturbation shows a slightly increased TAPV. These results are consistent with Heath et al. (1998).

Movement Time (MT): The perturbed trials show a significantly increased MT in

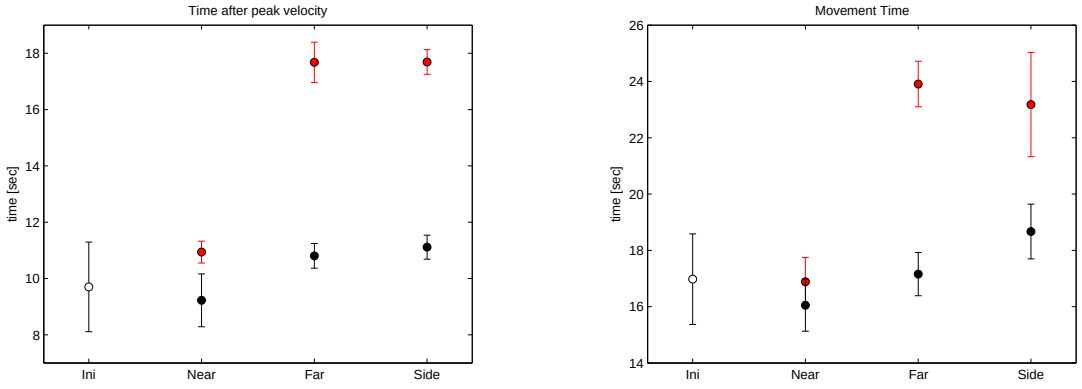

(a) (b)

Figure 5.11.: Results of the target location perturbation experiment. Shown are the mean values of TAPV (a) and MT (b) with their standard deviations of the different conditions. The colour code is similar to Figure 5.10. In contrast to the other measures, the TAPV of the perturbed conditions is greatly extended which also affects the MT.

comparison with both initial and the final target baseline (see Figure 5.11). As the MT is the sum of TPV and TAPV the results show that the (increased) TAPV has a much stronger influence than the (slightly decreased) TPV. This effect is caused by the *Onset* mechanism which caused a short but strong decrease of the velocity after the perturbation had been detected so that the TAPV was greatly extended. This result is also consistent with the experimental evidence of Heath et al. (1998).

An example trajectory and velocity profile can be seen in Figure 5.12. The velocity profile shows a characteristic double peak which often can be observed in perturbation experiments (e.g. Paulignan, MacKenzie, et al., 1991). The trajectory was corrected in flight towards the final target location.

5.5.3. Results perturbation target size

The overall effects of this second part of the experiment were similar to the target location perturbation conditions. However, here the perturbation showed no effect in the trajectory of the movement as the target location remained constant. The

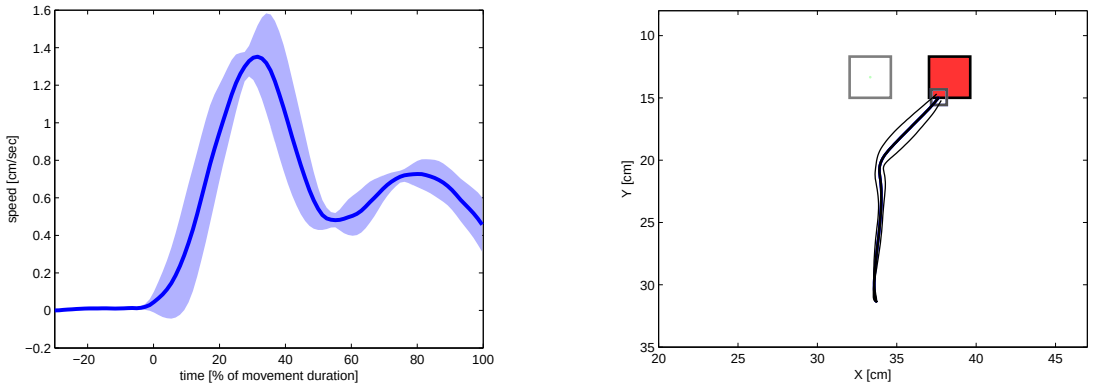

(a) (b)

Figure 5.12.: Results of the perturbed jump side condition: (a) The velocity profile (dark blue, with standard deviation in light blue) of the movement shows a secondary peak which often can be observed in perturbation experiments. (b) Here the trajectory of the movement with its standard deviation can be seen. Initially the movement is directed towards the unperturbed target (white square) and corrects later onto the final target object (red square).

results can be found in Table 5.6 and in the Figures 5.13 and 5.14. The results of the measures are as follows:

Peak velocity: The PV depended mainly on the initial target size. The PV of the smaller initial target (grow condition) is smaller than the one of the larger initial target (shrink). The same trend can be found in the baseline conditions, however, the baseline PVs are slightly higher than the PVs of the perturbed conditions (see Figure 5.13). This effect was also observed in the first part of the experiment.

Time to peak velocity: Also the TPV depended mainly on the initial target size, however the differences are smaller than in the PVs. The TPV is slightly smaller with larger initial target (shrink) and larger unperturbed target (see Figure 5.13). The TPVs of the perturbed conditions are smaller which is consistent with the experiments of the perturbed target location.

Time after peak velocity: Like in the perturbed target location conditions the TAPV of the perturbed conditions is significantly higher than in the baselines (see Figure

condition	MT [sec]	PV [cm/sec]	TPV [sec]	TAPV [sec]
far	23.9 (0.8)	1.29 (0.11)	6.2 (0.7)	17.7 (1.4)
near	16.9 (0.9)	1.51 (0.06)	5.9 (0.4)	10.9 (0.8)
side	23.2 (1.9)	1.46 (0.11)	5.5 (0.4)	17.7 (1.5)
BL				
near	16.1 (0.9)	1.32 (0.12)	6.8 (0.9)	9.2 (1.7)
initial	17.0 (1.6)	1.48 (0.24)	7.3 (1.6)	9.7 (1.8)
far	17.2 (0.8)	1.72 (0.12)	6.4 (0.4)	10.8 (0.5)
side	18.7 (1.0)	1.41 (0.04)	7.6 (0.4)	11.1 (1.2)

Table 5.5.: Results of the target location perturbation experiment. Displayed are mean values with their standard deviation in brackets.

5.14). The TAPV of the shrink condition (small final target) is slightly lower than the one of the grow condition (large), here the opposite effect was expected. This result is not fully consistent with the empirical evidence. The general increase is caused by the deceleration of the *Onset* mechanism.

Movement time: The MT depended on the behaviour of the TPV and the TAPV. The first was slightly decreased and the latter greatly increased. Hence, the MTs also show an increase. However, the grow condition is even slower than the shrink condition which was caused by the behaviour of the TAPV.

5.5.4. Discussion & Conclusion

The target perturbation experiments investigated the model's ability to deal with perturbations where the target changed its size or position after movement onset. Overall the model produced good results for the movement time and the kinematic markers. The results were mostly consistent with existing behavioural evidence even though it was difficult to achieve human-like behaviour in all measures. In comparison with the Fitts' law experiment where the target object remained constant the setting here was more complicated as the robot had to react towards a changing environment.

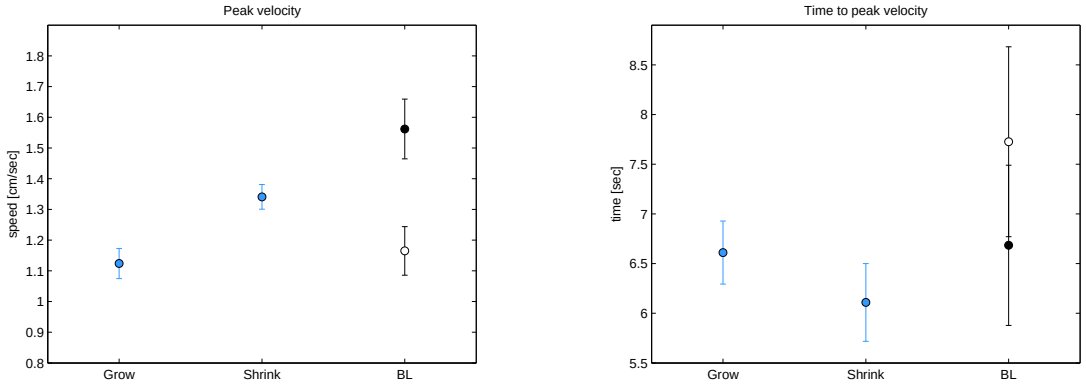

(a) (b)

Figure 5.13.: Results of the target size perturbation experiment. Shown are the mean values of (a) PV and (b) TPV of the different conditions. The colour code is similar to Figure 5.10, however, the perturbation conditions are now coloured blue. White data points show the results for the small and black for the large object baseline (BL) results. Both measures are influenced by the initial target size as they show similarities with the appropriate BL conditions: For instance the PV of the grow condition (small initial target) is smaller than the shrink condition (large initial target) which is similar to the BL behaviour where a small target shows lower PVs than a large target.

Humans easily deal with such situations by adapting their behaviour, however, before a reaction can take place a visual delay time is needed to fully process the sensory feedback and to adapt the already initiated movement. My model as well has a visual delay as it needs time to process changing visual information and to adapt the underlying DNFs. However, the model only relies on visual information while humans have access to a wider range of feedback and sensory input such as proprioceptive information and forward models (or efferent copies). This was tried to be simulated by increasing the delay for the target location map (T map) with the dead-time parameter, therefore the target information needs more time to be processed and is updated much slower than the hand position.

The results show that (with few exceptions) some of the measures are dominated by the properties of the initial target (namely PV and TPV) while other measures show a clear influence of the perturbation effect and the properties of the final target

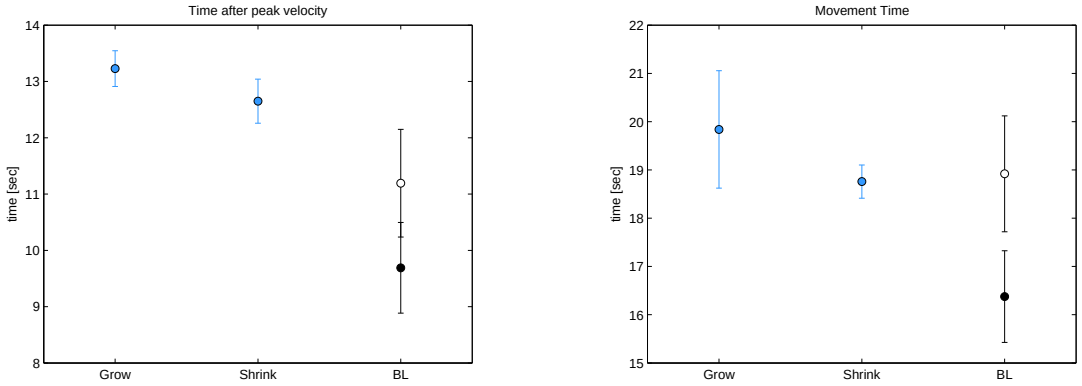

(a) (b)

Figure 5.14.: Results of the target size perturbation experiment. Shown are the mean values of (a) TAPV and (b) MT of of the different conditions. The colour code is similar to Figure 5.13. The perturbation greatly affected the TAPV which also influences the MT.

(TAPV and MT). Thus, generally the results are in harmony with the findings of perturbation studies (e.g. Heath et al., 1998).

Besides the visual delay the second reason for these results is the *Onset* mechanism which causes a short but strong deceleration effect once the perturbation has been processed by the moving blob in the V map. Similar "onset-effects" have been observed in experiments before (e.g. Castiello, 2001) and a common result of perturbation experiments of this kind is strongly increased MTs so that this implementation seems to be a natural way to effect the ongoing movement. This mechanism is responsible for the higher TAPVs that could be observed in all perturbation conditions. However, the *Onset* mechanism only shows human-like results with an appropriately chosen processing time of the model which can be controlled with the time constants of the DNFs and the dead-time parameter. When this processing time is too short, then the model would react quickly toward the perturbations and the measures would mainly depend on the final target properties. In contrast, a very high processing time would not allow corrective movements before the initial target had been reached. However, such behaviours would contradict the behavioural evidence. Hence, both, the *Onset*

condition	MT [sec]	PV [cm/sec]	TPV [sec]	TAPV [sec]
shrink	18.8 (0.3)	1.34 (0.04)	6.1 (0.4)	12.6 (0.6)
grow	19.8 (1.2)	1.12 (0.05)	6.6 (0.3)	13.2 (1.0)
BL				
small	18.9 (1.2)	1.17 (0.08)	7.7 (1.0)	11.1 (1.7)
big	16.3 (0.9)	1.56 (0.10)	6.7 (0.8)	9.7 (0.7)

Table 5.6.: Results of the target size perturbation experiment. Displayed are mean values with their standard deviation in brackets.

mechanism and the processing time, are responsible for the observed behaviour in my model.

Another important point is that the effect of the *Onset* mechanism is stronger when the target jumps from one location to another than when a stationary target changes its size. This effect is caused by the underlying DNFs as the observed "difference" in the T map is larger with a target displacement. The difference feeds into the control of the strength of the *Onset* mechanism which influences the moving blob. This is consistent with the experimental evidence (e.g. Heath et al., 1998; Paulignan, MacKenzie, et al., 1991; Paulignan, Jeannerod, et al., 1991).

With the visual delay (dead-time) and the *Onset* mechanism as main influence on the results it can be said that the results of the target perturbation experiments are caused by mechanisms that did not play a relevant role in the earlier goal-directed reaching experiments of chapter 5.3 and 5.4. This suggests that humans also possess separate mechanisms to account for perturbation effects.

5.6. Hand perturbation experiment

This final goal-directed reaching experiment applied a perturbation paradigm of the perceived hand location. The setup was inspired by the experiment of Saunders

and Knill (2005) who performed an experiment where participants were required to perform straight reaches towards target objects. In their experiment a perturbation occurred after the hand had moved 25% or 50% of the distance toward the target and affected only the perceived location of the hand. Hereby the hand's location was smoothly shifted a few cm nearer, further away or towards the sides. Saunders and Knill (2005) found that participants initiated online-controlled correction movements to account for these perturbations. Their main findings were that the perturbations were not fully compensated and perturbations that shifted the hand sideways were corrected with a smaller latency than perturbations along the movement direction.
In my model movement direction and amplitude are not independent as both are determined by the moving blob in the V map. The moving blob can move freely within the DNF without distinguishing between movement direction and distance. Therefore the expected outcome would be that my model shows no difference in the latency of the corrections of perturbations along the movement direction or sideways.

5.6.1. Methods

The experimental setup was similar to the previous experiments, however with the mentioned perturbation effects included. Besides a baseline condition without perturbation effect three conditions were implemented: the perceived hand location could move to a point closer (*near*), further away (*far*) or to the side (*side*) in relation to the actual hand location. The perturbation effect occurred six seconds after the initiation of the movement in the first half of the trajectory similar to the setup of Saunders and Knill (2005). Movement initiation was determined in a similar way than in previous experiments.
Target objects were again coloured markers and were placed in a distance of 20 cm in front of the hand. The perturbation effect changed the perceived location of the hand

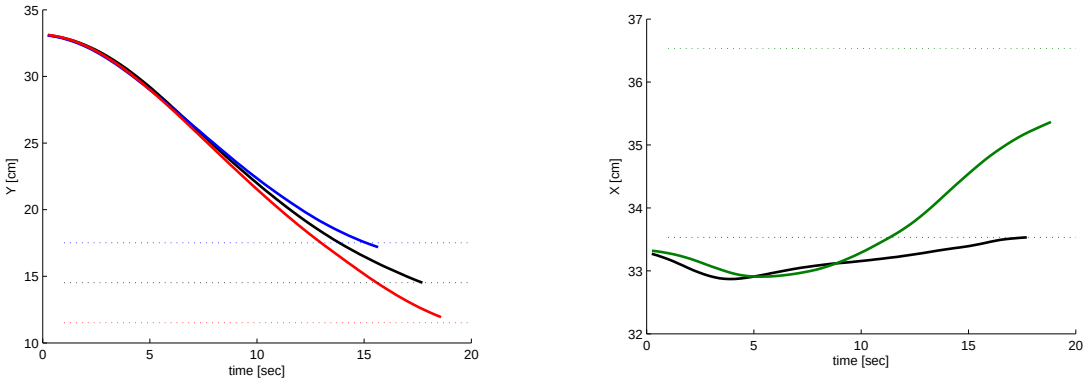

(a) (b)

Figure 5.15.: Trajectories of the hand perturbation experiment shown in the dimension of the perturbation. (a) Perturbation of the perceived hand location in the near (blue thick line) and far condition (red) in comparison with the baseline (black) in direction of the perturbation (y-axis). The endpoint location of the baseline and the amount of the perturbations are shown with the dotted lines. (b) Perturbation of the perceived hand location in the side condition (green) in comparison with the baseline (black) in direction of the perturbation (x-axis). Both graphs show that the perturbations were not fully compensated.

by applying a shift to the output of the H map in the sigma-pi unit. In this way the perturbation effected the ongoing movement as the hand-centred target location in the D map moved to account for the shift. The amount of the shift was five neurons in the H map and was applied immediately.

The trajectories of the movement were recorded and processed like in the previous experiments. The processed trajectories were used to investigate the effect of the perturbations. Furthermore, the time needed to effect the ongoing movement was calculated using the distance of the trajectories of the perturbed conditions to the baseline trajectory along the dimensions of the perturbation which were along the movement direction for the near and far condition (y-axis) and orthogonal for the side condition (x-axis). Moreover, all further model parameters remained unchanged.

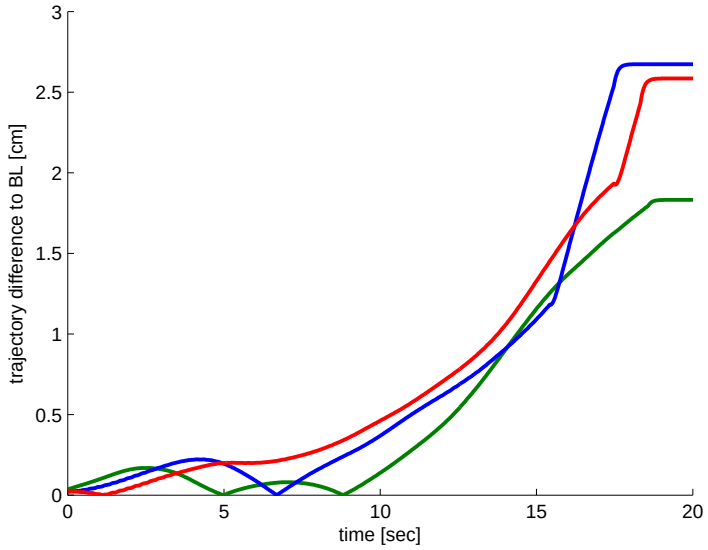

Figure 5.16.: Trajectory differences of the hand perturbation experiment along the movement duration. The perturbation occurred six seconds after movement onset. The lines of all conditions (blue - near, red - far and green - side) crossed the threshold at 1 cm at about the same time.

5.6.2. Results & Discussion

The perturbation had a visible effect on the movement trajectories (see Figure 5.15). The trajectory difference can be found in Figure 5.16. All perturbations caused the hand to veer away from the path of the baseline trajectory to compensate the shift in the perceived hand location. This behaviour was expected due to the closed-loop architecture of the model. However, the perturbations were not fully compensated as the differences of the perturbed endpoints and the baseline were smaller than the applied perturbation. This effect could be found in all conditions, however perturbations in movement direction were compensated to a slightly greater extend (86% in the far and 89% in the near condition) than in the side condition (61%). This result is partly consistent with the findings of Saunders and Knill (2005). They also found that the perturbations are not fully compensated, however to an equal extend across the conditions.

While it was expected by the model not to fully compensate the movements the fact that there was a difference in the compensation between the conditions is surprising. The movements of the robot arm are generated by the moving blob in the V map. This DNF encodes the movement vector for the desired movement. It takes some time to process the hand perturbation by the underlying DNFs so that the movement is initiated with the setting of the initial hand location. Therefore both initial and perturbed hand location play a role in determining the movement which results in the endpoint located in between initial and unperturbed location. However the V map does not make a difference in amplitude or direction encoding. Therefore it was expected that the compensation will be similar in all conditions. The results show that this is not the case. It seems that the moving blob is more sensitive towards changes in the movement direction then to perturbations orthogonal to the movement direction.

The time needed to effect the ongoing movement did not differ between the conditions (see Figure 5.16). The trajectory was considered to be different from the baseline when the trajectory difference crossed the threshold of 1 cm which was chosen high enough to filter the noise but as low as possible to detect an influence of the perturbation quickly. This happened at similar times in all conditions at 13.8 sec (far), 14.4 sec (side) and 14.5 sec (near). Thus the expected result of no influence of the direction of the perturbation was found.

However, even though this result was expected it is not consistent with the findings of Saunders and Knill (2005) who found that sideways perturbations are detected earlier. As described earlier the V map handles movements along the two dimensions in a similar way. In order to fully reproduce the results of Saunders and Knill (2005) modifications would be necessary. A possible extension could be a more sophisticated field dynamic that distinguishes between movement direction and side movements. With such a dynamic the V map could be able to reproduce their findings: if the

side perturbations could be initiated slightly earlier due to a modified field dynamic also their degree of compensation would increase. This would make the results of all measures fully consistent with the findings of Saunders and Knill (2005).

5.6.3. Conclusion

In this last experiment of the goal-directed reaching model I followed the paradigm of Saunders and Knill (2005) who applied a hand perturbation paradigm. In three conditions the hand position was perturbed after movement onset when reaching for a single target. The perceived hand location was shifted towards the target, away from the target or sideways. The results of my model were not fully consistent with the findings of Saunders and Knill (2005). Unlike in my experiment they found a similar effect of not fully compensated movements, however, the degree of compensation did not differ in their experimental conditions. Furthermore, they found that corrections toward sideways perturbations are initiated before corrections along the movement direction.

As my model does not distinguish between movement dimensions (along movement or sideways) this discrepancy with the behavioural evidence was expected to some extend. However, in order to achieve a more consistent simulation results my model would require modifications of the V map and the behaviour of the moving blob. As I did not have the possibility to implement the changes within this thesis I will only discuss them theoretically. With such a modification that gives a higher priority to the movement direction and a lower priority to the movement amplitude the simulation results would exactly match the behavioural evidence. My simulations are also a support for the explanation of Saunders and Knill (2005) who suggested that the brain distinguishes between movement direction and side movements.

Overall my model achieved good simulation results. However, in order to replicate

the behavioural evidence in detail modifications would be necessary. While there was no possibility to implement those modifications I was able to outline where and how they could improve the simulations which is also a demonstration on how my model can extend the knowledge of the human reaching process.

6. General Discussion

The general discussion is divided in several sections. First, I am going to summarise the findings of the different versions of my model in the simulated experiments. Afterwards I will review the functionality of the model and compare it with other theoretical and computational models. Finally, the model is discussed in the context of the neurobiological research before an outlook to possible future projects is given and the thesis is concluded.

6.1. Summary of the experimental findings

6.1.1. Summary of the original choice reaching model

In chapter 2.3 I presented a robotics-based approach to modeling the results of the odd-colour choice-reaching experiment of Song and Nakayama (2008b) and in chapter 3 three experiments were performed with the presented model. The model's abilities were tested in a single target setup and the odd-colour task. In order to simulate real-world reaching movements the output of my model is a robot arm built with LEGO Mindstorms NXT. The Target Selection module is the first or attentional stage of the model which implements a competitive selection process of the odd-colour target. In order to link the output of Target Selection stage with the robot arm I based the whole model on the dynamic field theory by Erlhagen and Schoener (2002).

Crucially, the motor control stage applies moving blob-dynamics in a neural field to ensure jerk-free (human-like) movements. The experiments demonstrated that the moving blob works as intended and that this principle is able to produce human-like trajectories with a bell-shaped velocity profile. An interesting point was that after I introduced a non-linear mapping the velocity profile was enhanced and the robot arm gained a better control when in vicinity of the target. Humans possess such a mapping already on the sensor level with the cortical magnification factor in the eye. The model shows that the motor cortex might apply both corrected (like in the T map) and non-linear mappings (like in the V map of the choice reaching model) to plan and generate movements.

Furthermore, the choice-reaching experiments successfully simulated the odd-colour task. Hereby, the simulations demonstrated that the Target Selection module not only is able to select the correct target, but also to reproduce the curved trajectories that were found by Song and Nakayama (2008b). This was achieved by applying preactivation or priming maps that gave an advantage of one colour or location and influenced the movement in an early stage. Colour priming effects where also suggested by Song and Nakayama (2008b) as reason for the curved trajectories. In the model it is also possible to prime locations; an effect that also has been found in experiments (e.g. Maljkovic & Nakayama, 1996). Interestingly, my model predicts that the priming of a location has a stronger influence on the movement and the trajectory than the colour priming. This prediction needs to be tested in future experiments.

The third experiment investigated how target and distractor objects are selected and passed onto the motor stage. Song and Nakayama (2008b) suggested that distractors have to reach a threshold in order to get activated. My model demonstrated that such a hard threshold is not necessarily required and pointed out the differences in the to be expected results of behavioural experiments to test this hypothesis. Future experiments will have to test those predictions.

Overall the model is consistent with Song and Nakayama's (2009) suggestions that there is a direct link between target selection and movement planning, that both processes work in parallel and that the target selection process is implemented in a dynamic competition.

6.1.2. Summary of the modified choice reaching models

In chapter 4 I presented and simulated further choice-reaching tasks with my model. All these simulated experiments required modifications of the control architecture due to new behavioural results like in the odd-colour Irrelevant Feature (IF) task or due to a different experimental setup like in the experiments to the spatial averaging and the Simon effect.

The experiments demonstrated that the original odd-colour model of chapter 2.3 is easily extendible to account for newer behavioural evidence. Hereby, the introduction of a new threshold and the adaptation of the DNF parameters enabled the model to simulate the difficult relationship of the two measures (reaction time and maximum curvature) which was found in the odd-colour IF experiment. Thresholds also played an important role in the Simon task. Interestingly, the role of thresholds already was a topic in the experiments of the previous section. My model demonstrates that such thresholds can explain multiple findings. I will discuss this feature in a greater detail in chapter 6.2.2.

The remaining experiments had setups that differed significantly from the odd-colour task of Song and Nakayama (2008b). However, with only few modifications to the Target Selection module these different choice-reaching tasks could be simulated. The results of those tasks resembled the existing behavioural experiments.

Overall it could be demonstrated that the control architecture of my model is general enough to simulate a wide range of tasks and to mimic human reaching trajectories.

Contrary, the model is also detailed enough to account for results like the complicated interplay of measures like the reaction time and the maximum curvature in various tasks.

6.1.3. Summary of the goal directed reaching model

In chapter 5 I presented the goal-directed reaching model and simulations of various goal-directed reaching tasks. The model I developed to simulate the goal-directed reaching process based on the original choice-reaching model of chapter 2.3. With the LEGO Mindstorms NXT robotic arm, the original hardware set-up and the new goal-directed reaching model I simulated various experiments. The first two experiments dealt with the speed-accuracy trade-off and its implications on movement parameters. The remaining experiments investigated the effects of perturbations on the movement.

One remarkable finding was that Fitts' law (which is the mathematical relation between movement time and size or distance of the target object) could be simulated with my model which mainly operates with the topological representations of movement parameters in the underlying neural fields. In this way my model offers an elegant approach to explain Fitts' law in a neurological plausible way. Also in the other experiments human-like behaviour could be simulated.

In order to simulate the experiments the functionality of the moving blob was extended by additional mechanisms that process further information such as perturbations and target properties. This information directly influences the moving blob and therefore the ongoing movement. I will continue to discuss this characteristic in chapter 6.2.4.

Traditionally, goal-directed reaching is explained with the two-component models that consist of a preplanned ballistic movement and a control phase at the end of the reach (see also chapter 2.1.2). The successful simulations showed that the

speed-accuracy trade-off and perturbation effects can also be mimicked applying the feedback-based closed-loop principle where no preplanning is necessary. Hence my model can contribute to the discussion about the underlying principle of goal-directed reaching movements. I will compare my model in detail with the existing models of goal-directed reaching in chapter 6.3.

6.2. Model characteristics

The different versions of my model have shown their abilities to simulate a wide range of choice-reaching and goal-directed reaching tasks. Despite the differences in the experiments all versions of the model share a number of common theoretical assumptions such as the closed-loop principle, dynamic neural fields (e.g. a target selection map, a map that converts the target location information into a hand-centred coordinate system etc.) or mechanisms like the moving blob in the velocity map that converts the hand-centred target information into specific movement attributes.
These characteristics play an important role for simulating visual attention and motor control which resulted in the the observed behaviour. Here I will discuss those characteristics in a greater detail. It is divided in several sections to discuss the distinct attentional and motor control features.

6.2.1. Visual attention

Visual attention was an essential feature in the choice-reaching tasks and is simulated in the Target Selection module. In contrast, for the goal-directed reaching experiments where only one target had to be attended this module did not play an important role and was simplified. Hence, I will focus on the attentional aspect of the choice-reaching models. There the Target Selection module consisted of two DNFs that represent target location (T map) and target colour (T_{col} map). In order to reach for the target

its location is the crucial feature, hence, only the T map passes its activation onto the motor stage. However, also the colour can influence the motor stage as both DNFs are interconnected. Moreover, colour was the relevant dimension to identify the target for the simulated choice-reaching tasks.

Both DNFs receive an input consisting of the colour maps from the image preprocessing. The exact interconnectivity and the role of the target colour map was task dependent to some extend, however, the model shows some common features: First, the colour maps are directly fed into the target selection map and create activations at the objects' locations. This can be interpreted as a default direct route where only the appearance of an object attracts attention whereas other object features require more processing time. The target determining colour information is processed in the T_{col} map which influences the target selection due to its connection to the T map. However, this pathway takes more time to be processed. Hence the T map already has established activations from the fast direct route which have to be overwritten in order to inhibit distractors. There is plenty of evidence of the existence of such a fast direct route and a slow indirect route from different tasks (e.g. Tipper et al., 1998; Kornblum et al., 1999).

There is evidence that suggests that more than one target or motor response can be activated at a time (see chapter 4.2.1 or Tipper et al., 1998; for a review). This fact is also featured in the T map which can establish several activations within its topological representation of the environment and passes them along to the motor stage. Note that this behaviour strongly depends on the parameters of the DNF which were chosen in a way to support this behaviour. For instance the usage of thresholds can limit this ability (see also chapter 6.2.2). However, there also is a maximum number of activations that the DNF can establish at a time depending on the parameters and its spatial resolution.

My implementation is consistent with behavioural evidence and theories of attention.

For instance the biased competition theory states that there are only limited resources in the brain to process visual information (e.g. Duncan, 2006). Hence when a target is presented with distractors all those objects compete for attention which affects measures such as the latency or the trajectory. This fact is represented by the neural field dynamics in the T map in my model which also can only represent a limited amount of target objects due to the neural field dynamics. There already exist a number of computational models that implement visual attention in a similar fashion (e.g. Trappenberg, Dorris, Munoz, & Klein, 2001; Heinke & Humphreys, 2003).
However, in contrast to most other models an important aspect of my model is that the Target Selection module does not operate isolated and independent from the other modules. Instead all modules operate in parallel and can influence the ongoing movement. This is an important aspect which should be considered when developing models of cognitive processes. In this way the Target Selection module continuously passes its information onto the Movement Velocity Control stage and can influence the movement at all times. Changes in the attentional stage affect the motor stage with only little processing delay. This is consistent with Song and Nakayama (2009) who found evidence for the parallel operation of movement control and visual attention in their choice-reaching tasks. My model shows a plausible implementation on how such a parallel structure could be realised.

6.2.2. Thresholds

In this section I am going to discuss the role of thresholds within the control architecture of my model. Generally, the information transfer in my model works in a continuous fashion so that the modules and DNFs receive inputs from earlier processing stages and pass it onto later stages. Hereby, all modules and DNFs operate in parallel and the DNFs pass all of their output activation along. However, as

demonstrated also the use of thresholds in between DNFs is applicable in such an architecture. Several experiments such as the odd-colour "threshold" experiment (see chapter 3.3) or the odd-colour irrelevant feature experiment (see chapter 4.1) investigated the influence of such thresholds on the behaviour of the robot arm.

In those experiments thresholds between target selection and motor stage play an important role for the simulation results. The relation between these two stages is not a simple single route from perception to action. This is reflected by the complex relation of measures such as the curvature and the latency. For instance, a typical effect in choice-reaching tasks is that with longer Reaction Times (RT) the Maximum Curvature (MC) decreases (e.g. Song & Nakayama, 2008b). In the simulations of the Simon task (see chapter 4.3) I demonstrated that a threshold behind the target location map can cause this effect. Moreover, a threshold at this location can also influence how many activated targets will be passed onto the motor stage as demonstrated in the experiment of chapter 3.3. A high threshold allows only fully activated targets to be passed on. Due to the global inhibition in the DNF dynamics then only one target can be activated at a time. A similar mechanism has been suggested by Song and Nakayama (2008b) to explain the curved trajectories. In contrast a lower threshold allows the target selection stage to pass more than one activated target onto the motor stage (e.g. chapter 4.2). The different experiments of my model demonstrated that several findings can be explained with different values of this threshold.

There are findings that differ from these results such as the outcome of the odd-colour irrelevant feature task where RT and MC show a similar pattern where conditions with a high RT also show a high MC and vice versa. There, my model demonstrated that this can be explained with a threshold at different neural layers between perception and motor stage like the target colour map threshold in the simulation of this task (see chapter 4.1). Hereby, the detection of a location independent feature (the colour)

controlled the movement initiation. My model could help to explain and understand the complexity of different experimental findings with thresholds between cognitive sub-processes.

Finally, with thresholds my model can demonstrate how the paradigm of the choice-reaching tasks works: The findings of those experiments base on the fact that due to the ongoing movement hidden cognitive processes "leak" into the movement trajectory. No such effect can be found when participants have sufficient time to terminate the target selection process (e.g Buetti & Kerzel, 2008; for an example in a Simon task). My model simulated such effects in several experiments with the application of threshold parameters (e.g. chapter 3.3 and 4.3). Moreover, my model can visualise those internal activations and threshold and can demonstrate their influence on reaction times and movement trajectories.

In a summary, my model shows how and where thresholds can be active to explain in-depth behavioural evidence of various measures. Then even complex relationships between different measures such as the latency and the curvature of the movement trajectory can be described by simple mechanisms. Hence, my model can be used as a tool to verify or to test theoretical assumptions or experimental evidence of choice-reaching tasks and therefore can contribute to the research in this area.

6.2.3. Motor control

As I aimed to simulate the human reaching process with a robot arm motor control is an important aspect in all experiments. The main parts of the motor control stage of my model are the hand target difference (D) map and the velocity (V) map. The D map converts birds-eye target information into a hand-related target position. This is realised using a sigma-pi unit which offers an easy way to combine two DNFs (McClelland et al., 1986). Note that the activation of the D map also

could be interpreted from the hand's point of view. Then the centre of the map would encode the target position and an activation in the map the current hand position. As humans tend to saccades towards attended objects (e.g. Abrams, Meyer, & Kornblum, 1990) this might be an alternative interpretation of the encoded information in the D map. However, the hand-centred target representation is supported by existing behavioural (e.g. Tipper et al., 1997) and neurobiological evidence (e.g. Buneo & Andersen, 2006; more details in chapter 6.4).

The V map is the centre piece of the motor control stage. Here the permanent activation of the moving blob encodes a speed vector of the upcoming movement. There is evidence that movements are encoded in the brain in cartesian coordinates as it is the case in the velocity map (e.g. Desmurget et al., 1998; for a review). It also has been suggested that movement amplitude and direction are not independently controlled (Sarlegna & Blouin, 2010) as it is the case in my model where the moving blob moves freely along those two dimensions. The moving blob itself has more features than simply encoding the speed. Its further functionality will be discussed in detail in the next section.

Another important point to note for the motor control is the usage of some form of "cortical magnification factor". In the original version of the model of chapter 2.3 a non-linear encoding schema was applied to the output of the V map. With this encoding more neurons in the V map encoded slower speed values and less neurons higher speed values. Note that for the goal-directed reaching model the non-linear encoding was moved to the D map. This was justified with better simulation results (i.e. no overshooting of the target and more natural velocity profile) and due to the fact that this can be a natural method to achieve a higher accuracy when the hand is close to the target object. Interestingly, the human body possesses such a non-linear encoding already at the sensory level in the eye (Rovamo & Virsu, 1979). Hence, it is possible that the brain utilises corrected linear and unchanged non-linear

encoded visual information which could still be present in the motor stage. Both representations contain important and distinct information such as size or distance of the target that can be useful for planning the movement like it was applied in the goal-directed reaching model with the *Acc* mechanism.

Not a direct part of the model but important for executing the movement of the robot arm is the Inverse Kinematics module. As my model generates the desired movement vector it is sufficient to apply a simple transfer function to convert the cartesian movement vector into a joint space vector. This is in contrast with many models that consider the mechanical and anatomical constraints of the arm. However, my model shows that the reaching process can be simulated in a human-like fashion with a simple transfer function.

6.2.4. The moving blob interface

The probably most remarkable feature of the model is the moving blob in the velocity map. The moving blob is a permanent activation that encodes a speed vector of an upcoming movement. It is designed in a way that it only slowly moves through the field to avoid sudden changes and jumps in the velocity. Although it remains open whether a mechanism like the moving blob really exists. The results of all experiments show that such an implementation is feasible and can generate straight human-like movement trajectories with a bell-shaped velocity profile.

However, the moving blob in my model is more than just a method to generate those trajectories. Moreover, it is an interface between attentional and target relevant information and the motor stage. In the original choice-reaching model the moving blob movement is determined by the default activation in the centre of the map and the (hand-centred) target location activation from the D map. More importantly, not only the target location but also further target properties and other task dependent

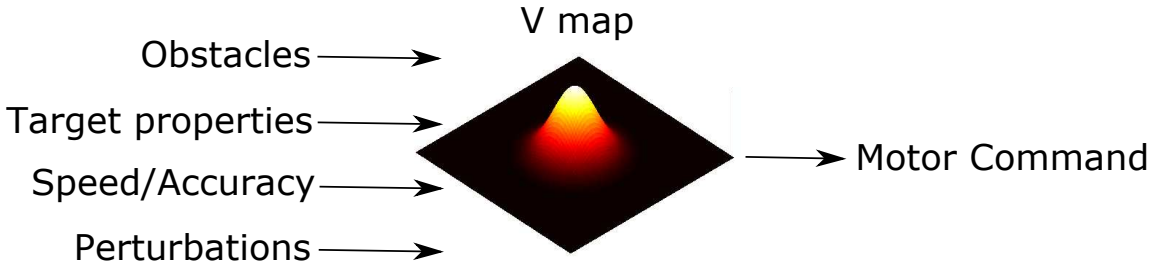

Figure 6.1.: The moving blob encodes the speed vector of a desired movement. It is designed in a way that it acts as an interface between the sensory/attentional and the motor control stage. Target features such as size or distance (encoded in the activation of the D map) have a direct influence on the behaviour of the moving blob in the V map. Moreover, multiple targets could be encoded which results in an averaged movement vector. Its functionality was greatly extended in the goal-directed reaching model. There also speed-accuracy constraints of the movement or perturbations can affect the moving blob due the new mechanisms (*Acc* and *Onset*) that connect the T and D with the V map. Future extensions could increase its functionality further. For instance an obstacle avoidance mechanism could be included.

constraints can influence the behaviour of the moving blob (see Figure 6.1). In the different version of the choice-reaching model the moving blob converts the current state of the encoded target objects into a speed vector to an average location of those objects. In the goal-directed reaching model where only one object was presented at a time the moving blob modulates the task requirements of speed and accuracy as well as considering the target size. Moreover, with the *Acc* and *Onset* mechanisms additional pathways were introduced that influence the movement substantially. Again these mechanisms work through the moving blob.

The moving blob mechanism is an example on how a single module can integrate sensor inflow and motor outflow. The existence of such a single feedback module in the motor control system has been proposed before (e.g. Desmurget & Grafton, 2000; Miall & Wolpert, 1996; Kirsch & Hennighausen, 2011). Also there is increasing evidence that there is no strict separation of planning and online-control mechanisms. For instance, a single mechanism that can adapt weightings for different kind of

feedback in the time course (e.g. proprioceptive feedback plays a big role in the early movement and visual feedback dominates in the late movement when it is available) has been suggested (e.g. Guigon, Baraduc, & Desmurget, 2008). Even though my model is solely based on visual feedback the moving blob mechanisms demonstrates how such a single mechanism that integrates different kinds of feedback and information might look like. Finally, to my knowledge there is no computational model that realises this mechanism and which is able to simulate multiple reaching experiments.

Summarising it can be said that the way the moving blob works is a neurological plausible integration mechanism for different kinds of information with the purpose to effectively plan and control movement parameter. Moreover, as already outlined in the previous section no extensive planning is necessary to integrate these information into an ongoing movement. Thus, the moving blob interface offers a parsimonious and neurological plausible way for generating movement trajectories.

6.2.5. The role of visual feedback and delay

Due to the closed-loop architecture of my model visual feedback is essential at all times to successfully reach for targets. Moreover, it is the only source of incoming sensory information as my model lacks of other kinds of sensors (like proprioceptive feedback).

As mentioned in chapter 2.1.2 the processing of visual feedback causes a delay in humans. This is also the case in my model where new visual information has to be processed by the different DNFs to adapt the movement of the hand.

Due to the lack of different kinds of feedback in the model faster feedback had to be simulated for the hand perturbation experiment. There the goal-directed reaching model simulates the influence of different kinds of sensory feedback of the arm in the

following way: The dead-time parameter leads to a delay for the processing of target information but does not influence the speed of updating the hand position. Hence changes in the hand position can be updated much quicker than changes in the target position. The delay in my model can be related to the reaction times which where in the goal-directed reaching model of chapter 5 between 2-3 seconds (without dead-time; approximate time for updating hand) to 7-9 seconds (with dead-time; approximate time for updating target). These values are faster than the movement times of the Fitts' law task which were between 13-20 seconds. In this way the presence of a faster source of feedback (e.g. proprioceptive) can be simulated even though the only available feedback remains the visual feedback. As mentioned before the visual delay in humans has been found to be as fast as 110 ms, while faster kinds of feedback were found in up to 30 ms (Elliott et al., 2001; for a review).

However, above principle of my model and the closed-loop principle in general have some important constraints. In this way my model crucially depends on the constant flow of incoming visual feedback as it represents the only source of information. Visual feedback has shown to offer a greater precision over proprioception (e.g. Guigon et al., 2008). Results of behavioural experiments show that when the hand and target position can only be seen before the movement and no visual information is available during the reaching process, the error rate typically increases while the accuracy decreases (see Elliott et al., 2001; for a review).

However, generally it is possible for humans to execute reaches without the permanent vision of hand and/or target. For instance experiments can be found where reaches are finished before visual information could be available or where reaches are performed in the absence of visual feedback (Elliott et al., 2001; for a review). Hence I want to discuss those conditions with respect to my model here.

My model would be able to perform reaches in conditions for very fast movements or without visual feedback only with an extension that includes non-visual feedback

to update the hand's position. Furthermore it would require an adjustment of the parameters in order to maintain the target activations in the DNFs. However, with such an extension the uncertainty about target and hand location would be increased which could possibly result in a "blur-out" effect that leads to broader activations in the underlying DNFs of hand and target and eventually would lower the accuracy for the velocity encoding. Hence, the model is not only able to handle those conditions but could also explain the behavioural evidence of such experiments.

Extensions also would be required for reaches that have to be executed and finished before the (visual) closed-loop cycle can be closed. This includes experiments where very fast reaches have to be made. However, following the philosophy of my model such reaches still had to be simulated following the closed-loop approach but applying different and faster kinds of feedback. Note that the model would be able to simulate such reaches with above dead-time mechanism where the faster proprioception feedback is simulated with non-delayed visual information while the (real) visual information receives the dead-time parameter and is perceived delayed by the model.

Other aspects of goal-directed reaching that were not the main issue of the simulated experiments, however, important for the human reaching process are learning and practice effects. Elliott et al. (2010) reviewed numerous findings of goal-directed reaching experiments. They found that when humans reach for targets in similar settings the reaching becomes faster and more accurate over time due to the practice effect. Also it seems that with more practice participants rely more on visual feedback than without. In my model this can be explained by an optimisation of the DNF parameters. In a new or unknown setting the model could fall back on default parameters which could be encoded in the motor cortex. A training effect is achieved when reaches in a similar environment are performed which adapts and optimises the parameter of the DNFs and in particular of the moving blob. In a following trial the new parameters would lead to a faster and more precisely moving blob. In order to

achieve this behaviour the exact position of hand and target must be known which could explain the fact that participants rely stronger on visual feedback.

6.2.6. Processing limitations

This section will give a further insight into the constraints and processing limitations of my model and humans. While the need of visual feedback was already discussed in the last section here I will focus here on different aspects.

One important point in my model is the choice of plenty parameters. The selection of these parameters was done manually. Hence, it is likely that there exist parameter values that are more optimal than the ones shown (see also chapter A.2). However, when the chosen values are modified slightly the behaviour of the model should not change significantly. In comparison with the human motor system it could be speculated that processes that select those parameter could be part of learning modules or a planning component for a reach.

Another aspect is the presence and the handling of noise. In my control architecture noise is mainly generated in the processing of the visual input and in the execution of the movement (the motors). The DNFs in the model typically require some (artificial) noise to work properly, however, due to the already present noise it was not necessary to include much noise there. Humans also possess noise in their perception-action system, however, the noise present there is not necessarily equivalent to the noise which is present in the model. For instance, humans possess a very efficient vision system so that the noise here might be lower than in my model. However, for arm movements humans have to take care of the handling of forces and the noise resulting from forces which was not necessary for controlling the robot arm. Summarised it can be said that my model - like humans - is able to handle a range of noise of different sources. However, the noise present in the model does not represent the same noise

that is present in the human perception-action system.

6.3. Comparison of my model with existing models

After having discussed the characteristics of my model I am going to compare those with existing models. There already exist plenty of models for simulating the human reaching process as a whole or parts of it such as visual attention, action selection, and movement control or distinct phenomena such as the Simon effect. Some models were already reviewed in chapter 2.1. Here two different kinds of models will be discussed. First, I will focus on goal-directed reaching models. Here I will compare my closed-loop model with recent versions of the popular two-component models. Later, in the second part my model will be compared with existing computational and mathematical models regarding visual attention and action selection. Hereby, I selected models that have demonstrated their ability to simulate human-like behaviour in areas that can be compared with my model such as response selection or movement control.

6.3.1. Goal directed reaching models

In chapter 2.1 I presented the main principles of models regarding the goal-directed reaching process which were the open-loop, closed-loop and hybrid models that are a mixture of the two. Amongst those the class of the (hybrid) two-component models are the most popular explanation and have a the longest tradition in explaining goal-directed reaching (Woodworth, 1899; see Meyer et al., 1990; for a review). The fact that I was able to simulate the goal-directed reaching experiments with a purely closed-loop architecture of my model changes the point of view for two-component models. As reviewed in chapter 2.1, in these models the first component is a pre-planned ballistic phase in which the hand moves towards the target. This component

plans the movement in an open-loop fashion depending on the target's characteristics, but also on the environment (e.g. obstacle avoidance). The second component applies the principle of online-control to successfully land on the target. More recent explanations distinguish between multiple processes within these two components (e.g. Elliott et al., 2010).

The simulation results of the goal-directed reaching experiments showed that phenomena such as the kinematic marker behaviour of reaches in a Fitts' law task of humans (see chapter 5.4) or perturbation effects can emerge with a continuous closed-loop model without an implementation of two distinguished and independent components. The model simply depends on visual information about arm and target location and permanently generates (cartesian) movement vectors which are processed into joint speeds by an inverse kinematics transfer function. Note that an observer without knowledge of my underlying model could interpret its results as well in the two-component way, however, the impression of an initial off-line phase only arises due to two characteristics of the model: First, the moving blob moves "like previously planned" to its peak velocity location (although completely input driven). Secondly, due to the processing time (or visual delay) of the model it can not react immediately to a changing environment which could also be seen in the results of the perturbation experiments where the model required some time to react toward the changing target properties. This fact could be misinterpreted by the observer who assumes that the first phase is pre-planned.

Although, my model is consistent with some aspects of the two-components models in general. I will compare some of its characteristics and explanations for the goal-directed reaching experiments with the most recent ones: the planning-control model of Glover (2004) and the multiple process model of Elliott et al. (2010).

As mentioned before in chapter 2.1, Glover's model (like all two-component models) distinguishes sharply between the planning and control processes. Glover describes

planning as a phase which operates prior to a movement where spatial and non-spatial characteristics of the target influence the selection of a suitable motor program and its kinematic parameters such as timing and velocity. Also in the multiple process model of Elliott et al. (2010) planning includes "specification of magnitude & timing of muscular forces" which is not the case in my model where these factors are purely driven by the neural field parameters and the target characteristics such as size and location.

In comparison with these explanations it is apparent that the planning component in my model turns out to be limited on selecting a target object and specifying parameters for the movement dynamic. Later the determination of velocity and direction of the movement takes place at all stages of the movement. This is solely driven by the activation of the selected target object. Hence, planning on a lower level is reduced to a minimum and takes place during the whole reaching process which is more similar to the second component of the two-component models. In this way it is not necessary to plan the timing of specific muscles, forces, or movement trajectories. The planning phase that takes place prior to the movement consists only of the target selection component and ends as soon as the moving blob moves away from its resting point in the centre. Hence in my model planning is a much smaller component than suggested by Glover (2004) and the predefined motor plans of the planning-control model only would encode parameter settings of the DNFs in the model. The Fitts' law behaviour then emerges directly from the dynamics of the movement and the encoding of the speed in the V map and is not pre-planned as suggested by Glover. From this point of view the moving blob could be interpreted as an interface of the incoming sensory information and the outgoing speed signals as it is the V map where the information of all pathways (and mechanisms) is integrated (see also chapter 6.2.4). Note that contrary to Glover's model non-spatial parameters such as fragility or function of the target do not play a role in my model. In fact such target characteristics

may require a further planning process. However, I think that an extension which handles these non-spatial parameters would solely influence the DNF parameters. From that point of view it could be said that the planning process could be reduced to a process which selects appropriate parameters for the underlying DNFs, the threshold between the different DNFs (T, D and V map) and particularly the parameters for the V map that controls the dynamic and the velocity of the movement with its moving blob. Note that my model is not able to plan or determine the parameters on its own. However, a "learning module" extension of the model could be able to optimize the parameters.

As my model is based on a closed-loop approach online-control plays a major role for guiding the hand to its target. After the initiation of the movement the model permanently generates movement vectors in a feedback-loop to adapt the ongoing movement. Hereby visual feedback is important to receive the location of target and hand. However, target and hand information is not perceived in the same way: Due to the dead-time parameter in the goal-directed reaching model the target map needs more time to update information about the target object. In contrast, the hand location is updated much quicker as the delay time does not apply here. This difference is supposed to reflect the fact that humans have mechanisms to achieve a similar functionality which the model lacks: efferent copies, forward models and proprioceptive feedback.

Glover's model works in a fairly similar way: the control phase relies fully on feedback loops that make use of visual information. This phase is responsible to guide the hand to the target location. Furthermore, Glover includes the usage of efference copies and proprioceptive feedback into this component. However, the main difference between his and my model is that in my model the control phase is active thorough the whole movement and not only towards the end of the trajectory. Elliott et al. (2010)'s multiple process model differs from above explanations: they include the usage of

early control mechanisms into the first phase of the two component models. Such a separation does not seem parsimonious as then the first phase would be ballistic in principle, however with the mentioned early online-control exceptions.

There already exist computational models that realise a closed-loop feedback based control of the goal-directed reaching process. For instance the already mentioned model of Hoff and Arbib (1993) which is based on the control theory and simulated reaches towards single target objects. My model offers some advantages over their model as it possesses a neurological plausible control architecture and includes features such as the target size in an elegant way. Another example is the model of Gawthrop, Lakie, and Loram (2008) who also followed a control-theory feedback-based approach. They found evidence that with this approach Fitts' law only can be modelled with a forward model and a predictor that estimates future states in order to calculate the movement. However, my model demonstrates that Fitts' law can emerge from a closed-loop approach with only visual feedback available and no included forward model or predictor which speaks against a purely control-theory based approach for simulating goal-directed reaching.

Summarised it can be said that my model offers an alternative perspective of the goal-directed reaching process. In contrast to the most popular approach of the two-component models my model utilises a single mechanism that continuously updates movement parameter solely driven by visual information about target and hand. Moreover, in the numerous goal-directed reaching experiments my model demonstrated that its novel DNF approach has advantages also compared with existing closed-loop models.

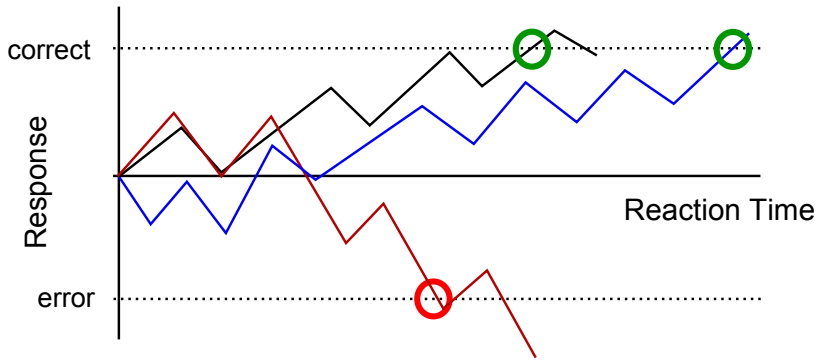

Figure 6.2.: Principle of the diffusion model (Ratcliff & Rouder, 1998) as an example of the decision models. Information is accumulated continuously over time until a response boundary is reached (dashed line). The upper response boundary represents correct decisions while the lower one represents error decisions. Three example paths can be seen: The black line leads quickly to a correct response, while the red one generates an error signal. The blue path evokes a correct response, however at a higher reaction time.

6.3.2. Mathematical & Computational models

Besides models for goal-directed reaching there exist numerous computational and mathematical models that simulate parts of the human reaching process. I will present the most important approaches here and discuss them with respect to my model.

Decision models

In this section I am going to present the diffusion model as an example of a mathematical decision model. Such mathematical models offer a more abstract way to explain cognitive behaviour. The diffusion model is a prominent example of the sequential sampling models (e.g. Ratcliff & Rouder, 1998; Smith & Ratcliff, 2004). It was developed to simulate the internal decision process of two choice decision tasks and is a useful tool to describe this process and to explain reaction times in such tasks. Its basic principle is that information for or against a particular response is accumulated over time. Once a (positive or negative) threshold has been reached an appropriate positive or negative response is evoked. The detailed functionality is explained in

Figure 6.2.

The functionality of the T_{col} map in my model is somewhat similar to the diffusion model. This map consists of only two neurons and is the location where the decision for the correct target colour is determined based on the amount of colour of the target and distractor objects (in the original odd-colour model of chapter 2.3). Hence, in theory a diffusion model could be implemented instead of the T_{col} map for simulating the colour selection. Experimental evidence demonstrated that the diffusion model simulates very well reaction times and their distributions for two choice decisions (Ratcliff & Rouder, 1998), however it is obvious that it accounts solely for the decision process. Hence, the underlying processes that first preprocess the necessary sensory input and on a later stage transform this decision into an action can not be explained with this kind of model. In contrast, my model implements all necessary steps to generate a motor command from a camera image. Even though some modules are implemented using technical solutions such as the Image Preprocessing or the Inverse Kinematics modules, the core of the model with its underlying dynamic neural fields implements the decision making process (and more cognitive processes) in a neurological plausible way. More abstract models like the diffusion model only convert an already preprocessed input into a decision but cannot explain how decisions are transformed into action. In this way my model offers the advantages of the cognitive robotics approach as it is a complete model that converts vision into action. Moreover, my model also could utilise more abstract models like the diffusion model in its control architecture to improve and extend their behaviour. Note that this was already discussed for the Simon models in chapter 4.3 as the there introduced models also can be categorised as decision models.

Continuous models

In contrast to the diffusion models which only can explain decisions with two possible outcomes my model encodes target activations and movement parameter in a continuous fashion. In fact this feature is inherited by the underlying framework of my model: the dynamic neural field theory by Erlhagen and Schoener (2002). They have applied the DNFs to a wide range of computational and psychological problems (see Schoener, 2008; for a review), however, to my knowledge a model to the human reaching process is a novelty with this framework.

There exists a range of computational models that also make use of a continuous representation of movement parameters. One that can explain the distractor influence in a reaching movement is the already mentioned response vector hypothesis of Tipper et al. (1997) (see also chapter 2.1.3). This model is able to calculate movement directions by averaging the activations of an underlying cell population. Potential target objects cause Gaussian-shaped activations in the cells and mechanisms can inhibit distractor objects. Tipper et al. (1997) were able to explain various behavioural evidence with this model. Even though the main principle of the response vector hypothesis is very similar to my model (encoding of movement parameters in a neural layer) there are big differences between my model and their approach. The most important one is that similar to the diffusion model the response vector hypothesis only simulates a part of the reaching process (one neural layer encoding movement directions) and can not explain how the activations are created from the sensor input and how the resulting movement direction is put into action.

Another example of a mathematical model that works with continuous activations is the reaching model of Cisek (2007). Due to the similarities with my model I am going to discuss it here briefly. His model consists of different neural layers that represent different brain regions in order to calculate movement directions of

encoded information	model	brain area
target (birds-eye)	T map	PPC (e.g. SPL, PRR)
target (hand-centred)	D map	PPC (e.g. SPL, PRR, MIP)
movement direction	V map	M1, PM
movement speed	V map	areas 2, 5

Table 6.1.: Brain areas with a similar representations of target properties or movement parameters than in my model. More details and references can be found in the introduction.

a reaching experiment where a spatial cue together with a colour cue determines a target object. Cisek's (2007) model is very similar to my model in some aspects and is able to simulate a wide range of neurological evidence of the reaching process. E.g. his model is made up of several neural layers that encode potential target objects and target properties such as colour or location. However, similar to Tipper et al.'s (1997) model essential parts are missing to give a complete explanation of the reaching process. Also Cisek (2007) only simulates one kind of experiments with his model.
In comparison with above models it can be said that my model implements the reaching process in a more general setting which enabled the simulation of a broad range of reaching experiments. In this way it works like Tipper's model with the distractor influence, however, in the same time the underlying DNFs possess a neurobiological plausibility (like in Cisek's model). Thus my model somewhat combines the advantages of these two models and offers a broader approach to the human reaching process.

6.4. The model in the context of neurobiology

In this section I am going discuss the recent neurological research with respect to my model (see also chapter 1.4; for an introduction). Support for the neurological plausibility of my model does not only come from the dynamic field theory and its background but also from recent brain research. For all of the DNFs in my model

counterparts with similar encoded information can be found in the human brain (see Table 6.1 and Figure 6.3). As mentioned in the introduction, the brain areas that are related to the reaching process like the PPC, M1 and PM receive their visual information from the parietal occipital visual area (PO) where there is evidence that visual information with and without foveal magnification is represented (Wise et al., 1997). In fact, I use in the model both, DNFs with (in the goal-directed reaching model D map with its eccentricity function) and without cortical magnification (T map). Moreover, my model applies target representations in different coordinate systems with an encoding in birds-eye view in the T map and in hand-centred coordinates in the D map. Such encoding schemes have been found in many sub-areas of the PPC (e.g. in the SPL, VIP, and LIP; Kalaska et al., 1997; Desmurget & Grafton, 2000). In my model the representations for movement direction and speed are encoded in the V map. Also in the brain neurons for encoding direction and amplitude were found in the M1 and PM areas (e.g. Wise et al., 1997; Toxopeus et al., 2011). Moreover, recent studies with monkeys found neurons that encode velocity (areas 5 and 2 of the parietal cortex; Averbeck, Chafee, Crowe, & Georgopoulos, 2005).

Moreover, the control architecture of my model sheds new light on the various interpretations of the functionality and encoded parameters of brain areas as it models all underlying processes of goal-directed reaching. For instance Buneo and Andersen (2006) discuss three different schemes for transforming the target position from an eye-centred to a hand-centred coordinate system. My model shows that there is no need for a sequential adding up of different positions and vectors such as in their "sequential" or "combinatorial method" where head, arm, hand vectors are added. With the sigma-pi unit of the model these information are combined in a direct fashion which speaks in favour of the "direct method" of Buneo and Andersen (2006).

Furthermore, my model gives an explanation on how the planning of the movement trajectory could take place. Hereby, the trajectory is planned rather simple as the

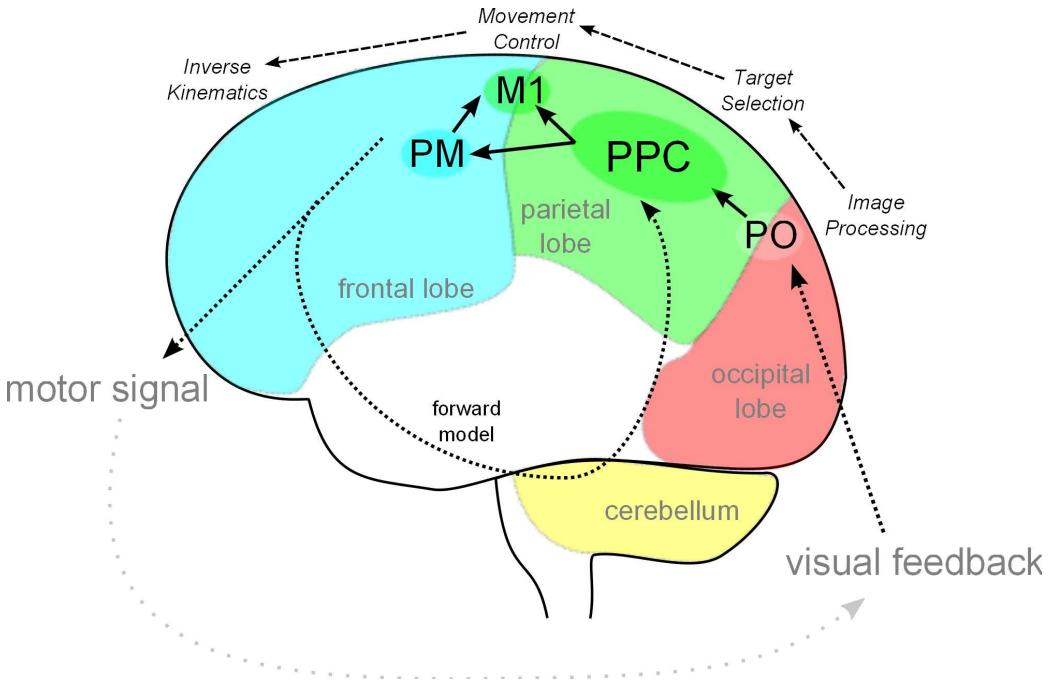

Figure 6.3.: Brain areas involved in the reaching process with the counterparts of my model (on top of the brain). Visual information originates in the occipital lobe and is processed into the area PO. This area serves as input for the PPC where attentional information is processed. The PPC area has connection to the premotor (PM) and motor (M1) areas from where the motor signal is sent to the muscles. The feedback loop is closed by the sensory processing of the visual feedback. Furthermore, the brain makes use of forward models and internal motor plan copies that can be used to predict the consequences of a planned movement. See the text for a discussion in a greater detail.

moving blob in the V map encodes only the current direction and speed of the movement. Evidence for such a "simple dynamic encoding scheme" has been found in the PPC in a study where monkeys performed a joystick task (Mulliken, Musallam, & Andersen, 2008). An alternative explanation is that M1 neurons encode more complex "pathlets" which are encoded on a single-cell level (Hatsopoulos, Xu, & Amit, 2007). Such pathlets then can be combined in order to generate the desired movement. However, my model demonstrated that it is not necessary to have such preplanned trajectories in order to mimic human reaching trajectories.

Evidence for sub-mechanisms in the goal-directed reaching model (*Acc*, *Onset*) which

were introduced to shape the velocity profile for smaller targets and in the perturbation experiments comes from the fact that there exist multiple connections between the visual area (PO) and the premotor areas (M1, PM). Moreover, the PM area was found to also process visuomotor information and non-spatial target properties (Wise et al., 1997) which gives support to the fact that features such as the target size actively influence the motor planning as it is the case in my model where the *Acc* mechanism influences the moving blob with target size and distance information.

There is evidence from a TMS study of Desmurget et al. (1999) that was interpreted as a proof against a purely closed-loop control of the human reaching process. There, TMS was applied on an area in the PPC and it was found that participants were not able to correct their movements toward a jumping target object. Instead the participants finished their already initiated hand movement towards the initial target object, however, with reduced accuracy. Desmurget and Grafton (2000) followed that there must exist some sort of pre-planning so that the initiated movement can be finished even in the absence of a visual feedback loop. With my model I propose a different interpretation for their results: The TMS could slow down the target selection stage which takes place in the T map (which also matches the PPC area). This would prevent that the perturbed target is perceived and detected in time. Additionally, as the T map does not receive new input due to the TMS its existing activation might "blur-out" and therefore reduce the accuracy of the ongoing movement. Note that I already have discussed a similar effect for a hypothetical non-visual feedback reach with my model in chapter 6.2.5.

Furthermore, there is neurological evidence of Cisek and Kalaska (2005) for the fact that potential target objects create activation in the PMd region even before movement execution. These so-called potential response neurons increased their fire-rate when a potential target object was close to their preferred direction. Then two targets created a bimodal distribution within a population of those cells. This gives further

support for the implementation in the Target Selection module where potential targets influence the motor output before the final target is selected.
With all the mentioned evidence of this section it can be concluded that my model demonstrated that its control architecture is neurologically plausible. All parts of the model can be related to a brain region that showed a similar functionality in experiments. Moreover, my model can help to answer open questions about how the brain processes information and how experimental findings can be explained on a neural level.

6.5. Outlook

This section will give an outlook of possible future extensions of my model and further experiments that could be simulated. Note that a few possible extensions regarding particular experiments already have been discussed in the experimental chapters.

6.5.1. Extensions of the model and further simulations

Several extensions for the model would be possible that could improve the hardware setup with the LEGO robot arm or the control architecture of the model. Regarding the hardware extensions one could think of a grasping component consisting of two fingers controlled by an additional motor. This would enable my model to simulate experiments were hand properties such as the grip aperture play an important role such as the perturbation experiments of Paulignan, MacKenzie, et al. (1991). The interplay of the grip aperture with the kinematic markers of the reach could extend the existing paradigm and give more support to my model in this kind of experiments. When talking about extensions of the control architecture the most obvious adaptation would regard the modules that are not yet implemented in a neurological plausible way utilising dynamical neural fields. This includes especially the Inverse Kinematics

module which is currently implemented as a simple mathematical function. While this does not offer new possible experiments it would increase the neurological plausibility of the model as a whole.

As discussed before, humans have shown to possess mechanisms to account for motor noise and other perturbation with forward models and proprioceptive feedback. Such feedback does not play a role in the current model, however, it could be included. Then the current motor signal and/or the joint positions of the arm could influence the processing of the future movement vector. Even an integration of this feedback into the moving blob mechanisms might be possible. Finally, extensions for more sophisticated movements (e.g. writing) could be included as well.

However, it is not necessary to introduce major extensions to the existing model and its variations in order to simulate new experiments. There is a range of choice-reaching tasks that could possibly be simulated with only small changes to the target selection module. This already has been demonstrated in chapter 4 with the experiments to the spatial averaging effect and the Simon task. Examples of tasks that were not yet simulated include reaching experiments with physical objects that could possibly be treated differently in the DNFs (e.g. Chapman & Goodale, 2008; Tipper et al., 1998). Other possible experiments could be performed with objects of different saliency (e.g. Wood et al., 2011).

6.6. Conclusion

The aim of my thesis was to develop a neurologically plausible computational model to explore the cognitive processes behind the human reaching process. Due to the cognitive robotics approach which I have taken it was required to implement all underlying cognitive processes of the reaching process. Moreover, with my model I investigated the role of visual attention and movement planning during the reaching

process.

The resulting model in its different variations was able to simulate various choice-reaching tasks such as the odd-colour task of Song and Nakayama (2008b) (see chapter 3), an extension of this task and experiments showing the spatial averaging effect of Chapman et al. (2010a) and the Simon effect (see chapter 4). Hereby, the model explored the interplay of target selection and movement coordination and gave a possible implementation of the cognitive processes involved in visual attention and movement planning.

Moreover, in chapter 5 several goal-directed reaching tasks simulating Fitts' law (Fitts & Peterson, 1964) and further speed-accuracy and perturbation phenomena (e.g. Heath et al., 1998; Saunders & Knill, 2005) were performed by a modified version of my model. The results of the numerous experiments were compared with human data in similar tasks and demonstrated that my model achieved good results. With its closed-loop approach my model offers an alternative explanation on how goal-directed reaching is planned and executed. While traditionally this is explained with two distinguished components of planning and control (e.g. Glover, 2004) my model demonstrates that such a separation is not required to achieve human-like behaviour in perturbation or Fitts' law tasks. The existence of a single process that integrates the available information and generates a motor signal was suggested before (e.g. Miall & Wolpert, 1996). With the moving blob interface my model gives an elegant explanation of this assumption and also demonstrates how such a process could be implemented in the human brain on a neural level.

Taking together the evidence of the experiments my model showed a possible implementation of all underlying cognitive processes of the human reaching process. The simulations demonstrated human-like behaviour in various reaching tasks and also can give predictions for future experiments. Additionally, the framework of the dynamic neural field theory gives my model a neurological plausible base and demonstrates how

the brain could encode the relevant information of the reaching process. Furthermore, my hardware setup offers an easy and inexpensive way to investigate aspects of visual attention and movement planning and control. Finally, due to its modular structure my model is easy to extend and modify and also can be used as a framework to utilise existing abstract models like the diffusion model in order to extend their applicability to choice-reaching experiments and to study their behaviour on reaching movements.

A. Appendix

The Appendix is divided into two sections. First, I present the mathematical details of my model. Afterwards, the second section lists all model parameters of the simulated experiments.

A.1. Mathematical details of the model

This first section of the appendix introduces the model's mathematics and equations in more detail. The qualitative description of the model's behaviour for the choice-reaching model can be found in chapter 2.3 and for the goal-directed reaching model in chapter 5.2. The first part of this section gives more details of the Image Processing module of my model. The second part describes the mathematical details of the dynamic neural fields in general. Subsequently, I will present details of the dynamic neural fields and their interconnectivity in the different versions of my model of chapter 2, 4, and 5 respectively. Finally, the mathematics of the Inverse Kinematics module will be presented.

A.1.1. Image processing

The Image Processing module converts the RGB camera image into three colour maps that directly feed as input into the DNFs of the model. First the 160 $\times$ 120 pixel camera image is downscaled to the size of 80 $\times$ 60 pixel. This downscaled image

then is processed with the following steps. First several parameters have to be set correctly to ensure that the colour detection works properly and the generated colour maps contain information about the marker without noise. The parameters have the following functions: The desired hue value (hue) and the hue tolerance (Δhue) determine the colour that has to be detected. In order to detect a pixel the hue value of the pixel must be in the range of $[hue - \Delta hue; hue + \Delta hue]$. As introduced in chapter 2.3.2 the image processing takes place in the HSV colour space. Hereby noise may occur if extreme values for S and V (which represent the colours white and black) are not filtered out. Therefore both Saturation (S) and Value (V) have to be larger than the value of the parameter sv. In the last step the erosion parameter ero determines the strength of an algorithm that decreases the noise of isolated pixel by deleting pixels if they have less activated neighbour pixels than the value of the parameter. Finally, the output of the Image Processing module are the three colour maps (blue, red, green) with a spatial resolution of 80×60 with values between 0 (no colour detected) and 1 (colour detected).

A.1.2. Dynamic neural fields

The model consists of multiple interconnected dynamic neural fields (DNFs) each serving a distinct purpose. The theory behind the framework was introduced in chapter 1.5 (see also Erlhagen & Schoener, 2002; for a review). The DNFs are: base map (B), hand map (H), target colour map (T_{col}), target location map (T), hand-target difference map (D), and velocity map (V). The maps without DNF dynamics are the three colour maps: the blue map (col_{blue}), the green map (col_{green}) and the red map (col_{red}). The colour maps are continuously generated from the camera image as described above and serve as input for some DNFs. Further maps without DNF dynamics are preactivation maps which were applied in some of the experiments

(e.g. in the odd-colour experiment of chapter 3.2). There is a preactivation map for colour (pre_{col}) and location (pre_{loc}). All DNFs and the non-dynamical maps are interconnected and influence each other. A description of their qualitative behaviour can be found in chapter 2.3.

Before I introduce the details of the interconnectivity of the DNFs in my model I am going to present the general mathematical details of the DNFs in more detail. The general equation to determine the neural activation of a DNF after Amari (1977) is as follows:

$$\tau \dot{u}(\boldsymbol{x}, t) = -u(\boldsymbol{x}, t) + h + s(\boldsymbol{x}, t) + \int w(\boldsymbol{x} - \boldsymbol{x}') f\big(u(\boldsymbol{x}', t)\big) d\boldsymbol{x}' + q(\boldsymbol{x}, t) \qquad \text{(A.1)}$$

This equation already has been presented in chapter 1.5, but is listed again to give a complete overview of the mathematical details here. Hereby, τ is a time parameter which defines how fast the DNF adapts towards changing inputs, $u(\boldsymbol{x}, t)$ stands for the field activation at time t and location $\boldsymbol{x}$, $h < 0$ is the resting level of the field, $s(\boldsymbol{x}, t)$ is the external input of the field, $w(\boldsymbol{x})$ is the activation kernel function and $q(\boldsymbol{x}, t)$ is normally distributed gaussian noise. Note that $\boldsymbol{x}$ is two-dimensional for the most DNFs in my model.

In the integral term of the equation there is the kernel function w. Before giving details of this function in A.7 I want to introduce details of the field output function f and the field equation that I implemented in my model. The field output function f is a sigmoidal function with parameters for the steepness of the slope (β) and the shift (u_0):

$$f(u) = \frac{1}{1 + e^{-\beta(u - u_0)}} \qquad \text{(A.2)}$$

For the implementation of the model, equation A.1 was adapted: the integral term was discretised according to the number of neurons and split up into separate excitatory

and inhibitory components. Furthermore a global inhibitory component was added. This is a common way to implement DNFs (see also Faubel & Schoener, 2008):

$$\tau \dot{u}(\boldsymbol{x},t) = -u(\boldsymbol{x},t) + h + s(\boldsymbol{x},t) + exc_{loc}(\boldsymbol{x},t) - inh_{loc}(\boldsymbol{x},t) - inh_{glob}(\boldsymbol{x},t) + q(\boldsymbol{x},t) \quad \text{(A.3)}$$

Thus, exc_{loc} and inh_{loc} define the local excitation and inhibition with the following equations:

$$exc_{loc}(\boldsymbol{x},t) = \sum_{\boldsymbol{x}'} w_{exc}(\boldsymbol{x}-\boldsymbol{x}') f\big(u(\boldsymbol{x}',t)\big) \quad \text{(A.4)}$$

$$inh_{loc}(\boldsymbol{x},t) = \sum_{\boldsymbol{x}'} w_{inh}(\boldsymbol{x}-\boldsymbol{x}') f\big(u(\boldsymbol{x}',t)\big) \quad \text{(A.5)}$$

Next, the global inhibition inh_{glob} depends on the summarised field activation and the parameter g_{inh}:

$$inh_{glob}(\boldsymbol{x},t) = g_{inh} \sum_{\boldsymbol{x}'} f\big(u(\boldsymbol{x}',t)\big) \quad \text{(A.6)}$$

Finally, the kernel w_k with its parameters σ_k (kernel width) and c_k (kernel strength) is defined with the following equation:

$$w_k(\boldsymbol{x}) = \frac{c_k}{\sigma_k\sqrt{2\pi}} \exp\left(-\frac{|\boldsymbol{x}|^2}{2\sigma_k^2}\right) \quad \text{(A.7)}$$

Kernel functions define how connections spread out through the DNF and how big the radius of influence of a neuron in its neighbourhood is. They are applied in all DNFs in the local excitation, inhibition and the noise term q. Additional kernels are applied in some DNFs to change input characteristics (e.g. to broaden activations in the V map).

Above equations are valid for every DNF in the model. However, the parameters (listed in chapter A.2) and input terms $s(x,t)$ of equation A.1 vary for different DNFs and for different variations of the model depending on the functionality and the

purpose of the DNF. The following sections present more details of the DNFs of the model for the different version of the simulations.

A.1.3. Choice reaching model

The mathematical details of the choice-reaching model as it was introduced in chapter 2.3 are presented here. This section is divided into subsections to point out the equations for the single DNFs of the model. If it is not stated differently the general DNF equations of the last section are valid. Generally the characteristics of the model are the following:

- The T_{col} map possesses only 2 neurons (one for each possible target colour) and is treated as a standard neural field with just one dimension. Also the corresponding non-dynamical pre_{col} map only has 2 neurons. All other DNFs and maps are two-dimensional with the spatial resolution of 80×60 neurons.

- The (non-dynamical) preactivation maps (pre_{col}, pre_{loc}) are manually defined. As these maps cannot change over time, they do not possess a time dimension. (Although their connection to the DNFs can be switched on and off in the model.)

- The input term $s(\boldsymbol{x}, t)$ differs in all DNFs according to the input the fields receive. The different input terms are described in the following subsections.

Each DNF receives a specific input according to its functionality. There are two states of inputs of the DNFs: before and during the simulation. Before the GO-signal is sent to the model which initiates the simulation, the input for all DNFs is by default a map without activation. However, due to the preactivation feature, some DNFs receive an input from preactivation maps instead of an empty map. The input maps of all different DNFs are described as follows.

Base map input

The base (B) map simply receives the blue colour map as input and selects the (larger) blue marker which is attached to the base of the robot arm. Its input is defined by the following equation:

$$s_B(\boldsymbol{x}, t) = col_{blue}(\boldsymbol{x}, t) \tag{A.8}$$

Hand map input

The endeffector or hand (H) map receives the blue colour map as positive and the output of the B map as negative input. Thus, after the B map has selected the arm base the H map selects the (smaller) blue marker which is attached to the arm endeffector (hand):

$$s_H(\boldsymbol{x}, t) = col_{blue}(\boldsymbol{x}, t) - f_B\big(u_B(\boldsymbol{x}, t)\big) \tag{A.9}$$

Target colour map input

The target colour (T_{col}) map consists of two neurons, each representing one possible target colour. It can be influenced by preactivation (*colour priming*) and therefore receives the pre_{col} map as input before the GO-signal is sent to start the simulation. After the simulation has been started each neuron receives the added field activation of the corresponding colour map weighted by a factor to account for the DNF parameters. Before GO-signal:

$$s_{T_{col}}(1, t) = pre_{col}(1) \text{ for neuron 1 (green)} \tag{A.10}$$

$$s_{T_{col}}(2, t) = pre_{col}(2) \text{ for neuron 2 (red)} \tag{A.11}$$

After GO-signal (The factor $\frac{1}{3}$ is a scaling parameter):

$$s_{T_{col}}(1,t) = \frac{1}{3}\sum_{\boldsymbol{x}} col_{green}(\boldsymbol{x},t) \text{ for neuron 1 (green)} \tag{A.12}$$

$$s_{T_{col}}(2,t) = \frac{1}{3}\sum_{\boldsymbol{x}} col_{red}(\boldsymbol{x},t) \text{ for neuron 2 (red)} \tag{A.13}$$

Target location map input

The target location (T) map receives a multiplicatively combined input of the T_{col} map and the colour maps (see also Figure 2.6). This way it is assured that the odd colour always has an advantage over the distractor colour in later stages of the simulation. The T map also can be influenced by preactivation (*spatial priming*) and it receives the pre_{loc} map as an input before the GO-signal.

Before GO-signal:

$$s_T(\boldsymbol{x},t) = pre_{loc}(\boldsymbol{x}) \tag{A.14}$$

After GO-signal:

$$s_T(\boldsymbol{x},t) = col_{green}(\boldsymbol{x},t) f_{T_{col}}\big(u_{T_{col}}(2,t)\big) + col_{red}(\boldsymbol{x},t) f_{T_{col}}\big(u_{T_{col}}(1,t)\big) \tag{A.15}$$

Hand-target difference map input

The input for the hand-target difference (D) map is the combined output activation of the H and the T map. It is realising a sigma-pi unit (McClelland et al., 1986) in a way that the location of the activation in the D map represents the difference of the location of the activations in the other two maps. Moreover, the origin in the center of the D map ($\frac{\boldsymbol{x}_{max}}{2}$) represents the position of the endeffector, while an activation somewhere in the DNF encodes a target. Therefore, an activation at the centre of the

D map would represent a target at the hand's position, while a target that is located in some distance to the hand would be represented with an activation far away from the map's centre.

The calculation is performed by applying the equation of a sigma-pi unit in the following way:

$$s_D(\boldsymbol{x}, t) = \sum_{\boldsymbol{x}_T} \sum_{\boldsymbol{x}_H} f_T\big(u_T(\boldsymbol{x}_T, t)\big) f_H\big(u_H(\boldsymbol{x}_H, t)\big) \tag{A.16}$$

$$\text{with: } \boldsymbol{x} = \frac{\boldsymbol{x}_{max}}{2} + \boldsymbol{x}_T - \boldsymbol{x}_H \tag{A.17}$$

In order to process the sigma-pi unit more efficiently, output activation thresholds th_T and th_H were introduced for the T and the H map for above equations. While the threshold for the H map th_H was introduced purely for efficiency reasons, the threshold th_T for the T map was an important parameter in the model. The thresholds cause that only neurons with activations higher than their value will be considered as input for the sigma-pi unit of the T and H map. The output value of neurons with values below the threshold value are set to 0 and will not influence the D map.

Velocity map input

The velocity (V) map performs the *moving blob* behaviour described in chapter 2.3. Hence, it possesses two fairly broad input activations: The first input is a predefined Gaussian activation in the centre of the map (*zero map*) which represents the resting hand (zero velocity) and assures the presence of an activation in the DNF at all times (see Equation A.19). The second input is a broadened output of the D map. The broadening is performed by an additional kernel function V_{inp} (see Equation A.20). With these two inputs a stable and slowly moving activation (rather than vanishing

or jumping activations) can be induced as described in chapter 2.3.

$$s_V(\boldsymbol{x}, t) = V_{zero}(\boldsymbol{x}) + D_{output}(\boldsymbol{x}, t) \tag{A.18}$$

$$V_{zero}(\boldsymbol{x}) = \frac{c_{zero}}{\sigma_{zero}\sqrt{2\pi}} \exp\left(-\frac{|\boldsymbol{x}|^2}{2\sigma_{zero}^2}\right) \tag{A.19}$$

$$D_{output}(\boldsymbol{x}, t) = \sum_{\boldsymbol{x}'} w_{V_{inp}}(\boldsymbol{x}') f_D\big(u_D(\boldsymbol{x}', t)\big) \tag{A.20}$$

Movement vector determination

The activation of the V map encodes a velocity vector which is the output of my model. The vector is determined by finding the maximum of the existing activation (the moving blob) in the DNF. From the resulting position $\boldsymbol{x}$ in the V map the origin or centre of the map $\frac{\boldsymbol{x}_{max}}{2}$ has to be subtracted to obtain the hand-centred velocity vector.

$$\boldsymbol{v} = \max_{\boldsymbol{x}} u_V(\boldsymbol{x}, t) - \frac{\boldsymbol{x}_{max}}{2} \tag{A.21}$$

In the next step the speed encoding of the velocity map is applied. The velocity vector $\boldsymbol{v}$ is normalized and raised to a higher power defined by the vector encoding power parameter m. For values $m \neq 1$ the encoding is non-linear (like in the experiments of chapter 3 where the encoding power was 1.5).

$$\boldsymbol{v}_{scaled} = |\boldsymbol{v}|^{m-1}\boldsymbol{v} \tag{A.22}$$

In order to generate a straight trajectory towards the target a desired future hand position is determined with the current hand position (obtained from the H map) and the scaled velocity vector $\boldsymbol{v}_{scaled}$. A further scaling parameter a of the velocity

vector is applied in order to ensure that the future point will not be located to far from the current hand position or behind the actual target, since the vector $\boldsymbol{v}_{scaled}$ can be extended significantly due to the nonlinear scaling. (If the future point is too far away from the hand then the arm cannot reach it and no joint angles could be calculated.)

$$\boldsymbol{x}_{current} = \max_{\boldsymbol{x}} u_H(\boldsymbol{x}, t) \tag{A.23}$$

$$\boldsymbol{x}_{future} = \boldsymbol{x}_{current} + a\boldsymbol{v}_{scaled} \tag{A.24}$$

Now the inverse kinematics can be applied for the current position $\boldsymbol{x}_{current}$ and the future position $\boldsymbol{x}_{future}$. Details of the inverse kinematics and the equations for the motor speed can be found in chapter A.1.6.

A.1.4. Modifications of the choice reaching model

The model description of the last section gave the details of the model of the odd-colour experiments of chapter 3. For simulating the single target baseline experiment and the choice-reaching experiments of chapter 4 parameters and the control architecture had to be modified slightly. Moreover, for the spatial averaging and Simon tasks the described interconnectivity had to be modified. The adaptations and differences to above model will be presented in the next sections.

Single target model

The single target experiment chapter 3.1 was the first experiment that was simulated with the control architecture. For this experiment the model is only modified in the Target Selection module to detect any object in the workspace. Hence, here the input for the T map is the additive combination of the red and the green map. Also the

T_{col} map and all its connections are inactive here. The input equations in the T map are as follows:

Before GO-signal (no priming was necessary here):

$$s_T(\boldsymbol{x}, t) = 0 \tag{A.25}$$

After GO-signal:

$$s_T(\boldsymbol{x}, t) = col_{green}(\boldsymbol{x}, t) + col_{red}(\boldsymbol{x}, t) \tag{A.26}$$

Odd-colour IF model

The modifications for the experiments of the odd-colour irrelevant feature experiment of chapter 4.1 affect only the Target Selection module. The input for the colour map is slightly changed and the weighting is modified. In the following equations the changes to the inputs of the old model are underlined.

After GO-signal:

$$s_{T_{col}}(1, t) = \underline{\frac{1}{20} max\Big(\sum_{\boldsymbol{x}} col_{green}(\boldsymbol{x}, t) - \sum_{\boldsymbol{x}} col_{red}(\boldsymbol{x}, t), 0\Big)} \text{ for neuron 1 (green)} \tag{A.27}$$

$$s_{T_{col}}(2, t) = \underline{\frac{1}{20} max\Big(\sum_{\boldsymbol{x}} col_{red}(\boldsymbol{x}, t) - \sum_{\boldsymbol{x}} col_{green}(\boldsymbol{x}, t), 0\Big)} \text{ for neuron 2 (red)} \tag{A.28}$$

Similar adaptations are applied to the input term of the T map.

After GO-signal:

$$s_T(\boldsymbol{x}, t) = \underline{(1 - 2.5 col_{red})}(\boldsymbol{x}, t) f_{T_{col}}\big(u_{T_{col}}(2, t)\big) + \underline{(1 - 2.5 col_{green})}(\boldsymbol{x}, t) f_{T_{col}}\big(u_{T_{col}}(1, t)\big) \tag{A.29}$$

Note that due to the new threshold of the T_{col} map activation can only be passed from the D to the V map if the activation of the T_{col} map surpasses the value of this threshold.

Spatial averaging model

The adaptations for the experiments of the spatial averaging effect in chapter 4.2 affect only the Target Selection module. Colours do not play a role in this experiment, but are used for the technical implementation to distinguish between potential and final target objects. Hereby both colours encode potential target objects but only the red object is considered as the final target object. The input for the T map is calculated by adding both colour maps with weights p_{green} and p_{red}:

$$s_T(\boldsymbol{x}, t) = p_{green} col_{green}(\boldsymbol{x}, t) + p_{red} col_{red}(\boldsymbol{x}, t) \tag{A.30}$$

The weights p account for the experimental setup as mentioned above. Before the GO-Signal both weights are set to 0, after the GO-signal and before movement onset the weights are both set to 1. Finally, after movement onset the weight p_{red} remains at 1 and p_{green} is set to 0.

After updating the T map the dead-time is applied. This parameter causes a delay of the information encoded in the T map for the following DNFs (D and V map). The deadtime is realised using a "first in, first out" approach by storing current output activation in an array. Then the oldest stored value is used for further processing steps (input for D map etc.).

Simon model

In the model for the simulations of the Simon effect in chapter 4.3 the Target Selection module had to be modified. The outputs of the T_{col} map here influence the weights of

the non-dynamical encoded target maps Target_{left} and Target_{right} which now serves as input to the T map. Those maps contain a Gaussian-shaped activation at the required target location on either the left or the right side.
Before GO-signal:

$$s_T(\boldsymbol{x}, t) = pre_{loc}(\boldsymbol{x}) \tag{A.31}$$

After GO-signal:

$$s_T(\boldsymbol{x}, t) = col_{green}(\boldsymbol{x}, t)\text{Target}_{left} + col_{red}(\boldsymbol{x}, t)\text{Target}_{right} \tag{A.32}$$

A.1.5. Goal directed reaching model

The goal-directed reaching model differs in some aspects from the choice-reaching model. Besides the DNFs for detecting the robot arm (B and H map) it consists of only three DNFs - the T, D and V map, however, it possesses some additional mechanisms.
Generally, before the simulation starts and a GO-signal is sent to the model, the input for the model DNFs is by default a map without activation:

$$s_T(\boldsymbol{x}, t) = s_D(\boldsymbol{x}, t) = \mathbf{0} \tag{A.33}$$

Note that this does not apply for the B and H map as they are used for the detection of the robot. The V map receives its default activation as described before (see Equation A.18).

Target map input

The T map encodes the birds-eye view location of the target object. In contrast to the choice-reaching model colour did not play a role in these experiments and

the two colour maps (red and green) are additively combined. However, for the target perturbation experiments different colours were used as part of a technical implementation in order to simulate changing location or size of target objects by combining or switching the colour input for the T map.

The input for the T map is calculated by adding both colour maps:

$$s_T(\boldsymbol{x}, t) = p_{green} col_{green}(\boldsymbol{x}, t) + p_{red} col_{red}(\boldsymbol{x}, t) \tag{A.34}$$

The weights p account for the experimental setup as mentioned before. For the Fitts' law experiment both weights are fixed at value $p_{green} = p_{red} = 1$, so that the colours were not distinguishable. However, for the perturbation experiments the values of the weights change after movement onset and cause the perturbation effect. In the location perturbation the active colour switches from green to red: $p_{green} = 1$, $p_{red} = 0$ (before) and $p_{green} = 0$, $p_{red} = 1$ (after the perturbation).

For the size perturbation condition the colours are combined: $p_{green} = 1$, $p_{red} = 1$ (big) and $p_{green} = 0$, $p_{red} = 1$ (small object). Then the target changes from big to small in the *shrink* and from small to big in the *grow* condition.

After updating the T map the dead-time is applied. This causes a delay of the information encoded in the T map for the following DNFs (D and V map). The dead-time is realized using a "first in, first out" approach by storing current output activation in an array in a similar fashion than in the spatial averaging experiment.

Hand-target difference map input

The input equations for the D map remain unchanged and are identical to the choice-reaching model. However, additionally a non-linear eccentricity function is applied besides the standard output function of the D map. This function causes a target close to the hand (and therefore close to the centre of the DNF) to activate more

neurons than a target object far away from the hand. The transfer function for the locations $\boldsymbol{x}$ is $x_{new} = x^3 + x$ in respect to the centre of the DNF. The implementation to convert the non-eccentric neuron positions $\boldsymbol{x}_D$ into the eccentric neuron positions $\boldsymbol{x}_D^{ecc}$ is as follows:

$$\boldsymbol{x}_D^{ecc} = \frac{1}{2}\big((\frac{\boldsymbol{x}_D}{hs} - 1)^3 + (\frac{\boldsymbol{x}_D}{hs} - 1)\big)hs + hs \tag{A.35}$$

Hereby hs stands for half the number of neurons of the DNF and is used to determine the distance toward the centre of the DNF in order to apply the function. Finally the output activation of the DNF is calculated with the magnified locations $\boldsymbol{x}^{ecc}$: $f_D\big(u_D(\boldsymbol{x}_D^{ecc}, t)\big)$.

For the hand perturbation experiment the technical implementation of the perturbation affected only the sigma-pi uni (see Equation A.17). There, with the applied perturbation the coordinates of the input of the H map are shifted towards the desired direction (near, far and sideways).

Velocity map input

The input equations for the V map of the choice-reaching model are extended to achieve the desired behaviour of the goal-directed reaching model. The zero map now consists of three parts to account for the newly introduced pathways in the model:

$$V_{zero}(t) = w_{st}Z_{st} + w_{acc}Z_{acc}(t) + w_{onset}Z_{onset}(t) \tag{A.36}$$

Hereby, Z_{st} is a time independent permanent input to ensure an activation around the centre when no target is present. This part is identical to the permanent activation of the choice-reaching model (see also Equation A.19). $Z_{acc}(t)$ is the input of the accuracy (Acc) mechanism and $Z_{onset}(t)$ of the onset ($Onset$) mechanism of the model.

All three terms possess weights w for balancing purposes.

The permanent input Z_{st} is identical to Equation A.19. It is a Gaussian around the centre of the V map and defined as follows:

$$Z_{st} = \frac{c_{st}}{\sigma_{st}\sqrt{2\pi}} \exp\left(-\frac{|\boldsymbol{x}_{centre}|^2}{2\sigma_{st}^2}\right) \tag{A.37}$$

Accuracy mechanism

The input of the *Acc* mechanism depends on T_{sum} which is the sum of the activation in the T map as its strength depended on the target size. With a threshold for the target sizes T_{sum} is determined using the following equation:

$$T_{sum}(t) = \frac{25 - \sum_{\boldsymbol{x}} f_T\big(u_T(\boldsymbol{x}_T, t)\big)}{100} \tag{A.38}$$

The constant parameters (25, 100) account for perceived object sizes in the experimental setting and balance the output. The *Acc* mechanism also received an input from the D map. With its eccentricity function the weighted sum of the DNF gives an estimate on how close the hand is located to the target.

$$D_{sum}(t) = \sum_{\boldsymbol{x}} w_{Gauss}(\boldsymbol{x}) f_D\big(u_D^{ecc}(\boldsymbol{x}, t)\big) \tag{A.39}$$

The weights $w_{Gauss}(\boldsymbol{x})$ are determined by applying a Gaussian around the centre of the D map:

$$w_{Gauss}(\boldsymbol{x}) = \frac{c_{Gauss}}{\sigma_{Gauss}\sqrt{2\pi}} \exp\left(-\frac{|\boldsymbol{x}|^2}{2\sigma_{Gauss}^2}\right) \tag{A.40}$$

Then the strength of the *Acc* mechanism is calculated using the following equation:

$$Z_{acc}(t) = T_{sum}(t) D_{sum}(t) \tag{A.41}$$

Finally, Z_{acc} can be used to calculate the input for the V map using Equation A.36.

Onset mechanism

The *Onset* mechanism can also influence the strength of the zero map in the V map. This mechanism detects variations in the activation of the T map and becomes active when an unexpected perturbation occurs. The strength of *Onset* is determined by:

$$Z_{onset}(t) = \max(\Delta_{act}(t) - th_{act}, 0) \tag{A.42}$$

Hereby, $th_{act} > 0$ is a threshold to filter noise and Δ_{act} is the change rate which is defined as the difference of the sum of the current activation and the running average of the activation. The change rate is calculated using following equation:

$$\Delta_{act}(t) = |\sum_{\boldsymbol{x}} f_T\big(u_T(\boldsymbol{x}_T, t)\big) - act(t)| \tag{A.43}$$

The running average *act* is required to calculate above equation. It is updated in every time step:

$$act(t) = act(t-1)(1 - \Delta t) + \sum_{\boldsymbol{x}} f_T\big(u_T(\boldsymbol{x}_T, t)\big)\Delta t \tag{A.44}$$

The above equations for *Acc* and *Onset* mechanism only configure the strength of the zero map in Equation A.36. In order to cause the blob to move away from the centre the target-depended input is needed which is determined similar to the choice-reaching model (see Equation A.20).

Movement vector determination

The determination of the movement vector is identical to the choice-reaching model. In contrast to the non-linear scaling of the choice-reaching model, here a linear equation

is applied in order to obtain the scaled movement vector. (The non-linear function here is included in the D map; see also Equation A.35.)

$$\boldsymbol{v}_{scaled} = \frac{\boldsymbol{v}}{4} \tag{A.45}$$

A.1.6. Inverse kinematics

Generally, the inverse kinematics deal with the problem of determining the angles of the joints of the robot arm when only the cartesian positions of the arm's joints are known. The Inverse Kinematics module is not part of the model and the problem is solved with a transfer function rather than applying DNFs or neural implementations. This section shows the mathematics and the implementation behind this transfer function.

In order to solve the inverse kinematics problem, knowledge about the cartesian position of the base and the endpoint is crucial. Furthermore, the length of the parts of the arm or the joint's coordinates must be known before a solution can be found. A common problem of the inverse kinematics is that a solution is not unique. Note that my robot arm only moves in the two-dimensional space and only possesses two joints which correspond to shoulder and elbow of a human. However, with the mentioned constraints it is obvious that only two solutions remain for my robot arm: one for a left and one for a right arm. As I assume the simulation of a right arm so that the left arm solution can be discarded here.

My model provides a movement vector which is converted with the current hand position $\boldsymbol{x}_{current}$ into a desired future hand position $\boldsymbol{x}_{future}$. The mathematical details of this processing were presented for the different versions of my model in the preceding sections (see Equations A.23 and A.24). The inverse kinematics now convert this cartesian positions ($\boldsymbol{x}_{current}$, $\boldsymbol{x}_{future}$) into the joint angles α and β for both current

and future positions of the robot arm. This is done using the equations A.55 and A.56. The following section presents the derivation of these equations with the trigonometry of the robot arm (see also Figure A.1). Subsequently, an angle difference of current and desired arm position can be determined which can be converted into speed values of the joint's motors which is explained in the last part of the section.

Inverse position kinematics with given arm positions and lengths

The problem of the inverse kinematics can be solved in different ways (see Jähne, 2008; for a review). The method that I have applied in my implementation makes use of the cartesian positions of the robot arm's shoulder and hand. As mentioned before the robot arm is a simplified model of a right arm of a human. Therefore restrictions for the joints apply e.g. the elbow angle β can not exceed 180° as it is physically not possible to bend the arm further than that (see Figure A.1; for the naming of the arm parts). As mentioned before this restriction of the angles make the inverse position kinematics problem unique, even when the joint position J is unknown. However, the length of both segments of the arm ($|\boldsymbol{b}| = length_{upperarm}$ and $|\boldsymbol{j}| = length_{forearm}$) must be known. The following derivation uses mainly trigonometrical relations to calculate the angles α and β with the vectors $\boldsymbol{b}$ (base to joint), $\boldsymbol{j}$ (joint to end) and $\boldsymbol{r}$ (*reach vector*, base to end). Additionally, the reach vector $\boldsymbol{r}$ is decomposed into two parts $\boldsymbol{r}_l$ (base to point H) and $\boldsymbol{r}_u$ (H to end). Moreover $\boldsymbol{r}$ separates α in a left and a right part. With the trigonometry of the triangle EE_xB the left part of α can be determined.

$$\alpha_{left} = \frac{\arcsin r_y}{|\boldsymbol{r}|} \text{ for } r_x < 0 \tag{A.46}$$

$$\alpha_{left} = \pi - \frac{\arcsin r_y}{|\boldsymbol{r}|} \text{ for } r_x \geq 0 \tag{A.47}$$

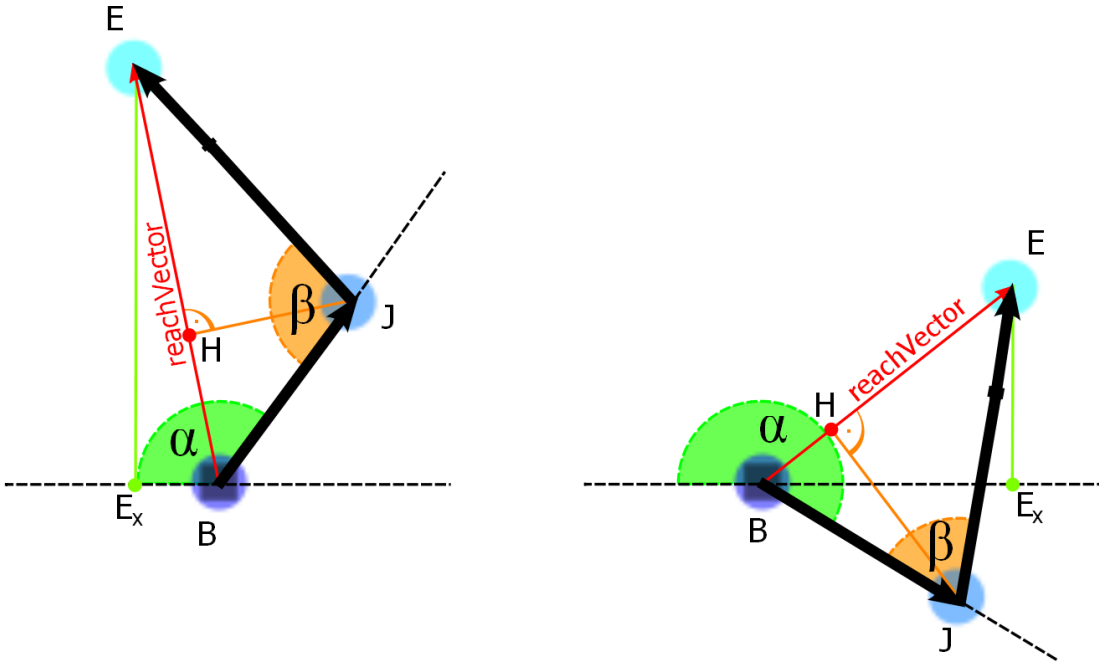

Figure A.1.: Vector model of the robot arm (black arrow) with the relevant angles and points: In order to calculate the kinematics with only the location of endpoint (or target), base and length of the arm segments some additional helping points are needed. Also two cases need to be distinguished: endpoint E left (left side) or right (right side) of the basis location B. See the text for the relevant equations regarding the inverse kinematics.

With the triangles HBJ and HJE the lengths of the two parts of the reaching vector $\boldsymbol{r}$ ($|\boldsymbol{r}_l|$ and $|\boldsymbol{r}_u|$) can be obtained. Note that the line HJ separates β in a left and a right part.

$$|\boldsymbol{r}_u| = \frac{|\boldsymbol{r}|^2 + |\boldsymbol{j}|^2 - |\boldsymbol{b}|^2}{2\,|\boldsymbol{r}|} \tag{A.48}$$

$$|\boldsymbol{r}_l| = |\boldsymbol{r}| - |\boldsymbol{r}_u| = \frac{|\boldsymbol{r}|^2 - |\boldsymbol{j}|^2 + |\boldsymbol{b}|^2}{2\,|\boldsymbol{r}|} \tag{A.49}$$

Now the remaining angle parts can be determined with the trigonometry of the triangles HBJ and HJE.

$$\alpha_{right} = \arccos\frac{|\boldsymbol{r}_l|}{|\boldsymbol{b}|} = \arccos\frac{|\boldsymbol{r}_l|}{length_{upperarm}} \tag{A.50}$$

$$\beta_{left} = \arcsin \frac{|\boldsymbol{r}_l|}{|\boldsymbol{b}|} = \arcsin \frac{|\boldsymbol{r}_l|}{length_{upperarm}} \tag{A.51}$$

$$\beta_{right} = \arcsin \frac{|\boldsymbol{r}_u|}{|\boldsymbol{j}|} = \arcsin \frac{|\boldsymbol{r}_u|}{length_{forearm}} \tag{A.52}$$

Finally the angle parts can be added up.

$$\alpha = \alpha_{left} + \alpha_{right} \tag{A.53}$$

$$\beta = \beta_{left} + \beta_{right} \tag{A.54}$$

The above equations can be combined to generate a single equation for both of the angles α and β, which results in the following equations for the inverse kinematics:

$$\alpha = \begin{cases} \arccos \frac{|\boldsymbol{r}_l|}{length_{upperarm}} + \frac{\arcsin r_y}{|\boldsymbol{r}|} \text{ for } r_x < 0 \\ \arccos \frac{|\boldsymbol{r}_l|}{length_{upperarm}} + \pi - \frac{\arcsin r_y}{|\boldsymbol{r}|} \text{ for } r_x \geq 0 \end{cases} \tag{A.55}$$

$$\beta = \arcsin \frac{|\boldsymbol{r}_l|}{length_{upperarm}} + \arcsin \frac{|\boldsymbol{r}_u|}{length_{forearm}} \tag{A.56}$$

Motor speed calculation

With the given positions $\boldsymbol{x}_{current}$ and $\boldsymbol{x}_{future}$ and the equations A.55 and A.56 the current angles $\alpha_{current}$, $\beta_{current}$ and the desired future angles α_{future}, β_{future} can be obtained. Finally, the desired angle changes $\Delta\alpha$ and $\Delta\beta$ are determined by calculating the difference of future and current angle and the motor speed commands are obtained by applying speed scaling parameters to the angle differences:

$$\Delta\alpha = \alpha_{future} - \alpha_{current} \tag{A.57}$$

The motor speed values $speed_\alpha$ and $speed_\beta$ are a result of a multiplication of the desired angle changes with the speed scaling parameters d_{gen}, $d_{shoulder}$ and d_{ellbow}.

$$speed_\alpha = d_{gen} d_{shoulder} \Delta\alpha \tag{A.58}$$

$$speed_\beta = d_{gen} d_{elbow} \Delta\beta \tag{A.59}$$

The general speed factor d_{gen} is utilised to correct the speed of the robot arm to an appropriate level, as the resulting speed values $speed_\alpha$ and $speed_\beta$ that will be sent to the robot arm have to be within the range of -100 and 100. However, an adaptation of d_{ellbow} and $d_{shoulder}$ can be necessary to correct gear ratios of the particular joints or slower running worn motors.

A.2. Parameters of the simulations

The model possesses plenty of parameters, some influence the reaching processes in an obvious way such as the speed scaling parameters that make the arm faster or slower, but many parameters have a more subtle influence on the movement characteristics or the model's behaviour. Their qualitative and quantitative influence have been discussed already in the chapters 2.3 and A.1. This chapter gives a review on how the values of the parameters were determined and lists all parameter values of the different simulations.

Typically two tables of parameters are documented: First the parameters for the DNFs of the model and second further parameters of the model. Where applicable a third table with preactivation, priming or conditional parameters will be shown.

Within the simulation software environment most of the parameters can be saved (and loaded) in a XML-File. The default XML-File always should to be loaded after

the start-up of the program.

The requirements for the camera parameters were independent from the experiment type and are listed in section A.2.2. Subsequently, the parameter values for the model in the different experiments can be found in the appropriate sections.

A.2.1. Choice of parameters

As mentioned above many parameter values had to be chosen appropriately to ensure the human-like behaviour of the model in the experiments. Especially the dynamic neural fields possess plenty of parameters to control their excitations, inhibition, randomness, etc. These parameters directly control the qualitative behaviour of the dynamic neural fields such as the size and number of allowed activations, the time it requires to decide for a target colour and many others. Besides the neural field parameters there is a range of further parameters.

Many parameter values had to be chosen carefully to ensure the desired behaviour while others allow a greater variance without significantly influencing the robot's behaviour. However, smaller changes (less than 5%) of the parameter values will not alter the behaviour of the robot significantly. Generally, I tried to modify as few parameter values as possible for the simulation of new experiments. For instance all three experiments of chapter 3 and all goal-directed reaching experiments of 5 have similar parameter values. Moreover, no automatised parameter optimisation or fitting took place. Hence, the parameter values listed in the following sections can be seen as example values that demonstrated the observed behaviour and are not necessarily the best or the only set of parameter values for the experiments.

A.2.2. Image processing

The parameter values for the image processing had to be adjusted before starting the simulations. This is necessary as different conditions such as the change of lights during the day, dawn or night require different parameter values. The following table documents typical values that could vary slightly with different conditions.

Image processing parameters

map	hue	Δhue	sv	ero
col_{blue}	250	50	15	1
col_{red}	5	15	40	1
col_{green}	100	50	35	2

A.2.3. Single target experiment

In the first experiment of chapter 3.1 the robot performed movements to single targets in the workspace. Two different simulations were performed with different encodings of the velocity vector v (*linear* and *non-linear*).

DNF parameters

map	τ	β	h	g_{inh}	c_{exc}	σ_{exc}	c_{inh}	σ_{inh}	c_q	σ_q
B	25	12	-2	0.3	80	3	20	10	0.05	1
H	2	12	-0.5	0.2	20	3	0	1	0.05	1
T_{col}	60	12	-0.1	7	10	0.1	10	1	0.05	1
T	30	1.5	-6	0.4	40	4	30	8	0.05	1
D	15	12	-1	1	30	5	20	10	0.05	1
V	20	12	-1	0.2	10	5	0	1	0.05	5

Further model parameters

parameter	description	value
th_t	sigma-pi threshold of T	0.1
th_h	sigma-pi threshold of H	0.95
c_{zero}	strength of zero activation in V map	10
σ_{zero}	width of zero activation in V map	40
$c_{V_{inp}}$	kernel strength of V_{inp}	10
$\sigma_{V_{inp}}$	kernel width of V_{inp}	40
m	magnification factor	1.5
a	vector scaling factor	0.1
d_{gen}	general speed factor	1.2
$d_{shoulder}$	shoulder speed factor	1
d_{elbow}	elbow speed factor	1

Parameters of the experimental conditions

parameter	description	value
linear encoding scheme		
m	magnification factor	1
d_{gen}	general speed factor	5
non-linear encoding scheme		
m	magnification factor	1.5
d_{gen}	general speed factor	1.2

A.2.4. Odd-colour experiment

This experiment from chapter 3.2 aimed for a simulation of the *curved trajectories* which were observed by Song and Nakayama (2009). The DNF and model parameter

values were identical to the single target experiment (with non-linear encoding scheme) and only the preactivation parameters were changed.

Parameters of the colour priming conditions

map	position	strength
straight trajectory		
pre_{col}	1 (green)	10
pre_{col}	2 (red)	20
curved trajectory		
pre_{col}	1 (green)	20
pre_{col}	2 (red)	26

The next table contains the parameters for the *spatial priming*. The first three rows describe the baseline parameter with no priming, the last rows the parameter for the curved trajectory condition. Displayed are the midpoints (neuron coordinates) of gaussian activations with their strength and σ.

Parameters of the spatial priming conditions

map	position	strength	σ
straight trajectory			
pre_{loc}	left $(23, 22)$	0	2
pre_{loc}	center $(40, 15)$	0	2
pre_{loc}	right $(58, 22)$	0	2
curved trajectory			
pre_{loc}	left $(23, 22)$	4	2
pre_{loc}	center $(40, 15)$	0	2
pre_{loc}	right $(58, 22)$	0	2

A.2.5. Odd-colour "continuous" vs. "threshold" experiment

In the experiment of chapter 3.3 of the influence of the threshold parameter th_T was explored. The DNF parameter values were identical to the single target experiment (see chapter A.2.3). In the baseline the parameter remained at the default value of $th_T = 0.1$, while in the other conditions $th_T = 0.6$ was applied. Additionally, the following colour priming was applied to generate curved trajectories.

Parameters

map	position	strength
pre_{col}	1 (green)	20
pre_{col}	2 (red)	5

A.2.6. Odd-colour IF experiment

DNF parameters

map	τ	β	h	g_{inh}	c_{exc}	σ_{exc}	c_{inh}	σ_{inh}	c_q	σ_q
B	25	12	-2	0.3	80	3	20	10	0.05	1
H	2	12	-0.5	0.2	20	3	0	1	0.05	1
T_{col}	225	6	-1	1	10	0.1	4	1	0.05	1
T	33	1.5	-0.1	0.15	160	2	385	4	0.05	1
D	40	12	-1	0.8	120	3	50	6	0.05	1
V	15	2	-1	0.4	20	5	0	1	0.05	5

Further model parameters

parameter	description	value
IF	size grouping (depended on condition)	*
	standard experiment	0
	with distractor grouping mechanism	4.7
th_t	sigma-pi threshold of T	0.1
th_h	sigma-pi threshold of H	0.95
c_{zero}	strength of zero activation in V map	5
σ_{zero}	width of zero activation in V map	40
$c_{V_{inp}}$	kernel strength of V_{inp}	15
$\sigma_{V_{inp}}$	kernel width of V_{inp}	40
m	magnification factor	1.5
a	vector scaling factor	0.1
d_{gen}	general speed factor	3
$d_{shoulder}$	shoulder speed factor	1
d_{elbow}	elbow speed factor	0.9

A.2.7. Spatial averaging experiments

DNF parameters

map	τ	β	h	g_{inh}	c_{exc}	σ_{exc}	c_{inh}	σ_{inh}	c_q	σ_q
B	25	12	-2	0.3	80	3	20	10	0.05	1
H	2	12	-0.5	0.2	20	3	0	1	0.05	1
T	120	1.5	-2	0.15	20	4	0	8	0.05	1
D	15	12	-1	0.4	30	3	0	3	0.05	1
V	15	2	-1	0.4	20	5	0	1	0.05	5

Further model parameters

parameter	description	value
$deadtime$	processing delay of T map	50
th_t	sigma-pi threshold of T	0.5
th_h	sigma-pi threshold of H	0.95
c_{zero}	strength of zero activation in V map	4
σ_{zero}	width of zero activation in V map	40
$c_{V_{inp}}$	kernel strength of V_{inp}	15
$\sigma_{V_{inp}}$	kernel width of V_{inp}	20
m	magnification factor	1.5
d_{gen}	general speed factor	1.2
$d_{shoulder}$	shoulder speed factor	1
d_{elbow}	elbow speed factor	0.9

Parameters of the priming conditions

map	position	strength	σ
P1 (left)	left $(27, 17)$	1	4
P2 (left)	left $(27, 17)$	2	4
P1 (right)	right $(53, 17)$	1	4
P2 (right)	right $(53, 17)$	2	4

A.2.8. Simon effect experiment

DNF parameters

map	τ	β	h	g_{inh}	c_{exc}	σ_{exc}	c_{inh}	σ_{inh}	c_q	σ_q
B	25	12	-2	0.3	80	3	20	10	0.05	1
H	2	12	-0.5	0.2	20	3	0	1	0.05	1
T	80	1.5	-3	0.3	15	4	30	8	0.05	1
T_{col}	60	12	-0.1	7	10	0.1	10	1	0.05	1
D	15	12	-1	0.4	30	3	0	3	0.05	1
V	24	2	-1	0.4	20	5	0	1	0.05	5

Further model parameters

parameter	description	value
th_T	sigma-pi threshold of T *condition low*	0.2
th_T	sigma-pi threshold of T *condition high*	0.95
th_H	sigma-pi threshold of H	0.95
c_{zero}	strength of zero activation in V map	4
σ_{zero}	width of zero activation in V map	40
$c_{V_{inp}}$	kernel strength of V_{inp}	15
$\sigma_{V_{inp}}$	kernel width of V_{inp}	20
d_{gen}	general speed factor	3
$d_{shoulder}$	shoulder speed factor	1
d_{elbow}	elbow speed factor	0.75

A.2.9. Goal-directed reaching experiments

DNF parameters

map	τ	β	h	g_{inh}	c_{exc}	σ_{exc}	c_{inh}	σ_{inh}	c_q	σ_q
B	25	12	-2	0.3	80	3	20	10	0.05	1
H	2	12	-0.5	0.2	20	3	0	1	0.05	1
T	30	1.5	-6	0.4	45	4	30	8	0.05	1
D	15	12	-1	0.4	30	3	0	3	0.05	1
V	24	2	-1	0.4	20	5	0	1	0.05	5

Further model parameters

parameter	description	value
$dead\ time$ –	dead time after T map	150
th_T	sigma-pi threshold of T	0.5
th_H	sigma-pi threshold of H	0.95
w_{st}	weight of Z_{st}	5
c_{st}	strength of zero activation in V map	10
σ_{st}	width of zero activation in V map	40
w_{acc}	weight of Z_{acc}	0.11
c_{acc}	strength of zero activation in V map	1
σ_{acc}	width of zero activation in V map	18
w_{onset}	weight of Z_{onset}	1
th_{act}	noise filter threshold in $Onset$	0.5
Δt	update speed in $Onset$	0.2
$c_{V_{inp}}$	kernel strength of V_{inp}	20
$\sigma_{V_{inp}}$	kernel width of V_{inp}	20
d_{gen}	general speed factor	3
$d_{shoulder}$	shoulder speed factor	1
d_{elbow}	elbow speed factor	0.75

Parameter of the conditions in the time-matching task

condition	value
low	$w_{st} = 5$
mid	$w_{st} = 7$
high	$w_{st} = 10$

References

Abrams, R. A., Meyer, D. E., & Kornblum, S. (1990). Eye hand coordination - oculomotor control in rapid aimed limb movements. *Journal of Experimental Psychology - Human Perception and Performance*, *16 (2)*, 248-267.

Adams, J. A. (1971). A closed-loop theory of motor learning. *Journal of Motor Behavior*, *3*, 111-150.

Amari, S. I. (1977). Dynamic of pattern formation in lateral-inhibition type neural fields. *Biological Cybernetics*, *27*, 77-87.

Andersen, R. A., & Buneo, C. A. (2002). Intentional maps in posterior parietal cortex. *Annu. Rev. Neurosci.*, *25*, 189-220.

Averbeck, B. B., Chafee, M. V., Crowe, D. A., & Georgopoulos, A. P. (2005). Parietal representation of hand velocity in a copy task. *J Neurophysiol*, *93*, 508-518.

Bagnall, B. (2007). *Maximum lego nxt: Building robots with java brains.* Variant Press.

Bastian, A., Schoener, G., & Riehle, A. (2003). Preshaping and continuous evolution of motor cortical representations during movement preparation. *European Journal of Neuroscience*, *18*, 2047-2058.

Buetti, S., & Kerzel, D. (2008). Time course of the simon effect in pointing movements for horizontal, vertical, and acoustic stimuli: Evidence for a common mechanism. *Acta Psychologica*, *129*, 420-428.

Buetti, S., & Kerzel, D. (2009). Conflicts during response selection affect response programming: Reactions toward the source of stimulation. *Journal of Experimental Psychology: Human Perception and Performance*, *35(3)*, 816-834.

Bullock, D., & Grossberg, S. (1988). Neural dynamics of planned arm movements: Emergent invariants and speed-accuracy properties during trajectory formation. *Psychological Review*, *95*, 49-90.

Buneo, C. A., & Andersen, R. A. (2006). The posterior parietal cortex: Sensorimotor interface for the planning and online control of visually guided movements. *Neuropsychologica*, *44*, 2594-2606.

Castiello, U. (2001). The effects of abrupt onset of 2-d and 3-d distractors on prehension movements. *Perception & Psychophysics*, *63 (6)*, 1014-1025.

Chapman, C. S., Gallivan, J. P., Wood, D. K., Milne, J. L., Culham, J. C., & Goodale, M. A. (2010a). Reaching for the unknown: Multiple target encoding and real-time decision-making in a rapid reach task. *Cognition*, *116*, 168-176.

Chapman, C. S., Gallivan, J. P., Wood, D. K., Milne, J. L., Culham, J. C., & Goodale, M. A. (2010b). Short-term motor plasticity revealed in a visualmotor decision-making task. *Behavioural Brain Research*, *214*, 130-134.

Chapman, C. S., & Goodale, M. A. (2008). Missing in action: the effect of obstacle position and size on avoidance while reaching. *Exp Brain Res*, *191*, 83-97.

Chelazzi, L., Müller, E., Duncan, J., & Desimone, R. (1993). A neural basis for visual search in inferior temporal cortex. *Nature*, *363*, 345-347.

Cisek, P. (2007). Cortical mechanisms of action selection: the affordance competition hypothesis. *Philosophical Transactions of the Royal Society of London Series B*, *362*, 1585-1599.

Cisek, P., & Kalaska, J. F. (2005). Neural correlates of reaching decisions in dorsal premotor cortex: Specification of multiple direction choices and final selection of action. *Neuron*, *45*, 801-814.

Cousineau, D. (2005). Confidence intervals in within-subject designs: A simpler solution to loftus and massons method. *Tutorials in Quantitative Methods for Psychology*, *1*, 42-45.

DeJong, R., Lian, C.-C., & Lauber, E. (1994). Conditional and unconditional automaticity: A dual-process model of effects of spatial stimulus-response correspondence. *Journal of Experimental Psychology: Human Perception and Performance*, *20(4)*, 731-750.

Desimone, R., & Duncan, J. (1995). Neural mechanisms of selective attention. *Annual Review of Neuroscience*, *18*, 193-222.

Desmurget, M., & Grafton, S. (2000). Forward modeling allows feedback control for fast reaching movements. *Trends in Cognitive Science*, *4 No.11*.

Desmurget, M., Pelisson, D., Rossetti, Y., & Prablanc, C. (1998). From eye to hand: Planning goal-directed movements. *Neuroscience and Biobehavioral Reviews*, *22 No. 6*, 761-788.

Desmurget, M., Prablanc, C., Jordan, M., & Jeannerod, M. (1999). Are reching movements planned to be straight and invariant in the extrinsic space? kinematic comparison between compliant and unconstrained motions. *The Quartely Journal of Experimental Psychology*, *52A (4)*, 981-1020.

D'Mello, S., & Franklin, S. (2011). Computational modeling/cognitive robotics complements functional modeling/experimental psychology. *New Ideas in Psychology (Special Issue on Cognitive Robotics and Theoretical Psychology)*, *29*, 217-227.

Duncan, J. (2006). EPS Mid-Career Award 2004: Brain mechanisms of attention. *The Quarterly Journal of Experimental Psychology*, *59*(1).

Elliott, D., Hansen, S., Grierson, L. E. M., Lyons, J., Bennett, S. J., & Hayes, S. J. (2010). Goal-directed aiming: Two components but multiple processes. *Psychological Bulletin*, *136(6)*, 1023-1044.

Elliott, D., Helsen, W. F., & Chua, R. (2001). A century later: Woodworth's (1899) two-component model of goal-directed aiming. *Psychological Bulletin*, *127(3)*, 342-357.

Erlhagen, W., & Bicho, E. (2006). The dynamics neural field approach to cognitive robotics. *J. Neural Eng.*, *3*, R36-R54.

Erlhagen, W., & Schoener, G. (2002). Dynamic field theory of movement preparation. *Psychology Review*, *109(3)*, 545-572.

Faubel, C., & Schoener, G. (2008). Learning to recognize objects on the fly: A neurally based dynamic field approach. *Neural Networks*, *21*, 562-576.

Feigenson, L., Dehaene, S., & Spelke, E. (2004). Core systems of number. *Trends in Cognitive Science*, *8*(7), 307-314.

Findlay, J. M. (1982). Global visual processing for saccadic eye movements. *Vision Research*, *22(8)*, 1033-1045.

Fitts, P. M. (1954). The information capacity of the human motor system in controlling the amplitude of movement. *Journal of Experimental Psychology*, *47*, 381-391.

Fitts, P. M., & Peterson, J. R. (1964). Information capacity of discrete motor responses. *Journal of Experimental Psychology*, *67*, 103-112.

Flanagan, J. R., Ostry, D. G., & Feldman, A. G. (1993). Control of trajectory modifications in target-directed reaching. *Journal of Motor Behavior*, *25(3)*, 140-152.

Gallivan, J. P., Chapman, C. S., Wood, D. K., Milne, J. L., Ansari, D., Culham, J. C., et al. (2011). One to four, and nothing more: Nonconscious parallel individuation of objects during action planning. *Psychological Science*, *22(6)*, 803-811.

Gawthrop, P., Lakie, M., & Loram, I. (2008). Predictive feedback control and fitts' law. *Biological Cybernetics*, *98*, 229-238.

Georgopoulos, A. P., Schwartz, A. B., & Kettner, R. E. (1986). Neuronal population coding of movement direction. *Science*, *233(4771)*, 1416-1419.

Glover, S. (2004). Separate visual represenations in the planning and control of action. *Behavioural and Brain Sciences*, *27*, 3-78.

Grierson, L. E. M., & Elliott, D. (2009). Goal-directed aiming and the relaitve contribution of two online control processes. *American Journal of Psychology*, *122(3)*, 309-324.

Guigon, E., Baraduc, P., & Desmurget, M. (2008). Computational motor control: feedback and accuracy. *European Journal of Neuroscience*, *27*, 1003-1016.

Haggard, P., & Richardson, J. (1996). Spatial patterns on the control of human arm movement. *Journal of Experimental Psychology: Human Perception and Performance*, *22(1)*, 42-62.

Hatsopoulos, N. G., Xu, Q., & Amit, Y. (2007). Encoding of movement fragments in the motor cortex. *Journal of Neuroscience*, *27(19)*, 5105-5114.

Heath, M., Hodges, N. J., Chua, R., & Elliot, D. (1998). On-line control of rapid aiming movements: Unexpected target perturbations and movement kinematics. *Canadian Journal of Experimental Psychology*, *52(4)*, 163-173.

Heath, M., Weiler, J., Marriott, K. A., Elliott, D., & Binsted, G. (2011). Revisiting fitts and peterson (1964): Width and amplitude manipulations to the reaching environment elicit dissociable movement times. *Canadian Journal of Experimental Psychology*, *65(4)*, 259-268.

Heinke, D., & Humphreys, G. W. (2003). Attention, spatial representation, and visual neglect: Simulating emergent attention and spatial memory in the selective attention for identification model (saim). *Psychology Review*, *110*(1), 29-87.

Hoff, B., & Arbib, M. A. (1993). Models of trajectory formation and temporal interaction of reach and grasp. *Journal of Motor Behavior*, *25(3)*, 175-192.

Hommel, B. (1994). Spontaneous decay of response-code activation. *Psychological Research*, *56*, 261-268.

Hommel, B. (2011). The simon effect as tool and heuristic. *Acta Psychologica*, *136*, 189-202.

Howard, L. A., & Tipper, S. P. (1997). Hand deviations away from visual cues: indirect evidence for inhibition. *Exp Brain Res*, *113*, 144-152.

Jähne, B. (2008). *Digital Image Processing: Concepts, Algorithms, and Scientific Applications*. Springer-Verlag Berlin Heidelberg.

Jeannerod, M. (1984). The timing of natural prehension movements. *Journal of Motor Behavior*, *16, 3*, 235-254.

Kalaska, J. F., Scott, S. H., Cisek, P., & Sergio, L. E. (1997). Cortical control of reaching movements. *Current Opinion in Neurobiology*, *7*, 849-859.

Kirsch, W., & Hennighausen, E. (2011). Kinematic markers of distance-specific control in linear hand movements. *Journal of Motor Behavior*, *43 (3)*, 253-262.

Kornblum, S., Stevens, G. T., Whipple, A., & Requin, J. (1999). The effects of irrelevant stimuli: 1. the time course of stimulus-stimulus and stimulus-response consistency effects with stroop-like stimuli, simon-like tasks, and their factorial combinations. *Journal of Experimental Psychology: Human Perception and Performance*, *25(3)*, 688-714.

Lee, D. (1999). Effects of exogenous and endogenous attention on visually guided hand movements. *Cognitive Brain Research*, *8(2)*, 143-156.

Lu, C.-H., & Proctor, R. W. (1995). The influence of irrelevant location information on performance: A review of the simon and spatial stroop effects. *Psychonomic Bulletin & Review*, *2(2)*, 174-207.

MacKenzie, E. L., Marteniuk, R. G., Dugas, C., Liske, D., & Eickmeier, B. (1987). Three-dimensional movement trajectories in fitts' task: Implications for control. *The Quartely Journal of Experimental Psychology*, *39A*, 629-647.

Maljkovic, V., & Nakayama, K. (1996). Priming of pop-out: II. The role of position. *Memory & Cognition*, *58*(7), 977-991.

McClelland, J., Rumelhart, D., & Hinton, G. (1986). The appeal of parallel distributed processing. In *Parrallel Distributed Processing: Explorations in the microstructure of cognition. Volume I: Foundations.* Cambridge MA: MIT Press/Bradford Books.

Metzker, M., & Dreisbach, G. (2009). Bidirectional processes in the simon task. *Journal of Experimental Psychology: Human Perception and Performance*, *35(6)*, 1770-1783.

Meyer, D. E., Kornblum, S., Abrams, R. A., & Wright, C. E. (1988). Optimality in human motor performance: Ideal control of rapid aimed movements. *Psychological Review*, *95(3)*, 340-370.

Meyer, D. E., Smith, J. E. K., Kornblum, S., Abrams, R. A., & Wright, C. E. (1990). Attention and performance xiii. In L. Erlbaum (Ed.), (p. 174-225). M. Jeannerod.

Miall, R. C., & Wolpert, D. M. (1996). Forward models for physiological motor control. *Neural Networks*, *9(8)*, 1265-1279.

Morse, A. F., Herrera, C., Clowes, R., Montebelli, A., & Ziemke, T. (2011). The role of robotic modelling in cognitive science. *New Ideas in Psychology*, *29*, 312-324.

Muller, H., & Krummenacher, J. (Eds.). (2006). *Visual Search and Attention* (Vol. 14) (No. 4/5/6/7). Psychology Press.

Mulliken, G. H., Musallam, S., & Andersen, R. A. (2008). Forward estimation of movement state in posterior parietal cortex. *PNAS*, *105 no. 24*, 8170-8177.

Munro, H., Plumb, M. S., Wilson, A. D., Williams, J. H. G., & Mon-Williams, M. (2007). The effect of distance on reaction time in aiming movements. *Exp Brain Res*, *183*, 249-257.

Nakano, E., Imamizu, H., Osu, R., Uno, Y., Gomi, H., Yoshioka, T., et al. (1999). Quantitative examinations of internal representations for arm trajectory planning: Minimum commanded torque change model. *Neurophysiol*, *81*, 2140-2155.

Nothdurft, H. C. (1992). Feature analysis and the role of similarity in pre-attentive vision. *Perception and Psychophysics*, *52*, 355-375.

Paulignan, Y., Jeannerod, M., MacKenzie, C., & Marteniuk, R. (1991). Selective perturbation of visual input during prehension movements: 1. the effects of changing object size. *Exp Brain Res*, *87*, 407-420.

Paulignan, Y., MacKenzie, C., Marteniuk, R., & Jeannerod, M. (1991). Selective perturbation of visual input during prehension movements: 1. the effects of changing object position. *Exp Brain Res*, *83*, 502-512.

Petreska, B., & Billard, A. (2009). Movement curvature planning through force field internal models. *Biological Cybernetics*, *100*, 331-350.

Plamondon, R., & Alimi, A. M. (1997). Speed/accuracy trade-offs in target-directed movements. *Behavioural and Brain Sciences*, *20*, 279-349.

Proulx, M. J. (2010). Size matters: Large objects capture attention in visual search. *PLoS ONE*, *5 (12)*.

Proulx, M. J., & Egeth, H. E. (2008). Biased competition and visual search: the role of luminance and size contrast. *Psychological Research*, *72*, 106-113.

Ratcliff, R., & Rouder, J. N. (1998). Modeling response times for two-choices decisions. *Psychological Science*, *9 (5)*, 347-356.

Rosenbaum, D. A., Cohen, R. G., Meulenbroek, R. G. J., & Vaughan, J. (2006). *Plans for grasping objects.* Book.

Rovamo, J., & Virsu, V. (1979). Estimation and application of the human cortical magnification factor. *Exp Brain Res*, *37(3)*, 495-510.

Rubichi, S., & Pellicano, A. (2004). Doe the simon effect affect movement execution? *European Journal of Cognitive Psychology*, *16(6)*, 825-840.

Sarlegna, F. R., & Blouin, J. (2010). Visual guidance of arm reaching: Online adjustments of movement direction are impaired by amplitude control. *Journal of Vision*, *10(5)*, 1-12.

Saunders, J. A., & Knill, D. C. (2005). Humans use continuous visual feedback from the hand to control both the direction and distance of pointing movements. *Exp Brain Res*, *162*, 458-473.

Scherbaum, S., Dshemuchadse, M., Fischer, R., & Goschke, T. (2010). How decisions evolve: The temporal dynamics of action selection. *Cognition*, *115*, 407-416.

Scherberger, H., & Andersen, R. A. (2007). Target selection signals for arm reaching in the posterior parietal cortex. *The Journal of Neuroscience*, *27(8)*, 2001-2012.

Schmidt, R. A., Zelaznik, H., Hawkins, B., Frank, J. S., & Quinn, J. T. (1979). Motor-output variability: A theory for the accuracy of rapid motor acts. *Psychological Review*, *86(5)*, 415-451.

Schmidt, R. A., Zelaznik, H. N., & Frank, J. S. (1978). Information processing in motor control and learning. In G. E. Stelmach (Ed.), (p. 183-203). New York: Academic Press.

Schoener, G. (2008). *Dynamical systems approaches to cognition* (Vol. ???). In: The Cambridge Handbook of Computational Psychology, Ron Sun, (ed.), Cambridge University Press (in press, 2008).

Siciliano, B., & Khatib, O. (Eds.). (2008). *Springer handbook of robotics*. Springer-Verlag Berlin Heidelberg.

Simon, J. R. (1990). Stimulus response compatibility. In R. W. Proctor & T. G. Reeve (Eds.), (p. 31-86). Elsevier Science Publishers B.V.

Smith, P., & Ratcliff, R. (2004). Psychology and neurobiology of simple decisions. *Trends Neurosci*, *27*, 161-168.

Song, J.-H., & Nakayama, K. (2006). Role of focal attention on latencies and trajectories of visually guided manual pointing. *Journal of Vision*, *6*, 982-995.

Song, J. H., & Nakayama, K. (2008a). Numeric comparison in a visually-guided manual reaching task. *Cognition*, *106*, 994-1003.

Song, J. H., & Nakayama, K. (2008b). Target selection in visual search as revealed by movement trajectories. *Vision Research*, *48*, 853-861.

Song, J. H., & Nakayama, K. (2009). Hidden cognitive states revealed in choice reaching tasks. *Trends in Cognitive Science*, *13(8)*, 360-366.

Spivey, M. J., Grosjean, M., & Knoblich, G. (2005). Continous attraction toward phonological competitors. *Proceedings of the National Academy of Sciences of the USA*, *102*, 10393-10398.

Strauss, S., & Heinke, D. (2012). A robotics-based approach to modeling of choice reaching experiments on visual attention. *Frontiers in Psychology*, *3*, Article 105.

Strauss, S., & Heinke, D. (2013). Neurologically plausbile implementation of goal directed reaching: A closed-loop model. *TBA - in preparation*, -, -.

Strauss, S., Woodgate, P., & Heinke, D. (2013). Reaching to the odd-one-out: The role of target-distractor size. *TBA - in preparation*, -, -.

Tagliabue, M., Zorzi, M., Umilta, C., & Bassignani, F. (2000). The role of long-term-memory and short-term-memory links in the simon effect. *Journal of Experimental Psychology: Human Perception and Performance*, *26(2)*, 648-670.

Taube, J. S., & Bassett, J. P. (2003). Persistent neural activity in head direction cells. *Cerebral Coretx*, *13 (11)*, 1162-1172.

Thompson, S. G., McConnell, D. S., Slocum, J. S., & Bohan, M. (2007). Kinematic analysis of multiple constraints on a pointing task. *Human Movement Science*, *26*, 11-26.

Tipper, S. P., Howard, L. A., & Houghton, G. (1998). Action-based mechanisms of attention. *Philosophical Transactions of the Royal Society of London Series B-Biological Sciences*, *353(1373)*, 1385-1393.

Tipper, S. P., Howard, L. A., & Jackson, S. R. (1997). Selective reaching to grasp: Evidence for distractor interference effects. *Visual Cognition*, *4(1)*, 1-38.

Toxopeus, C. M., Jong, B. M. de, Valsan, G., Conway, B. A., Leenders, K. L., & Maurits, N. M. (2011). Direction of movement is encoded in the human primary motor cortex. *PLoS ONE*, *6, Issue 11*.

Trappenberg, T. P., Dorris, M. C., Munoz, D. P., & Klein, R. M. (2001). A model of saccade initiation based on the competitive integration of exogenous and endogenous signals in the superior colliculus. *Journal of Cognitive Neuroscience*, *13:2*, 256-271.

Webb, B. (2009). Animals versus animats: Or why not model the real iguana? *Adaptive Behavior*, *17(4)*, 269-286.

Welsh, & Elliot. (2004). Movement trajectories in the presence of a distracting stimulus: Evidence for a response activation model of selective reaching. *The quarterly journal of experimental psychology*, *57A(6)*, 1031-1057.

Welsh, Elliot, D., & Weeks, D. (1999). Hand deviations toward distractors. *Exp Brain Res*, *127*, 207-212.

Wise, S. P., Boussaoud, D., Johnson, P. B., & Caminiti, R. (1997). Premotor and parietal cortex: Corticocortical connectivity and conmbinatorial computations. *Annu. Rev. Neurosci.*, *20*, 25-42.

Wolfe, J., & Horowitz, T. S. (2004). What attributes guide the deployment of visual attention and how do they do it. *Nature Reviews Neuroscience*, *5*, 495-501.

Wolfe, J. M. (1998). Visual Search: A Review. In H.Pashler (Ed.), *Attention* (p. 13-74). Psychology Press.

Wood, D. K., Gallivan, J. P., Chapman, C. S., Milne, J. L., Culham, J. C., & Goodale, M. A. (2011). Visual salience dominates early visuomotor competition in reaching behavior. *Journal of Vision*, *11(10)*, 1-11.

Woodworth, R. S. (1899). The accuracy of voluntary movement. *Psychological Review*, *3*, 2, whole No. 13.

Yantis, S., & Egeth, H. E. (1999). On the distinction between visual salience and stimulus-driven attentional capture. *Journal of Experimental Psychology: Human Perception and Performance*, *25 (3)*, 661-676.

Ziemke, T. (Ed.). (2011). *Special issue: Cognitive robotics and reevaluation of piaget concept of egocentrism* (Vol. 29) (No. 3).